

Dissertation
Submitted to the
Combined Faculties for the Natural Sciences and for Mathematics
of the Ruperto-Carola University of Heidelberg, Germany
for the degree of
Doctor of Natural Sciences

presented by

Dipl.-Chem. Dmitry Kuchenov
born in Ulan-Ude, Russia
Oral-examination: June 26, 2017

The sensing and processing of multiple extracellular cues by living cells

Referees: Dr. Rainer Pepperkok

Prof. Dr. Ursula Klingmüller

This work was carried out at the European Molecular Biology Laboratory (EMBL) in Heidelberg, Germany, from October 2014 to April 2017 under supervision of Dr. Carsten Schultz.

Summary

Cells have an amazing ability to monitor complex extracellular environment, constantly deciding whether they, for example, migrate, survive, proliferate or differentiate. This ability is achieved through extremely dynamic cellular signaling networks that use the limited number of signaling components. Despite signaling networks of individual receptors are characterized in details, it is not fully understood how cells, employing shared signaling pathways, process and encode information from *multiple cues* that are physiologically common scenario.

In this study, I have first established a quantitative high-throughput FRET-based multi-parameter imaging platform (FMIP) which allows monitoring activity of multiple signaling pathways in living cells with high spatial and temporal resolution. The general applicability of this method was proven by profiling epidermal growth factor (EGF)-induced signaling network activity. FMIP was further employed in investigations of: (i) fatty acid dependent DAG signaling, (ii) the perturbation of EGF-induced signaling caused by the EGFR mutations; and (iii) the effects of an MEK inhibitor on EGF network activity. This platform will be a useful tool for investigating diverse signaling networks including growth factors, cytokines, hormones and GPCRs.

To understand the mechanisms underlying the signal integration and processing from multiple extracellular cues by living cells, I have further focused on receptor tyrosine kinases. Using FMIP I identified the dynamic signaling interactions (synergy, additivity, antagonism) between growth factors and cytokines at the system level. We find that those concentration dependent dynamic signaling interactions tune signaling network in the order of seconds or minutes to achieve specific activity state. While the signaling network state specifies unique gene

Summary

expression the gene expression profile shapes signaling network state in the order of hours. We further showed the potentiation and the tuning of dynamic EGF signaling under quasi-physiological concentration in non-starved cells. Overall the results suggest that under physiological conditions, in the presence of multiple signaling cues of low concentrations, the cellular signaling network is pre-activated and tuned to achieve specific strong responses to low concentrations of ligands. Thus, we provide mechanistic understanding of specific cell adaptation to the extracellular environment in the presence of multiple cues.

Zusammenfassung

Zellen haben die verblüffende Fähigkeit, komplexe extrazelluläre Umgebungen zu überwachen, konstant auf Stimuli zu reagieren und dabei zu bestimmen, ob sie sich zum Beispiel fortbewegen, teilen oder differenzieren sollen. Diese Fähigkeit wird durch ein höchst dynamisches zelluläres Signalnetzwerk ermöglicht, das mit einer begrenzten Anzahl von Komponenten auskommt. Obwohl die Netzwerke einzelner Rezeptoren bereits detailliert charakterisiert wurden, konnte noch nicht vollständig geklärt werden, wie Zellen mit Hilfe von gemeinsamen Signalwegen die Informationen von mehreren verschiedenen Botenstoffen verarbeiten und kodieren, wie es in einem physiologischen Szenario die Regel ist.

In im Rahmen dieser Arbeit wurde zunächst eine Hochdurchsatz, FRET-basierte Multi-Parameter-Bildgebungsplattform (FRET-based multi-parameter imaging platform; FMIP) etabliert, die es erlaubt, die Aktivität mehrerer Signalwege in lebenden Zellen mit hoher räumlicher und zeitlicher Auflösung zu beobachten. Die generelle Anwendbarkeit dieser Methode wurde anhand der Messung EGF-induzierter Aktivität im Signalnetzwerk gezeigt. Weiterhin wurde FMIP angewendet für die Untersuchung von: (i) Fettsäure-abhängiger DAG-Signalweitergabe, (ii) der Störung EGF-induzierter Signalweiterleitung aufgrund von EGFR-Mutationen und (iii) den Effekten eines MEK-Inhibitors auf die EGF-Netzwerkaktivität. Diese Plattform ist daher ein nützliches Werkzeug zur Untersuchung von vielfältigen Signalnetzwerken, darunter Wachstumsfaktoren, Hormonen und GPCRs.

Um den Mechanismus zu verstehen, der der Integration und Verarbeitung von mehreren gleichzeitigen extrazellulären Signalen zugrunde liegt, wurde im Weiteren der Schwerpunkt auf Rezeptor-Tyrosinkinasen gelegt. Mit Hilfe von FMIP konnten die dynamischen Signalwechselwirkungen (Synergie, Additivität und Antagonismus) zwischen

Wachstumsfaktoren und Zytokinen auf einer systemischen Ebene untersucht werden. Dabei wurde entdeckt, dass konzentrationsabhängige, dynamische Signalwechselwirkungen das Signalnetzwerk auf einer Zeitskala von Sekunden bis Minuten einstellen, um einen spezifischen Aktivitätszustand zu erreichen. Während der Zustand des Signalnetzwerks die Expression von bestimmten Genen reguliert, formt das Genexpressionsprofil den Zustand des Netzwerks im Zeitraum von Stunden. Weiterhin konnte in nicht ausgehungerten Zellen gezeigt werden, wie das dynamische EGF-Signal unter quasi-physiologischen Konzentrationen potenziert und eingestellt wird. Insgesamt deuten die Resultate darauf hin, dass das zelluläre Signalnetzwerk unter physiologischen Bedingungen und in Gegenwart von mehreren niedrig konzentrierten Botenstoffen voraktiviert und so eingestellt ist, dass starke Reaktionen auf niedrige Ligandenkonzentrationen erzielt werden können. Dies liefert das mechanistische Verständnis der Anpassung von Zellen an ihre extrazelluläre Umgebung in der Gegenwart von unterschiedlichen Signalen.

Contents

Summary	i
Zusammenfassung	iii
Contents	v
List of Figures	viii
Abbreviations	x
Chapter 1 - Introduction	1
1.1 RTKs are crucial regulators of cellular processes.....	1
1.2 RTKs signaling initiation and termination	3
1.2.1 RTKs signaling initiation	3
1.2.2 RTKs signaling duration and termination	5
1.3 Intracellular signaling of RTKs	6
1.3.1 Signal-induced assembly of multiprotein complexes and signaling network	8
1.3.1.1 Ras/MAPK signaling pathway	9
1.3.1.2 PI3K/AKT/mTOR signaling pathway	11
1.3.1.3 PLC- γ /PKC signaling pathway.....	13
1.3.1.4 Src/FAK signaling pathway.....	14
1.3.1.5 Mechanisms of signaling pathway cross-talk	16
1.3.2 Spatiotemporal control of signaling activity	19
1.4 RTKs cross-talk as an additional level of signaling complexity	22
1.5 Biosensors are useful tools for studying intracellular signaling in living cells.....	24
1.5.1 Fluorescent proteins as a reporting unit in biosensors	25

Contents

1.5.2	Single-fluorescent-protein-based biosensors.....	25
1.5.3	Fluorescence resonance energy transfer-based biosensors.....	26
	Aim of the thesis.....	29
	Chapter 2 – Experimental methods.....	31
2.1	Materials.....	31
2.2	Buffers and Media.....	36
2.2.1	Western Blot Buffers.....	36
2.2.2	Bacterial Culture media.....	37
2.2.3	Eukaryotic cell media and solutions.....	38
2.2.4	Starvation media.....	39
2.3	Cell culture.....	40
2.4	Methods.....	41
2.4.1	Molecular work.....	41
2.4.2	Live-cell microscopy.....	43
2.4.2.1	Forward transfection and imaging.....	43
2.4.2.2	Solid-phase reverse transfection.....	43
2.4.2.3	Cell microarray imaging.....	46
2.4.2.4	Cross-contamination assay.....	47
2.4.3	Image processing.....	47
2.4.3.1	FRET quantification.....	47
2.4.3.2	Automated cell counting.....	48
2.4.4	Western blotting.....	48
2.4.5	RNA extraction and evaluation.....	50
2.4.6	Statistical and data analysis.....	51
2.4.6.1	Outliers removal.....	51
2.4.6.2	Synergy score.....	52
2.4.6.3	Analysis of RNA-Seq data.....	53
2.4.6.4	General statistical analyses and data visualization.....	53
	Chapter 3 – Results and discussions.....	55

3.1	FRET-based multi-parameter imaging platform (FMIP) as a tool to study intracellular signaling networks	55
3.1.1	Transfection optimization	57
3.1.2	Monitoring EGF signaling network activity and platform validation	64
3.1.3	FMIP applied to various experimental designs	68
3.1.3.1	Monitoring EGF signaling perturbations caused by EGFR mutations and a clinically relevant inhibitor	70
3.1.3.2	Monitoring fatty acid dependent diacylglycerol induced signaling	74
3.1.4	Conclusions and Outlook	75
3.2	Signaling network integration and processing of multiple extracellular cues	78
3.2.1	Overview of the approach	79
3.2.2	Single stimulus treatment experiments	81
3.2.3	Pairwise treatment experiments	82
3.2.4	Signal integration from the pair of extracellular cues	84
3.2.5	Signaling interactions tune gene expression profile	87
3.2.6	Signaling interactions shape signaling response under quasi-physiological conditions	91
3.2.7	Conclusions and Outlook	94
	Bibliography	98
	Acknowledgements	118

List of Figures

Figure 1.1 Family members are listed under receptor representations.	2
Figure 1.2 Schematic representations of four modes of receptor tyrosine kinase dimerization. .	4
Figure 1.3 Multidomain architecture of signaling proteins.....	7
Figure 1.4 Schematic representation of Ras/ERK signaling pathway.....	11
Figure 1.5 Schematic representation of the PI3K/AKT/mTOR signaling pathway.	13
Figure 1.6 Schematic representation of PLC- γ /PKC signaling pathway.	14
Figure 1.7 Schematic representation of p130CAS signal integration.....	15
Figure 1.8 Schematic representation of motifs featured in biological networks.....	17
Figure 1.9 Schematic representation of signaling dynamics processing by Ras/ERK module.	20
Figure 2.1 Image analysis pipeline of an in-house developed macro FluoQ.....	49
Figure 3.1 FRET-based multi-parameter imaging platform (FMIP).	57
Figure 3.2 Substitution of Opti-MEM with DMEM or imaging buffer.	58
Figure 3.3 The substitution of gelatin in transfection mixes.....	59
Figure 3.4 Transfection optimization.....	60
Figure 3.5 The influence of the splitting time before reverse transfection on efficacy.....	61
Figure 3.6 Efficacy optimization when cell were split 24 hours before reverse transfection.....	62
Figure 3.7 cross-contamination analysis.	63
Figure 3.8 EGF-induced signaling in HeLa and H838 cells.	66
Figure 3.9 Heterogeneous cellular responses.	67
Figure 3.10 The impact of the FRET biosensor expression level on cellular signaling.	69
Figure 3.11 Perturbation of EGF signaling network by the MEK inhibitor AZD6244.	71

Figure 3.12 Changes of the EGF signaling network by constitutively active EGFR carrying L858R and T790M mutations.....	72
Figure 3.13 Comparison of global signaling responses.	73
Figure 3.14 Fatty acid composition dependent DAG signaling.	74
Figure 3.15 K-means clustering of single cell S6K activation as representative example of 4 clusters.....	80
Figure 3.16 The identity of the extracellular cues specifies characteristic dynamic signaling responses in living HeLa cells.....	81
Figure 3.17 The identity of the extracellular cues specifies their location in PCA space.....	82
Figure 3.18 Crosstalk of two growth factors shapes signaling dynamics.	83
Figure 3.19 Composite interaction map reflecting antagonism, additivity and synergy due to GFs signaling interaction.....	85
Figure 3.20 The dynamics of signaling interactions.	86
Figure 3.21 Schematic overview of the RNA-seq screen performed with GFs.	87
Figure 3.22 Gene and signaling response dynamics after single or pairwise stimulation.	89
Figure 3.23 Volcano plots of differentially expressed genes (DEGs).....	89
Figure 3.24 Signaling pathway enrichment analysis of DEGs.....	90
Figure 3.25 Quasi-physiological condition shape EGFR response.....	93
Figure 3.26 Intracellular information processing from multiple cues.....	96

Abbreviations

(p70) S6K1 – (p70) S6 kinase homolog 1

(p90) RSK (2) – (p90) ribosomal S6 kinase (2)

4E-BP1 – eIF4E binding protein 1

AA – arachidonic acid

Abl1 – v-abl Abelson murine leukemia viral oncogene homolog 1

Akt/PKB – AKR mouse thymoma kinase/Protein kinase B

ATP – adenosine triphosphate

BAD – Bcl-2-associated death promoter

BDNF – brain derived neurotrophic factor

BiFC – bimolecular fluorescence complementation

Ca²⁺ – calcium ions

CaMKII – Ca²⁺/calmodulin dependent protein kinase II

cAMP – 3',5'-cyclic adenosine monophosphate

Cent – centromere

c-Fos – v-Fos FBJ Murine Osteosarcoma Viral Oncogene Homolog

c-MET(or HGFR) – cellular met proto-oncogene (hepatocyte growth factor receptor)

CREB – cAMP response element binding protein

Cyto – cytosole

DAG – diacylglycerol

DMEM – Dulbecco's Modified Eagle Medium

DMSO – dimethylsulfoxide

DNA – desoxyribonucleic acid

ECD – extracellular domain

EGF(R) – epidermal growth factor (receptor)

eIF4E – eukaryotic translation initiation factor 4E

ERBB2 – v-Erb-B2 Avian Erythroblastic Leukemia Viral Oncogene Homolog 2
ERK1/2 – extracellular signal-related kinase homolog 1 or homolog 2
FAK – focal adhesion kinase
F-BAR – FCHo2-Bin/Amphiphysin/Rvs domain
FGDI – membrane-targeted Rho guanine nucleotide exchange factor
FGF(R) – fibroblast growth factor (receptor)
FNIII – fibronectin type III domain
FOXO – forkhead homeobox type O
FOXO 3A – forkhead homeobox type O 3A
FOXO1 – forkhead homeobox type O 1
FP – Fluorescent protein
FPS/FES – Tyrosine-protein kinase Fes/Fps
FRET – fluorescence resonance energy transfer
FRS2 – Fibroblast Growth *Factor Receptor Substrate 2*
FYVE – Fab-1, YGL023, Vps27, and EEA1 domain
G6Pase – glucose-6-phosphatase
GAB (1) – grb2 associated binding protein (1)
GRB2 – growth factor bound 10
Grb2 – growth factor receptor-bound protein 2
GSK3(β) – glycogen synthase kinase 3 (beta)
GTP – guanosine-5'-triphosphate
HER1/2/3/4 – human epidermal growth factor receptor 1/2/3/4; same as ERBB1/2/3/4
ICD – intracellular domain
IEG – immediate early gene
Ig – immunoglobulin-like domain
IGF1 – insulin-like growth factor 1
IGFR-1 – insulin-like growth factor-1 receptor
IP3(R) – inositol (1,4,5)-triphosphate (receptor)
IRS – insulin receptor signaling protein
IRS1 – insulin receptor signaling protein homolog 1
IRS2 – insulin receptor signaling protein homolog 2
KSR1/2 – kinase suppressor of ras 1/2
Mad1 – basic helix–loop–helix leucine zipper protein; mitotic arrest deficient-like protein 1
MAPK – mitogen-activated protein kinase
MAPKK – MAPK kinase
MEK1/2 – MAPK/ERK kinase homolog 1 or homolog 2

Abbreviations

MeOH – methanol

mTOR – mammalian target of rapamycin

mTORC1 – mammalian target of rapamycin complex 1

mTORC2 – mammalian target of rapamycin complex 2

MYC – avian myelocytomatosis virus oncogene

Nck – non-catalytic region of tyrosine kinase adaptor protein 1

NF- κ B – nuclear factor kappa-light-chain-enhancer of activated B cells

NGF(R) – nerve growth factor (receptor)

Nuc - nucleus

p130CAS – BCAR, breast cancer anti-estrogen resistance 1

PAABD – phosphoamino-acid-binding domain

PBS – phosphate buffered saline

PCR – polymerase chain reaction

PDGFR α – platelet-derived growth factor receptor, alpha polypeptide

PDGFR β – platelet-derived growth factor receptor, beta polypeptide

PDK1 – 3-phosphoinositide dependent protein kinase-1

PH – pleckstrin homology domain

PHLPP – PH domain and leucine-rich repeat protein phosphatases

PI3K – phosphatidylinositol-3 kinase

PIP2 – phosphatidylinositol(4,5)bisphosphate

PIP3 – phosphatidylinositol(3,4,5)trisphosphate

PKC – protein kinase C

PLA₂ – phospholipase A2

PLC- γ – phospholipase C-gamma

PM – plasma membrane

PP2A – protein phosphatase 2A

PTB – pTyr-binding domain

PTEN – phosphatase and tensin homolog deleted on chromosome 10

PTP – protein tyrosine phosphatase

Rac1 – ras-related C3 botulinum substrate 1

RAF(1) – v-raf-1 murine leukemia viral oncogene (homolog 1)

Raptor – regulator-associated protein of mTOR

Ras – Rat sarcoma or PROTO-ONCOGENE PROTEIN P21

RET – rearranged during transfection; ret proto-oncogene

Rheb – ras homolog enriched in brain

RhoA – ras homolog family member A

Rictor – rapamycin-insensitive companion of mTOR
ROI – region of interest
RT – room temperature
RTK(s) – receptor tyrosine kinase(s)
SBD – Src binding domain
SCF – stem cell factor
SD – substrate binding domain
SDS – sodium dodecylsulfate
SH2 – Src homology 2 domain
SH3 – Src homology 3 domain
Shc – SHC-transforming protein
SHIP – Src homology homain 2-containing inositol 5-phosphatase
SHP – SH2 containing phosphatase
SHP – SH2 containing phosphatase homolog 1
SOC – super optimal broth with catabolite repression
SOS – son of sevenless
Src – v-src sarcoma (Schmidt–Ruppin A-2) viral oncogene homolog (avian)
STAT – signal transducer and activator of transcription
TBC1D7 – TBC1 domain family, member 7
TBE – Tris buffered EDTA
TKD – tyrosine kinase domain
TrkA – tropomyosin receptor kinase A
TrkB – *tropomyosin receptor kinase B*
TSC1 – tuberous sclerosis complex 1 (Hamartin)
TSC2 – tuberous sclerosis complex 2 (Tuberin)
ULK1 – unc-51-like kinase 1
VAV1 – guanine nucleotide exchange factor 1
VEGFR – vascular endothelial growth factor receptor

Chapter 1 - Introduction

1.1 RTKs are crucial regulators of cellular processes

Receptor tyrosine kinases (RTKs) are crucial for cell-to-cell communication in multicellular organisms. Being able to regulate critical cellular processes such as proliferation, differentiation, survival, metabolism and migration, it is not surprising that RTKs are involved in embryogenesis and the development of many diseases including cancer. In humans, RTKs comprise 58 members distributed in 20 families based on their sequence homology and structure (Figure 1.1) (Lemmon and Schlessinger, 2010). All RTKs are manufactured as a single polypeptide chain with the highly conserved architecture composed of an extracellular domain (ECD), a single transmembrane domain and intracellular region (van der Geer et al., 1994). The latter contains a juxtamembrane domain, the catalytic domain with kinase activity, and the C-terminal tail that varies from few to 200 residues (van der Geer et al., 1994). Interestingly, the most variable part is localized in ECD, the major function of which is to bind to a specific ligand. The major principle of RTK activation is dimerization or oligomerization upon the binding of ECD to a secreted ligand (Honegger et al., 1989). Subsequent conformational change induces RTK autophosphorylation of critical intracellular docking sites to initiate the assembly of multiple signaling complexes. In turn, these complexes trigger several parallel intracellular signaling pathways in vertebrates including Ras/MAPK, PI3K/AKT PLC/PKC, STATs pathways (Kolch and Pitt, 2010; Zheng et al., 2013). Newly emerging data suggest that there are notable differences among RTKs in the mechanisms of activation. Moreover, RTK-induced signaling was shown to be much more complex due to the network-like architecture formed by signaling pathways having feedback and feed-forward loops (Lemmon and Schlessinger, 2010).

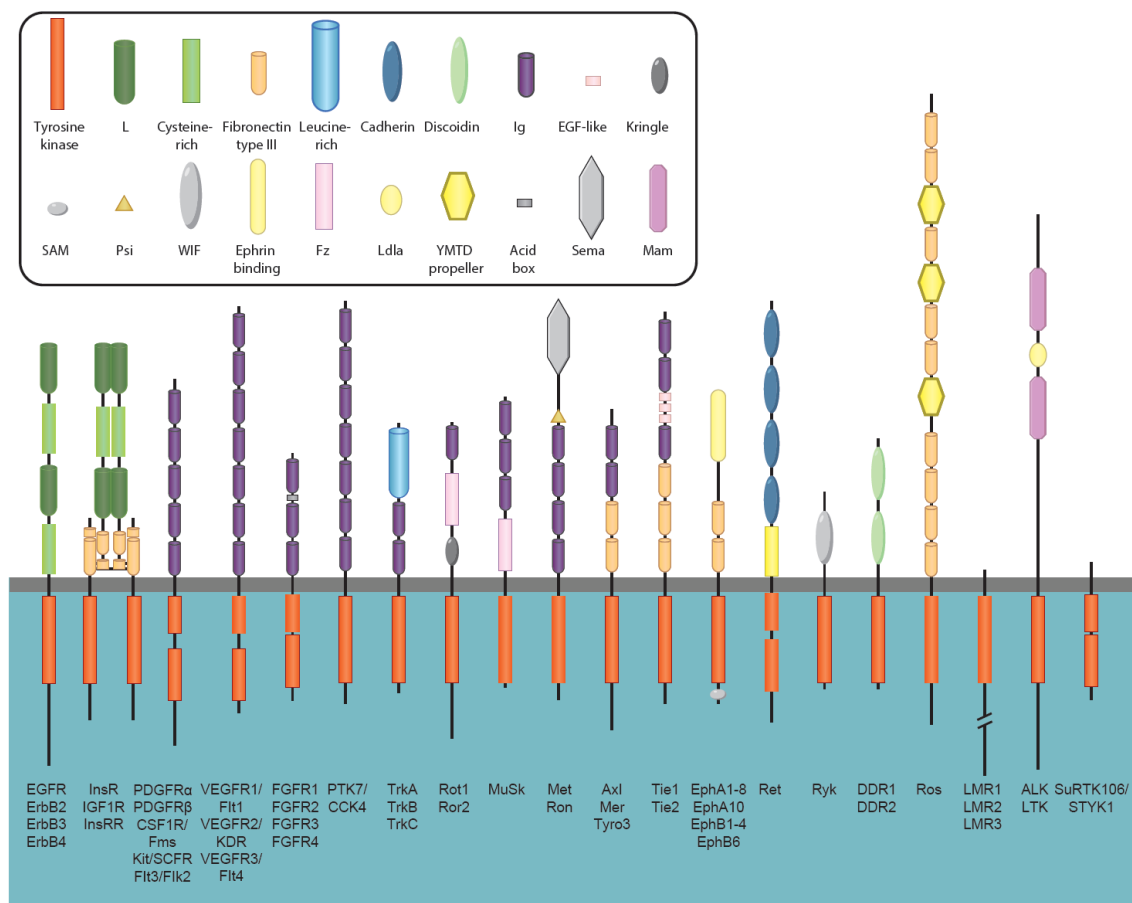


Figure 1.1 Family members are listed under receptor representations. Figure is adapted from (Lemmon and Schlessinger, 2010).

The dysregulation of RTK-activated pathways due to, for example, gene amplification and genetic mutations often underlies numerous diseases including cancer. U.S. Food and Drug Administration therefore approved many anticancer therapies targeting aberrant RTKs signaling. However, substantial improvement in survival rate by newly developed anti-cancer therapies is often compromised by primary or acquired drug resistance. Over the past few decades, many diverse mechanisms of drug resistance have been discovered. They could be classified in at least three different groups: (i) Competing with drug binding (Yonesaka et al., 2011; Yun et al., 2008); (ii) Masking or loss of the drug-binding site (Anido et al., 2006; Nagy et al., 2005); (iii) Pharmacodynamic and pharmacokinetic mechanisms (Burger et al., 2005; Illmer et al., 2004). Although huge progress has been made in the exploration of major principles underling drug resistance mechanisms, the emerging complexity and plasticity of signaling networks suggests

that additional mechanisms are involved in the development of drug resistance. For example, by exploiting signaling network plasticity cancer cells are able to remodel signaling network activity by the dysregulation of feed-forward and feedback loops to overcome drug potency (Chaturvedi et al., 2009; Duncan et al., 2012; Lai et al., 2014). Moreover, redundancy of RTK signaling is also involved in the development of drug resistance (Liu et al., 2009; Wilson et al., 2012). Therefore, the deeper understanding of the basic principles of RTK signaling as well as its plasticity in normal and diseased tissues will facilitate the development of effective therapeutic approaches to prevent cancer progression.

1.2 RTKs signaling initiation and termination

RTKs control of important cellular processes and aberrant signaling as well as its duration might lead to the failure in embryo development or to the development of various diseases. Therefore cells have evolved complex mechanisms to precisely control the initiation, duration and termination of RTKs signaling on the receptor level.

1.2.1 RTKs signaling initiation

The general model of RTK activation, as previously mentioned, proposes ligand-induced receptor dimerization or oligomerization. In support of this model, it was shown that EGFR (epidermal growth factor receptor, ErbB1) expressed at physiological levels exists as a monomer on the cell membrane whereas dimerization and clustering of EGFR was detected upon stimulation with EGF (epidermal growth factor) (Nagy et al., 2010). Interestingly, the overexpression of EGFR induced ligand-independent formation of clusters that are promoted by membrane-mediated interactions (Nagy et al., 2010). Although the functional role of these clusters is not clear, the cluster formation might be involved in the aberrant signaling upon overexpression of receptor in various tumors. However, it is important to note that the insulin receptor and its closely related member, insulin-like growth factor-1 receptor (IGFR-1), are expressed as dimers linked with disulfide bonds in the absence of their ligand (Ward et al.,

2007). Ligand binding by those dimers induces structural changes leading to the increase of kinase activities. Regardless of initial state of the receptor (monomeric, dimeric or oligomeric) the binding to the ligand is an essential prerequisite to effectively stabilize the active configuration of the dimeric/oligomeric receptor and initiate signal transduction.

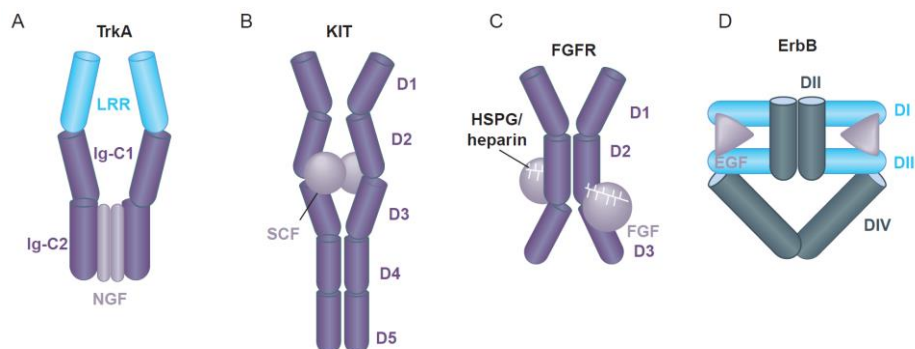


Figure 1.2 Schematic representations of four modes of receptor tyrosine kinase dimerization. (A) Ligand-mediated dimerization without receptor contacts. Interaction between neural growth factor and TrkA is depicted as an example. (B) Ligand-mediated dimerization with receptor contacts illustrated through the interaction of stem cell factor with the KIT receptor. (C) Dimerization by forming a ternary complex with an accessory molecule. As an example, the complex is illustrated via FGFR, heparin and FGF interaction. (D) Receptor-mediated dimerization. The formation of EGFR homodimer upon EGF binding is illustrated. Receptors are represented as protein domains in form of colored cylinders. Figure is adapted from (Heldin et al., 2016).

The extracellular region of RTKs, enabling the recognition of specific ligands, is mainly made of the varying set of specific domains such as fibronectin type III (FNIII) and *immunoglobulin*-like (Ig) domains (Figure 1.1). Combinatorial domain architecture allows the multimodal strategy of ligand binding and signaling initiation. In general, four modes of RTK-ligand binding and dimerization are described (Figure 1.2). For example, nerve growth factor (NGF), a homodimeric ligand, acts as a cross-bridge between two monomers of TrkA (tropomyosin receptor kinase A) (Wehrman et al., 2007). This dimerization is induced without receptor monomers interaction (Figure 1.2 A.). The second mode is also a symmetric binding of dimeric stem cell factor (SCF) to an RTK kit but the receptor dimer forms homotypic contacts additionally stabilizing receptor-receptor interaction (Yuzawa et al., 2007) (Figure 1.2 B.). Another mode is demonstrated by the fibroblast growth factor receptor (FGFR) that forms a dimer upon binding to its ligand, fibroblast growth factor (FGF), and an accessory molecule, heparin or heparin sulfate (Stauber et al., 2000) (Figure 1.2 C.). Receptor-ligand, receptor-heparin/heparin sulfate and ligand-heparin interactions

are cooperatively involved into the stabilization of the receptor dimer. The last mode is represented by the EGFR family where each molecule of monomeric EGF binds to a single receptor causing a conformational change. The latter initiates direct binding of two EGF-bound receptors and their activation (Figure 1.2 D.). Considering the unique modular composition of ECD, it is very likely that further investigation of the 58 RTKs in humans will lead to the discovery of new RTK dimerization mechanisms.

Regardless of the dimerization mechanism, RTKs have evolved effective ligand-dependent activation mechanisms requiring coordinated changes in the surfaces of ECDs and intracellular domains (ICDs) in order to induce the kinase domain association between the two receptors. Although crystal structures of activated tyrosine kinase domains (TKDs) are very similar, the activation mechanisms are extremely different among RTKs due to a wide diversity in the structures of inactive TKDs. These inactivated structures are defined by a receptor-specific set of cis-autoinhibitory intermolecular interactions to precisely control the TKD activity of the receptor (Hubbard, 2004; Niu et al., 2002; Zhang et al., 2006). Thus, phosphorylation that regulates kinase activity occurs on RTK specific residues in various regions of the intracellular domain. As the most common scenario, RTKs are auto-phosphorylated in the activation loop of the kinases that leads to the stabilization of the open conformation and the subsequent binding of ATP as well as the protein substrate to the kinase domain of RTK (Hubbard and Till, 2000). The fully activated kinase domain then catalyzes auto-phosphorylation of tyrosine residues that serve as docking sites for Src homology 2 (SH2) and pTyr-binding (PTB) domain-containing proteins and causes the formation of multiprotein signaling complexes activating signaling pathways (Pawson, 2004; Ronan et al., 2016).

1.2.2 RTKs signaling duration and termination

RTK initiation induces massive phosphorylation of the receptors and associated adaptor proteins. The maximum level of phosphorylation is achieved within 10 min and gradually decreases to the basal level in about 2 hours. Surprisingly, the phosphotyrosine turnover on activated RTKs is extremely rapid with the half-life time of 10-30 seconds (Kleiman et al., 2011). Such rapid cycle

of phosphorylation/dephosphorylation implies several important properties of this dynamic system. First, it enables integration of positive feedback loops through production of reactive oxygen species that in turn transiently inhibit protein tyrosine phosphatases (PTPs) activity. As a result of this positive regulation, a switch-like response can be achieved (Tischer and Bastiaens, 2003). Second, it was suggested as a mechanism of proofreading that effectively terminates the signal upon the binding of a receptor to a non-specific ligand (McKeithan, 1995). Finally, it was also reported that the rapid turnover of phosphorylation sites might be an important mechanism damping the signals from SH2 domains with high dwell times and low specificity (Oh et al., 2012).

The signal termination occurs by ligand-induced endocytosis that subsequently leads to a first step in the receptor deactivation, the dephosphorylation (Goh and Sorkin, 2013). It was proposed that endocytosis is needed to transport an active RTK to the internal membranes, the location of protein tyrosine phosphatases (PTPs), in order to dephosphorylate and inactivate the receptor (Haj et al., 2002). However, it was also noticed that RTK internalization may maintain or even amplify the signaling activity of a receptor supporting the concept of endosomal RTK signaling (Grecco et al., 2011; Kermorgant and Parker, 2008; Murphy et al., 2009). Moreover, the endosomal RTK signaling may differ from plasma membrane signaling suggesting unique regulatory mechanisms that are not fully understood (Murphy et al., 2009). Thus, the future challenge is to prove the relevance and mechanistic regulation of endosomal signaling in various cell types under physiological conditions.

1.3 Intracellular signaling of RTKs

After the activation of an RTK, its main task is to diffuse information from the plasma membrane through the cytoplasm to the correct cellular location and at the right time. In order to adjust the cellular state the information is transmitted to the nucleus to start the transcriptional program enabling the adaptation of the cell to the environmental changes. This is achieved through several general processes of information propagation in a cell: (i) the signal-dependent activation or assembly of multiprotein complexes; (ii) temporal control of signaling activity and (iii) the precise control of protein activity by subcellular localization (Kholodenko et al., 2010;

Lee and Yaffe, 2016; Pawson, 2004). In order to fulfill those complex processes cells have evolved modular organization of signaling proteins comprising domains with diverse functions such as binding and/or catalytic properties (Figure 1.3). Cells also employ clever ways to dynamically regulate the functionality of those domains by posttranscriptional modifications (Deribe et al., 2010) and binding to small molecules and/or ions (GTP, cAMP, Ca^{2+}) (Ni et al., 2011). Thus, the multi-domain protein architecture and the diverse mechanisms regulating the domain functionality result in the formation of an interconnected network forming a protein machinery that is able to reliably transmit extracellular information and adapt to the external and internal perturbations, a property of the signaling network that is often called plasticity.

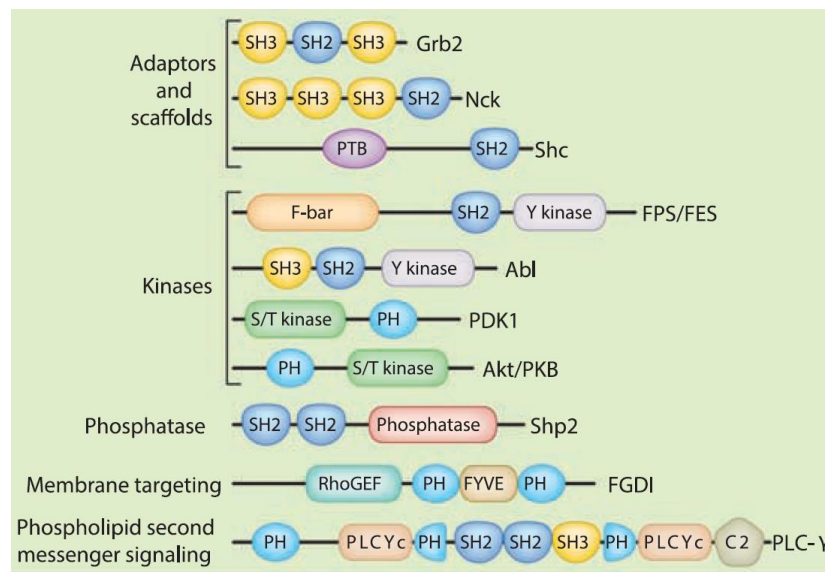


Figure 1.3 Multidomain architecture of signaling proteins. Schematic representations of selected adaptor and scaffolding proteins (Grb2, Nck, Shc); the serine/threonine (S/T) kinases (PDK1 and Akt/PKB); the tyrosine kinases (FPS/FES and Abl); the protein tyrosine phosphatase (Shp2); a membrane-targeted Rho guanine nucleotide exchange factor (FGDI); and phospholipase C- γ (PLC- γ). Protein domains are also shown: Src homology 2 (SH2); Src homology 3 (SH3); phosphotyrosine binding (PTB); FCHo2-Bin/Amphiphysin/Rvs domain (F-BAR); Fab-1, YGL023, Vps27, and EEA1 domain (FYVE); and Ca^{2+} -dependent membrane-targeting (C2) domain. Enzymatic domains in each protein are named. Figure is adapted from (Deribe et al., 2010).

1.3.1 Signal-induced assembly of multiprotein complexes and signaling network

The autophosphorylation of active RTKs, as mentioned above, leads to the recruitment of proteins containing SH2 and PTB domains that enables the signal-dependent activation of downstream signaling proteins. While PTB domain-containing proteins typically serve as scaffold proteins (Shc, FRS2), SH2 domain-containing proteins might have at least three distinct functions such as an adaptor/scaffold (Grb2, Nck), an enzyme (Shp2, Abl1, Vav1) and a transcription factor (STAT1-6) (Liu et al., 2006) (Figure 1.3). The recruitment of signaling proteins may be initiated through direct binding to the autophosphorylated receptor or indirect by enrolling additional proteins, called adaptor proteins. These adaptor proteins form complexes with the activated receptor and are phosphorylated by RTKs with which they are associated. In turn, the phosphorylated sites of adaptors serve as docking sites for a distinct repertoire of downstream signaling molecules. For simplicity, the signaling events at the level of the receptor and downstream signaling are often separated into the different steps of information transduction. Therefore two main questions are raised and discussed below: (1) how does a single receptor achieve specificity in the regulation diverse cellular processes and (2) how are different RTKs using the same set of signaling pathways but induce different responses.

Two possible mechanisms of specificity and information integration by a RTK were proposed: the individual binding of a specific effector molecule could trigger distinct signaling outcome or alternatively, the binding of multiple effectors is combinatorially decoded to drive the desired signaling and physiological response. The examination of embryos expressing a PDGFR α (platelet-derived growth factor receptor, alpha polypeptide) bearing a mutation in one autophosphorylation site to impair binding to specific effector identified unique phenotypes suggesting that each effector regulates a distinct biological response (Klinghoffer et al., 2002). In contrast, the combination of effectors binding to PDGFR β (platelet-derived growth factor receptor, beta polypeptide) determined the total number of vascular smooth muscle cells/pericytes indicating that combinatorial input from several effectors is also able to induce specific physiological response (Tallquist et al., 2003). Thus using point mutations at tyrosine

residues abrogating the recruitment of specific effectors by PDGF receptor α and PDGF receptor β highlighted that both mechanisms occur at least during mouse development.

RTKs are complex and dynamic multiprotein hubs that are able to activate multiple signaling pathways including Ras/MAPK, PI3K/AKT/mTOR, PLC- γ /PKC, STAT, and Src/FAK that are shared among various RTKs. Therefore, a physiologically relevant question is how different RTKs induce distinct cellular responses. For example, PDGF and FGF that are required for craniofacial mouse development elicit divergent transcriptional programs (Vasudevan et al., 2015). These two programs seem to result from differential usage of signaling pathways. PDGF regulates PI3K-dependent differentiation whereas FGF promotes ERK-dependent cell proliferation. Nevertheless, both of these growth factors are able to activate ERK although with significantly different dynamics. FGF-induced ERK activation is greater in magnitude and longer in duration in comparison to PDGF-dependent ERK activation indicating the complex mechanisms of information processing by RTK signaling networks. However, the purpose and regulation of the PDGF-induced ERK signaling dynamics remain unclear. Further studies are needed to elucidate the role of signaling dynamics in the multi-pathway information integration by RTK, but strong hints (chapter 1.3.2) point towards the importance of temporal patterns within the signal transduction network.

1.3.1.1 Ras/MAPK signaling pathway

The Rat sarcoma (Ras)/Mitogen-activated protein kinase (MAPK) signaling pathway is important for proliferation, differentiation and survival programs. MAPKs are a highly conserved family including 15 members, the best characterized being ERK1/2. A simple view of ERK1/2 activation is usually initiated by translocation of the growth factor receptor-bound protein 2/Son of sevenless (Grb2/Sos) protein complex to an autophosphorylated RTK by direct binding to the activated receptor or through interaction with SHC-adaptor protein (Shc) that is also phosphorylated by the receptor (Figure 1.4) (Salcini et al., 1994). Grb2/Sos protein complex is formed through an interaction mediated by SH3 domain of Grb2 and the proline rich region of Sos. On the plasma membrane Sos, a small GTP binding protein, forces prenylated Ras (H-Ras,

K-Ras, N-Ras) to release bound GDP and to bind GTP. This GDP/GTP exchange results in Ras activation.

Ras activation is followed by sequential activation of cytoplasmic protein kinases (Figure 1.4). It is well known that Ras is responsible for the recruitment of Raf1 to the plasma membrane where Raf1 is activated (Stokoe et al., 1994). Then the activated Raf1 phosphorylates MAPK kinases (MAPKKs), MEK1 and MEK2, at two serine residues (Ser217 and Ser221) triggering their activation (Alessi et al., 1994). In turn, activated MAPKKs initiate phosphorylation of two adjacent threonine and tyrosine residues of ERK1/2 (Haystead et al., 1992) resulting in substantial conformational changes and subsequent ERK catalytic activation. MAPK has a wide variety of downstream targets including protein kinases (RSK) and transcription factors (CREB, FOXO and MYC). The aforementioned complex mechanism of MAPK signaling is tightly regulated by scaffold proteins. MAPK scaffold proteins contain several domains and serve as a platform for multiprotein complex assembly. By bringing specific players of a MAPK cascade in close proximity, scaffold proteins facilitate activation of a particular MAPK providing increased specificity and the mechanism to regulate compartmentalized signaling. For example, in response to the activation of RTK, kinase suppressor of Ras 1 (KSR1) interacts with Raf, MEK and ERK bringing effectors and their upstream activator into close proximity (Therrien et al., 1996).

In the past, the Ras/MAPK signaling pathway was considered as a simple linear cascade of biochemical reactions. However, it became apparent in the scientific community that signal attenuation and reversion to the basal state via negative feedback loops are crucial for most Ras/MAPK-dependent biological processes. One of the key attenuation mechanisms of Raf activity is direct phosphorylation of Raf by ERK on several specific residues (Dougherty et al., 2005). It was also suggested that ERK can control Ras activity through a RSK2-dependent mechanism (Douville and Downward, 1997). Another important feedback loop involves the ERK-induced expression of genes encoding Sprouty and MAPK phosphatases that negatively regulate the signaling of this pathway. Such complex regulatory mechanisms of Ras/MAPK signaling allow achieving distinct signaling dynamics after activation of specific RTKs.

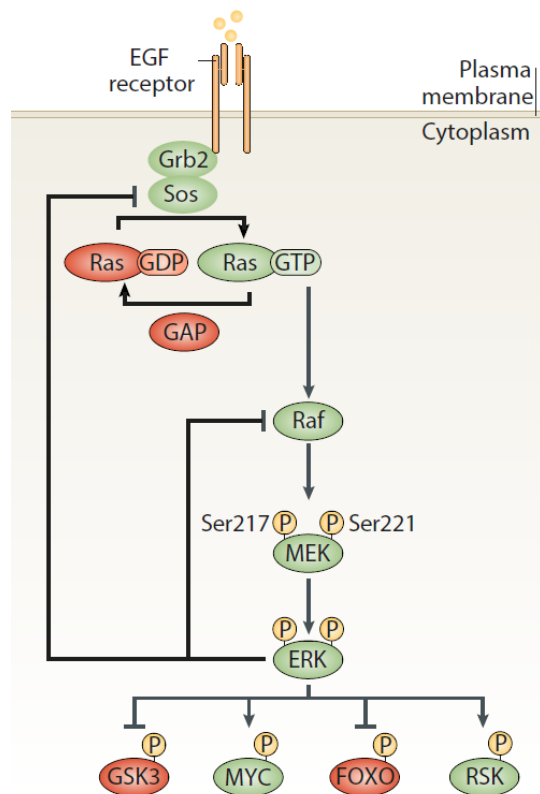


Figure 1.4 Schematic representation of Ras/ERK signaling pathway. Figure is adapted from (Mendoza et al., 2011).

1.3.1.2 PI3K/AKT/mTOR signaling pathway

The phosphatidylinositol 3-kinase (PI3K)/mammalian target of rapamycin (mTOR) pathway controls distinct cellular functions including cell survival, metabolism and division and is triggered by PI3K a lipid kinase, and its recruitment to the active RTK. The recruitment of PI3K is achieved through the direct binding of PI3K to the receptor or indirect association of active PI3K with docking proteins such as insulin receptor substrate (IRS) or GRB2-associated binder (GAB) (figure 1.5). The translocation of PI3K to the plasma membrane leads to the generation of phosphatidylinositol 3,4,5-trisphosphate (PIP3) by the phosphorylation of phosphatidylinositol 4,5-bisphosphate (PIP2). In turn, the increased concentration of PIP3 on the plasma membrane initiates the recruitment of AKT through pleckstrin homology (PH) domains that recognizes PIP3. AKT, being in close proximity, is activated by 3-phosphoinositide-dependent kinase 1 (PDK1). Subsequently, AKT phosphorylates tuberous sclerosis complex 2 (TSC2) at multiple

sites to suppress the GAP activity of the TSC1-TSC-TBC1D7 complex (Inoki et al., 2002). The later leads to the activation of the small GTPase RAS homologue enriched in brain (Rheb) that directly activates mTORC1 (figure 1.5). It is well known that mTOR can be associated with two distinct complexes, mTOR complex 1 (mTORC1) or complex 2 (mTORC2), and both of these complexes are activated by growth factors. While regulation of mTORC1 kinase activity is described in detail, the regulation of mTORC2 is poorly understood. AKT and mTORC1 are essential signaling hubs to integrate multiple signals and control distinct cellular processes. For instance, AKT is able to modulate distinct cellular process by phosphorylation of GSK3 β , regulating cell-cycle entry, and Bcl-2-associated death promoter (BAD) inhibiting apoptosis. Active mTORC1 phosphorylates the translational regulator eukaryotic translation initiation factor 4E (eIF4E) binding protein 1 (4E-BP1) and S6 kinase 1 (p70S6K1) promoting protein synthesis. Importantly, mTORC1 also phosphorylates and stimulates growth factor receptor-bound protein 10 (GRB10) which is a negative regulator of insulin/PI3K signaling providing mechanism for the temporal control of PI3K/AKT/mTOR signaling (Yu et al., 2011). Moreover, mTORC1 can prevent autophagy by direct phosphorylation of UNK-51-like kinase 1 (ULK1) Ser758 (Ganley et al., 2009). The mTORC1 activity is not only regulated by RTK signaling but also by many signaling cues such as lipids, amino acids and the ATP/AMP ratio (Long et al., 2005). Recently, it was also shown that mTORC2 can phosphorylate AKT at Ser473 to potentiate lipogenesis in liver (Hagiwara et al., 2012). Thus, the ability of the PI3K/AKT/mTOR signaling pathway to regulate numerous cellular process and phenotypes is achieved through complex non-linear topology of this pathway, illustrating the complexity of the cellular signaling machinery.

The PI3K/AKT/mTOR signaling is tightly controlled by multiple mechanisms attenuating the activity of the pathway. For example, several inositol phosphatases such as PTEN and SHIP are known to decrease amount of PIP3 on the plasma membrane (Yuan and Cantley, 2008). AKT can also be directly inactivated by protein phosphatase 2A (PP2A) and PH domain and leucine-rich repeat protein phosphatases (PHLPP) that dephosphorylate the kinase. Several feedback loops are engaged in the regulation of AKT activity at the pathway and transcriptional level. S6K phosphorylates IRS and rapamycin-insensitive companion of mammalian target of rapamycin

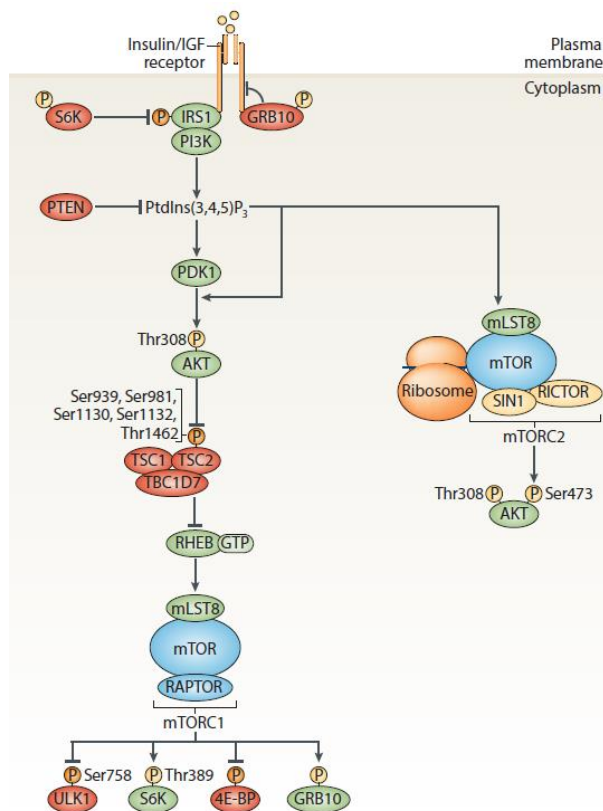


Figure 1.5 Schematic representation of the PI3K/AKT/mTOR signaling pathway. Figure is adapted from (Shimobayashi and Hall, 2014).

(RICTOR) damping AKT activity and mTORC1 signaling. Moreover, AKT negatively regulates Forkhead box *protein O* (FOXO)-mediated RTK transcription as well as IRS1 transcription through mTORC1 (Chandarlapaty et al., 2011). Collectively, multiple mechanisms of PI3K/AKT/mTOR signaling inactivation allow the differential activation of signaling components and hypothetically diversify the combinatorial signaling code regulating cellular responses.

1.3.1.3 PLC- γ /PKC signaling pathway

Phospholipase C gamma (PLC γ) was characterized as the first substrate directly interacting with activated EGFR in 1989 (Margolis et al., 1989) (figure 1.6). This binding to the active EGFR

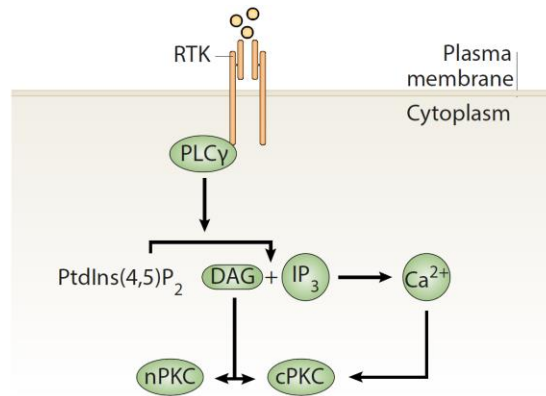


Figure 1.6 Schematic representation of PLC- γ /PKC signaling pathway.

occurs through the N-terminal and C-terminal Src homology 2 (SH2) domains of PLC- γ and releases its catalytic activity. After activation, PLC- γ hydrolyses phosphatidylinositol 4,5-bisphosphate (PIP₂) producing two second messengers: inositol 1,4,5-trisphosphate (IP₃) and diacylglycerol (DAG). The soluble IP₃ diffuses to the surface of endoplasmic reticulum (ER) and binds with the IP₃ receptor (IP₃R) inducing the release of calcium ions (Ca²⁺) to the cytoplasm. This leads to the activation of Ca²⁺/calmodulin dependent protein kinases (for example, CaMKII). Concurrently, the increase of cytoplasmic Ca²⁺ ions and production of DAG on the plasma membrane contributes to the activation of classical and novel isoforms of PKC, a central hub of this signaling pathway. The *in vivo* relevance of this pathway was explicitly demonstrated in transgenic and knockout mice suggesting the involvement of PLC- γ /PKC signaling pathway into tumor-related phenotypes.

1.3.1.4 Src/FAK signaling pathway

The Src/FAK signaling pathway is involved in the regulation of cell migration and the promotion of anchorage-independent growth as well as cell survival. It was shown that Src can be activated via direct association with RTKs including EGFR, c-Met (or HGFR) and platelet-derived growth factor (PDGFR) by binding its SH2 domain to RTK phosphorylated site (Bromann et al., 2004). This interaction releases the inhibitory effect of the SH2 domain bound to the tail of the protein in the auto-inhibited state (Boggon and Eck, 2004). Subsequently, activated Src phosphorylates FAK at Tyr576 and Tyr577 that leads to the Src-dependent FAK activation (Frame et al., 2010).

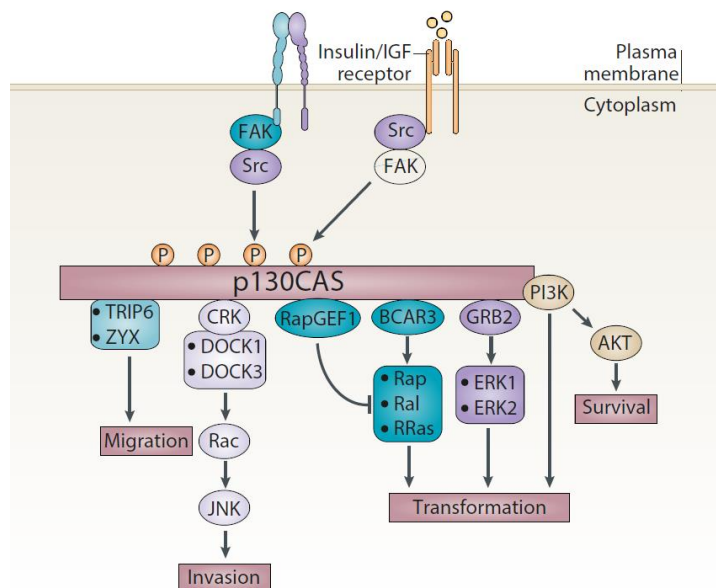


Figure 1.7 Schematic representation of p130CAS signal integration. Figure is adapted from (Cabodi et al., 2010a).

The following phosphorylation of the p130Cas adaptor protein that has multiple protein-protein interaction domains including an SH3 domain, a large tyrosine kinase substrate binding domain (SD) and a Src binding domain (SBD), can result in the formation of the p130Cas-Src-FAK complex (Cabodi et al., 2010a). This complex mediates the integration of Src/FAK signaling with multiple signaling pathways such as PI3K/AKT and Ras/ERK producing the high density network of cross-talk. Moreover, p130Cas-Src-FAK complex is able to couple RTK signaling to integrin signaling (Sieg et al., 2000) (figure 1.7). The relevance of such signaling integration by the p130Cas protein was illustrated in the preclinical studies suggesting that p130Cas/ ERBB2-transformed cells facilitate invasive properties and strengthening PI3K/AKT and ERK/mTOR/S6K signaling (Cabodi et al., 2010b; Tornillo et al., 2011). The latter in turn cause increased MMP9 secretion whereas PI3K/AKT promoted RAC1 signaling. Thus, Src/FAK signaling pathway serves as a platform integrating multiple extracellular signals with diverse downstream signaling pathways that are able to control various aspects of cell behavior (figure 1.7). This example vividly illustrates one of the difficulties in studying basic principles of signal transduction which is originated in the high interconnectivity of the network, where many pathways come together to induce distinct cellular responses.

1.3.1.5 Mechanisms of signaling pathway cross-talk

RTKs are able to activate multiple signaling pathways that, in turn, intertwine together forming a densely interconnected network. Describing specific pathways I have partially demonstrated the complexity of this signaling machinery by illustrating cross-talk between distinct pathways. Pathways are able to antagonize, enhance, or complement each other leading to synergistic, additive or inhibitory effects. These signaling principles allow context-dependent changing the nature of responses to a stimulus, encoding vast variety of cellular responses with relatively few signaling pathways and, most importantly, adapting to an external and an internal perturbation. The latter is often an inevitable obstacle in drug efficacy of the targeted therapeutics for cancer patients (Pazarentzos and Bivona, 2015). Understanding basic principles of signal transduction and operation of signaling machinery at the system level will help to develop new therapeutic strategies for the disease prevention or intervention. In this chapter, I would like to introduce general regulatory mechanisms used by cells to integrate several pathways employed downstream of activated RTKs.

In the past two decades many mechanisms and modes of cross-talk have been discovered. An abstract view on these seemingly diverse and complex regulatory mechanisms leads to highlighting common patterns achieving particular functions and properties (Alon, 2007; Buchler et al., 2003; Kolch et al., 2015; Sneppen et al., 2010). These patterns can be separated into regulatory functional units (or motifs, see figure 1.8) such as feedback and feedforward loops and serve as elemental building blocks to integrate information not only within a pathway but also between distinct pathways.

One of the common regulatory units of biochemical networks is a feedback loop that can be both positive OR negative. A negative feedback loop was illustrated within the Ras/MAPK signaling pathways (1.3.1.1) when phosphorylation and deactivation of Raf by ERK limits the duration of ERK activity in response to the RTK stimulation. The negative feedback loop presents important properties to signaling networks such as the filtering and smoothing out fluctuations generated by the varying input strength or the stochastic activation of upstream signaling (Fritsche-Guenther et al., 2011; Sauro and Kholodenko, 2004). The positive feedback loop is involved in

PKC regulation through the indirect activation of PLA₂ by ERK leading to the increased production of arachidonic acid (AA). In turn, AA and DAG together are able to facilitate the activity of PKC resulting in the prolonged activation of ERK. Such positive-feedback loop can function as a bistable system allowing to switch from inactive to a constitutively active state.

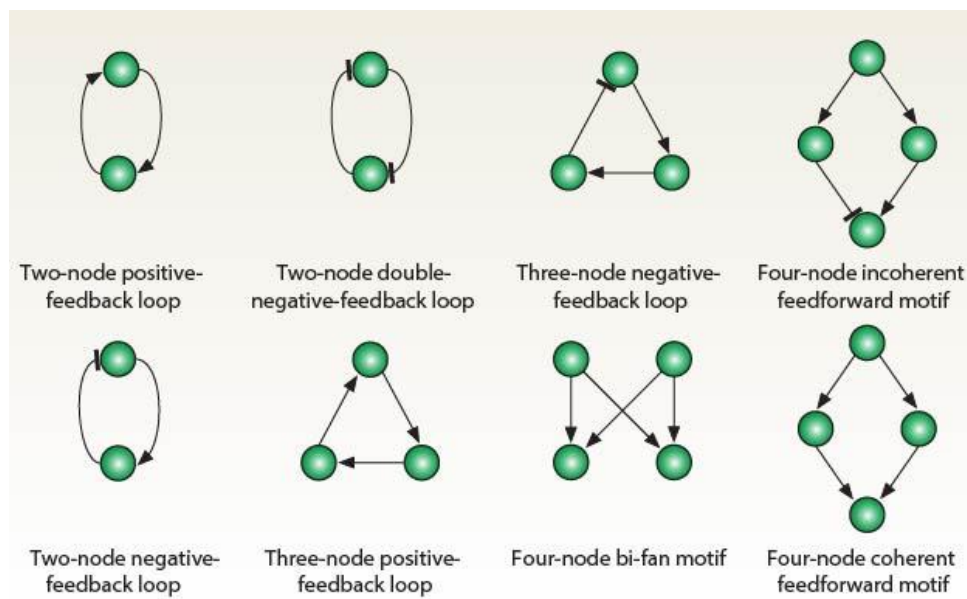


Figure 1.8 Schematic representation of motifs featured in biological networks. Figure is adapted from (Azeloglu and Iyengar, 2015).

A cross-inhibition mechanism involves the component of one signaling pathway that negatively regulates the upstream component of another pathway inhibiting its activity. A good example is the signal from the MAP kinase ERK that phosphorylates Grb2-associated binder1 (Gab1) and subsequently inhibits recruitment of PI3K to the EGF receptor (Lehr et al., 2004; Yu et al., 2002). The similar mechanism of pathway cross-inhibition is also induced by IGF-1 stimulation. In this case, AKT negatively regulates ERK activity by phosphorylating inhibitory sites in RAF (Guan et al., 2000; Zimmermann and Moelling, 1999). It was shown that cross-inhibition mechanism might be involved in emerging resistance to the target therapy indicating therapeutic relevance in the clinics.

Cross-activation is another cross-talk mechanism found in signaling networks. In this case the signaling molecule of one pathway regulates the activity of the upstream component of another

pathway, facilitating its activity. It was, for example, shown that Ras is able to potentiate the activity of PI3K by direct binding (Rodriguez-Viciano et al., 1994). As mentioned in 1.3.1.2, TSC2 that integrates information from different growth factors, stress as well as metabolic signals, is a heavily phosphorylated protein. The strong activation of ERK and RSK upon stimulation with EGF leads to phosphorylation of TSC2 inhibiting the GAP function of the TSC1-TSC-TBC1D7 complex. The latter increases the activity of mTORC1, another example of the cross-activation (Ma et al., 2005). Moreover, ERK and RSK are able to directly phosphorylate Raptor, the component of mTOR complex 1, and promote the phosphorylation of 4E-BP by mTORC1 (Carriere et al., 2011). Thus, a crosstalk between two distinct pathways employs negative as well as positive regulation, illustrating the complexity of signaling interaction modes.

A wide variety of signaling pathways can often positively or negatively act on the same protein or complex that is called pathway convergence. A good example is the c-Myc transcription factor accumulation that is regulated by Ras/ERK and PI3K/mTOR pathways independently. While ERK stabilizes c-Myc via its phosphorylation on Ser62 (Sears et al., 2000), RSK and S6K phosphorylate Mad1, a repressor of c-Myc, facilitating its degradation (Zhu et al., 2008). Mad1 degradation results in the c-Myc-Max dimerization and the initiation of survival transcriptional programs (Mendoza et al., 2011). The transcription factor FOXO is another crucial hub of pathway convergence. ERK-mediated phosphorylation of FOXO3A induces its degradation. FOXO1 and FOXO3A can also be phosphorylated by AKT. Phosphorylation induced association with 14-3-3 proteins sequester FOXOs in the cytosol preventing the induction of pro-survival gene expression.

The experimental observation that the same signaling molecules are able to participate in distinct pathways raises broad questions: what are the molecular mechanisms that couple components from different pathways. Although it is just the beginning of a long journey, a common mechanism was identified across many signaling pathways (Good et al., 2011; Langeberg and Scott, 2015; Zheng et al., 2013). For example, cells have evolved a clever mechanism to bring components of different signaling pathways in close proximity using scaffold proteins that compose of multiple distinct domains. The modular structure of the scaffold proteins allows the

interaction with multiple signaling components and shaping signaling network architecture on the molecular level. Bringing distinct signaling components to close proximity determines the specificity of information flow within intracellular networks. As mentioned in 1.3.1.1 and 1.3.1.4 chapters, the examples of scaffold proteins are KSR and p130Cas that coordinates MAPK pathway and couples Src/FAK signaling with other pathways in mammals, respectively (Cabodi et al., 2010a; Therrien et al., 1996). In general, scaffold proteins are able to regulate subcellular pathway activation (Brennan et al., 2002; Garrenton et al., 2006), provide additional means to control pathway activity by competing with distinct inputs of different functionality (Patterson et al., 2010) and efficiently promote downstream signaling (Good et al., 2009). Importantly, scaffold proteins can also coordinate negative and positive feedback loops shaping downstream responses (chapter 1.1.3.1). Overall, those functions can be tuned by inputs directly modifying scaffold proteins that often make scaffold proteins a direct target for pathway activity regulation. Thus, scaffold proteins increase plasticity of the signaling network that allows encoding wide range of cellular responses by the relatively limited number of signaling components.

1.3.2 Spatiotemporal control of signaling activity

Cellular signaling networks are able to transmit information through the temporal dynamics of network components that is described by the signal delay, the frequency, the fold change, the amplitude and the duration. The first attention has been given to distinct dynamics of ERK emerging after stimulation with separate growth factors. For example, epidermal growth factor (EGF) induces transient ERK activation resulting in the proliferation of PC12 cells whereas nerve growth factor (NGF) stimulation induced sustained ERK activation causing cell differentiation (Heasley and Johnson, 1992; Nguyen et al., 1993). These observations spiked subsequent extensive work linking the signaling molecule dynamics to the identity of an upstream stimulus and cellular outcomes in distinct cell types (McCawley et al., 1999; Nagashima et al., 2007).

To a big surprise for a scientific community, it was shown that single cells within a cellular population respond with high heterogeneity. The measurement of signaling activity at the population level may mask the real single-cell patterns due to averaging (Ferrell and Machleder, 1998). Modern technologies including optogenetics and biosensors allowing the manipulation of

signaling activity and the instantaneous measurement of cellular response at the single cell level facilitated numerous studies that are focused on whether signaling dynamics is driving cellular responses. The use of a FRET biosensor enables monitoring ERK activity at the single live cell level. A recent study has demonstrated that different EGF concentrations are able to modulate the frequency and duration of ERK activity pulses in MCF-10A cells (Albeck et al., 2013). At the same time it was illustrated that oscillatory ERK activity resulted in a greater proliferative response than continuous ERK signaling (Aoki et al., 2013). Although single-cell responses are highly heterogeneous (Frechin et al., 2015; Hiratsuka et al., 2015; Kumagai et al., 2015), it was demonstrated that the dynamic nature of the ERK, Ca^{2+} and nuclear factor kappa-light-chain-enhancer of activated B cells (NF- κ B) signaling provided high fidelity of information processing in an individual cell (Selimkhanov et al., 2014). By utilizing optogenetics, Toettcher et al. were

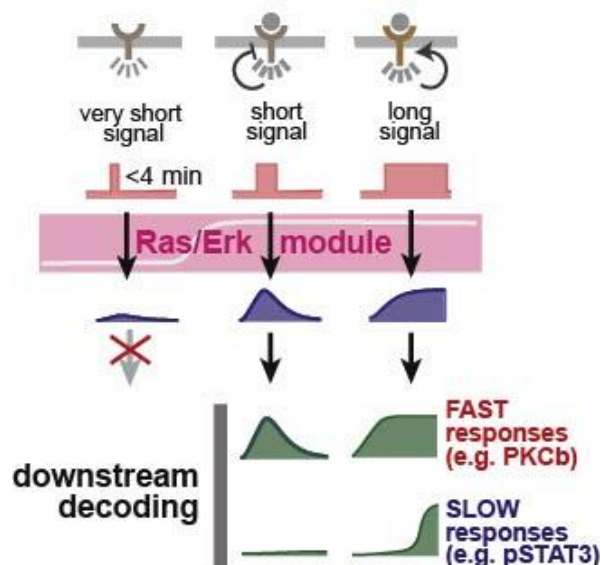


Figure 1.9 Schematic representation of signaling dynamics processing by Ras/ERK module. Figure is adapted from (Toettcher et al., 2013).

able to selectively control ERK activity and dissect the role of its frequency modulation in signaling (Toettcher et al., 2013). They proved that the ERK signaling pathway has properties of a low-pass, high-bandwidth filter that can transmit a broad range of signals, with the exception of high-frequency responses (Figure 1.9). By combining optogenetics with reverse phase protein arrays they were able to identify downstream effectors sensing different ERK dynamics. Overall, it was extensively shown that temporal dynamics are able to specify different cellular responses such as differentiation, proliferation and migration. Moreover, complex signaling dynamics

including oscillations and pulses can increase the accuracy of information propagation through signaling networks.

The dynamic features of cellular networks are principally determined by the connectivity of signaling components along and/or between distinct pathways (chapter 1.3.1). Exploiting modular response analysis, it was demonstrated that EGF and NGF shape the topology of the signaling network to induce distinct temporal patterns of ERK activity in PC12 cells (Santos et al., 2007). The EGF stimulation induces negative feedback attenuating ERK signaling, whereas NGF elicits positive feedback potentiating ERK activity. The decoding of complex temporal patterns is also based on the network motifs (chapter 1.3.1.5) that are able to sense the dynamic change of an up-stream signal. For example, PC12 cells utilize a feedforward loop to distinguish transient and sustained ERK activity (Nakakuki et al., 2010). The transient ERK activation leads to the induction of immediate early gene (IEG) products expression including c-Fos and their rapid degradation. However, the sustained ERK activation in the cytoplasm induces direct c-Fos phosphorylation and its stabilization. Interestingly, the aforementioned two feedforward loops that interpret upstream signal duration are spatially separated and act in different cellular compartments: the fast nuclear arm induces transcription and slow cytosolic arm modulates protein degradation. Thus, the compartmentalized network topology not only programs the signaling patterns but also decodes signaling dynamics by downstream effectors.

In many cases, the concentration of extracellular cues that cells are exposed to such as insulin is highly dynamic. Therefore, Kubota et. al. were puzzled by how a signaling network encodes and processes the dynamics of extracellular cues. They showed that temporal patterns of insulin stimulation are encoded by AKT dynamics (Kubota et al., 2012). The later employing network motifs can induce distinct activation of downstream effectors such as glycogen synthase kinase-3 β (GSK3 β), glucose-6-phosphatase (G6Pase) and ribosomal protein S6 kinase (S6K) that regulates different cellular processes. For example, an incoherent feedforward loop enable S6K to adapt to the level of insulin assuring transient response upon change of insulin concentration whereas direct activation of GSK3 β by AKT lead the detection of sustained insulin stimulation. Thus, their study provides an example of how dynamics of a ligand concentration can be encoded and decoded by signaling network topology.

With the development of new technologies it becomes obvious that signaling pathways form a highly dynamic and interconnected network transmitting information from an ocean of extracellular cues. In fact, recent studies have demonstrated that the spatio-temporal organization of signaling network architecture regulates specific cellular responses (Housden and Perrimon, 2014; Nakakuki et al., 2010). Although the majority of signaling network studies illustrates the biological relevance of the signaling dynamics, the molecular mechanisms that encode and decode this dynamics still remain unclear. A better understanding of these mechanisms will allow manipulating key parameters in a highly controlled way and therefore stimulate the development of new pharmacological approaches. Therefore, further studies are needed to elucidate basic principles of signaling networks operation.

1.4 RTKs cross-talk as an additional level of signaling complexity

RTKs using largely overlapping downstream effectors to transmit information can often have distinct physiological functions. Although individual RTK signaling networks have been characterized in detail, the understanding how cells, using the limited number of signaling components, integrate and process information from many external cues is one of the major challenges of cell biology. The information from multiple RTKs is integrated at different signaling levels: physical interaction between different receptors, downstream pathways cross-talk or transcriptional regulation.

One of the well-studied mechanisms of RTKs cross-talk occurs at the level of receptors that involves physical interaction between different RTK and transactivation by downstream effectors. The direct dimerization of EGFR with ErbB-3, for instance, facilitates the signaling through PI3K/AKT pathway (Olayioye et al., 2000), whereas, EGFR interaction with ErbB-2 potentiates MAPK signaling (Karunagaran et al., 1996). Moreover, RTK heterodimerization can occur not only within one but also between members of different protein families. For example, IGF-1R can result in the activation of EGFR (Ahmad et al., 2004) or ErbB-2 (Balana et al., 2001) through physical interaction. It was also demonstrated that Src, downstream effectors of IGF-1R, can transactivate EGFR in MCF-7-derived tamoxifen-resistant breast cancer cells

(Knowlden et al., 2005) illustrating cross-activation via downstream signaling. These examples support a very attractive concept that explains the additional mechanism of signaling diversification based on RTK trans-activation. Importantly, the RTK transactivation has been suggested as one of the mechanisms of drug-resistance in cancer cells (Kim et al., 2016).

An entirely different mechanism of RTK cross-talk is mediated by downstream effectors without affecting receptors themselves. This type of the interplay between RTKs can lead to unpredicted signaling behavior such as synergistic and antagonistic responses that are regulated by network topology (Volinsky and Kholodenko, 2013). Mathematical modeling proposed the mechanism of the synergistic ERK activation by EGF and insulin in HEK293 cells (Borisov et al., 2009). This study showed that EGFR and insulin signaling is linked by GRB2-associated binding protein (GAB). The insulin stimulation activates the production of PIP3 on the plasma membrane that in turn facilitates GAB1 translocation. Active EGFR stimulates GAB1 phosphorylation thereby recruiting multiple signaling molecules including PI3K, Grb2/SOS and SH2 domain-containing tyrosine phosphatase 2 (SHP2). In turn, PI3K recruitment generates a positive feedback loop for GAB1 translocation whereas the translocation of Grb2/SOS and SH2 potentiates the ERK activation. At the same time, another study also showed that IGF-1 potentiates the ability of EGF to activate ERK whereas the AKT phosphorylation was decreased upon dual stimulation in comparison with “IGF-1 only” stimulation in PC12 cells (Martin et al., 2009). Moreover, they demonstrated that pairwise RTK activation can induce time dependent signaling interaction effects on network components, differential gene expression and, most importantly, physiological responses such as cell survival and neurotransmitter production that are not predictable from individual treatments (Martin et al., 2009).

The RTK receptor cross-talk can also occur via transcriptional induction of RTK or its signaling components by another RTK. For example, in breast cancer cells EGF treatment induces expression of insulin receptor substrate 1 and 2 (IRS1 and IRS2) that is diminished by the EGFR inhibitors (Cui et al., 2006). Another recent study revealed that blocking MEK signaling in triple negative breast cancer cells in which poor prognosis is often characterized by EGFR and c-Met phosphorylation, induced expression and activation of multiple RTKs including PDGFR β , VEGFR2, and HER2/3 (Duncan et al., 2012). Moreover, this study showed that activation of the

RTKs is accompanied with increased expression of cytokines establishing positive paracrine/autocrine loops. In neuroblastoma cells lines, retinoic-induced activation of the RTK Ret leads to the increased expression of tropomyosin receptor kinase B (TrkB), an RTK, and its ligand brain derived neurotrophic factor (BDNF) (Esposito et al., 2008). Importantly, the knockdown of TrkB or ret proto-oncogene (Ret) by siRNAs impairs differentiation in neuroblastoma cells indicating an important role of TrkB/Ret cross-talk in this process. Overall, these examples reveal the clinical relevance of the RTK cross-talk at the transcription level.

In conclusion, the comprehensive understanding of the basic principles of RTK signaling and the mechanisms of a complex RTK cross-talk is of major interest for fundamental and translational research. Recent discoveries revealed underappreciated complexity of the cellular signaling machinery that could be addressed only after the evolution of currently available experimental and computational tools enabling to study this complexity at the different regulatory levels and, most importantly, to link those levels of complexity in a single concept.

1.5 Biosensors are useful tools for studying intracellular signaling in living cells

Ideally, to study basic principles of the signaling network operation one would like to follow the localization, concentration and activity of the investigated signaling molecules in living cells with high accuracy and temporal resolution. Fluorescence microscopy of genetically encoded sensors (or biosensors) effectively satisfies these stringent requirements as an experimental approach. Typically, biosensors are composed of a sensing element that is associated with a reporting unit (Bolbat and Schultz, 2017; Newman et al., 2011). The sensing unit communicates the change of interest and can comprise of the whole protein or specific protein domain as well as the synthetic peptide sequence (Oldach and Zhang, 2014). Two or more components such as protein domains and synthetic peptide sequences are often used to engineer a modular sensing unit.

1.5.1 Fluorescent proteins as a reporting unit in biosensors

Fluorescent proteins (FPs) are typically used as the reporting unit in biosensors. Over the past 20 years a wide variety of FPs have been isolated from different biological species and optimized by introducing specific mutation in the protein to improve their photophysical properties such as brightness, contrast, photostability and spectral characteristics. The development of FPs with diverse spectral characteristics that are described by wavelengths of the excitation and emission resulted in multiplexing imaging (imaging several FPs). For example, cyan (Goedhart et al., 2012), green (Shaner et al., 2013), red (Bajar et al., 2016) and near-infrared (Shcherbakova and Verkhusha, 2013) were recently developed with improved optical properties. Moreover, FPs with specialized optical characteristics such as large Stokes shifts that are highly desirable for multiplexing were also developed and utilized for dual FRET sensor imaging (Shcherbakova et al., 2012). Although researchers now have access to the large repertoire of FPs that meets diverse needs of experimental setup limitations of the FPs have been discovered by the long-term imaging and targeting subcellular compartments. For instance, it was shown that red FPs often tend to accumulate in lysosomal compartments, probably due to resistance to proteases (Costantini et al., 2015; Katayama et al., 2008). The dimerization or oligomerization of FPs fused to the protein of interest is another caveat that one should be cautious about. It was shown that FPs initially characterized as monomeric have residual tendency to oligomerize when fused with membrane proteins (Cranfill et al., 2016). Finally, thermodynamic stability such as the formation of intermolecular disulfide bonds is a crucial FP characteristic that may influence oligomeric state as well as chromophore establishment (Costantini et al., 2015). The wide range of FPs led to developing biosensors of diverse operating principles and design that can at least be divided into the two largest groups: single-fluorescent-protein- and fluorescence resonance energy transfer (FRET)-based biosensors.

1.5.2 Single-fluorescent-protein-based biosensors

The simplest single-fluorescent-protein-biosensor is a translocation reporter that consists of fusion of protein or protein domain of interest with a FP. Fluorescently labeled ERK (Cohen-

Saidon et al., 2009) and FOXO3A (Zanella et al., 2008), for example, were used to monitor activity of upstream signaling pathways by quantifying their distribution between cytoplasm and nucleus. Alternatively, a biosensor can be engineered by fusion of FP with a protein domain specifically binding to the molecule of interest. This strategy is typically exploited to measure the lipid concentration at cellular membranes. However, one should employ this approach cautiously due to the failure of particular domains to recognize respective lipids at the organelles or plasma membrane (PM). For instance, PI(3,4,5)P3 and DAG on the PM can be observed by the PH domain of AKT (Laketa et al., 2014) and the C1 domain of PKC- γ (Wilke et al., 2014), respectively. The production of PI(3,4,5)P3 and DAG on the PM induces translocation of those sensors and can be measured as an increase in the fluorescence intensity.

Another strategy to generate single-fluorescent-protein-biosensors involves complex protein engineering that exploits the photophysical properties of FPs. The majority of biosensors of this kind was based on the fact that FPs can tolerate certain structural modifications such as insertions of proteins or engineered sequence and still remain fluorescent (Baird et al., 1999). Importantly, the conformational change of the insertion strongly modulates optical characteristics of the FP including fluorescence intensity. This strategy was successfully used in the development of the Ca²⁺ (Chen et al., 2013; Inoue et al., 2015), hydrogen peroxide (Ermakova et al., 2014), ATP (Tantama et al., 2013), NADH (Hung et al., 2011), cAMP (Odaka et al., 2014), and DAG (Tewson et al., 2012) biosensors. Surprisingly, some FPs split into several fragments are able to restore the structure of β -barrel and become fluorescent due to sufficient affinity of the fragments. A method that is called bimolecular fluorescence complementation (BiFC) is based on this unique principle and has been extensively used to monitor protein-protein interactions (Kodama and Hu, 2012). In this case the stimulus induced dimerization of the proteins or sensing elements fused with fragments of a FP lead to the assembly of the β -barrel and appearance of fluorescence.

1.5.3 Fluorescence resonance energy transfer-based biosensors

The largest family of biosensors are based on the principle of fluorescence resonance energy transfer (FRET), a phenomenon that was first described in 1948 (Förster, 1948). FRET is the mechanism of energy transfer from a donor fluorophore to an acceptor fluorophore via non-

radiative dipole-dipole coupling occurring in close proximity to each other (<10 nm). Another requirement for efficient energy transfer is the sufficient overlap of the emission donor spectra with the excitation (or absorption) acceptor spectra. FRET efficiency is extremely sensitive to the relative orientation of fluorophore dipoles as well as to the distance between fluorophores that makes it ideal to visualize protein-protein binding as well as changes in the protein conformation (Bolbat and Schultz, 2017).

One of the typical FRET biosensor designs is generated by placing a protein domain or engineered molecular switch that undergoes conformational change upon binding to a specific ligand or enzymatic modification between a pair of fluorescent proteins that exhibits FRET (unimolecular FRET biosensors). These sensors are expressed as a single protein containing all parts of the sensor: a donor, an acceptor and a molecular switch. For example, the molecular switch of biosensors measuring the activity of protein kinases and phosphatases is composed of two parts that are linked together: a kinase-specific substrate and phosphoamino-acid-binding domain (PAABD). The kinase-specific substrate phosphorylation by an activated kinase induces the interaction between substrate and PAABD and leads to the conformational change. The resulting conformational rearrangement in the sensing unit then produces a substantial changes in FRET. This design was employed to develop FRET biosensors for monitoring activity of numerous protein kinases including ERK (Harvey et al., 2008), PKA (Depry et al., 2011), PKC (Schleifenbaum et al., 2004), AKT (Miura et al., 2014), RSK (Komatsu et al., 2011), and many others. The modular architecture of FRET biosensors allows developing biosensors to measure not only the activity of protein kinases but also the activity of other enzymes and a variety of signalling process. Using the rationally designed switches led to the development of several biosensors measuring the activation of small G-proteins such as Ras (Mochizuki et al., 2001), Rac1 (Itoh et al., 2002), RhoA (Yoshizaki et al., 2003) by fusion the small G-protein of interest with effector domain that specifically recognizes active (GTP-bound) form of the small GTPase. Moreover, the similar modular architecture was employed to monitor dynamics of diverse range of post translational modifications including methylation (Lin et al., 2004), acetylation (Sasaki et al., 2009) and O-GlcNAcylation (Carrillo et al., 2006). More recently, Nakaoka et. al. have developed the sensor to detect histone 3 acetylation at the Lys 9 and Lys 14 (Nakaoka et al., 2016). Thus, the rational design of modular molecular switches that undergo a substantial

conformational rearrangement will further broaden the spectrum of biosensors monitoring diverse biological processes and reactions including protein-protein interaction, the concentration of second messengers, post-transcriptional modifications and protein activities in living cells.

Another way to engineer FRET biosensor is dividing FRET sensor into two separately expressed protein chains. Each part of such bimolecular FRET biosensor contains either donor or acceptor. Typically this approach is used for monitoring protein-protein interactions whereas bimolecular FRET sensors are useful to visualize a protein conformational change. However, additional differences between these designs have to be taken in consideration prior to the development and the use of a FRET biosensor (Miyawaki, 2011). Although bimolecular FRET biosensors have higher FRET change they are prone to the signal damping due to disruption of 1(donor):1(acceptor) ratio and undesired interaction of biosensor's parts with native cellular proteins (Miyawaki and Niino, 2015). In contrast, unimolecular FRET sensors are less apt to interact with native cellular proteins and assumed to have constant donor:acceptor ratio (1:1) resulting in a reliable signal (Miyawaki and Niino, 2015). Thus the use of unimolecular FRET biosensors is mostly restricted by the labour intensive optimization of the biosensor architecture and the low response.

Overall, biosensors provide a unique ability to monitor diverse signaling events with high spatio-temporal resolution in living cells which is of great relevance for basic and clinical research. Although the dozens of biosensors were developed only a minor portion of them is used in clinical and fundamental studies due to both labour and time intensive imaging. The further development of novel approaches allowing high-throughput biosensor imaging will accelerate studies of basic principles of signal transduction.

Aim of the thesis

Due to the complexity of an intracellular signaling network, discussed in the introduction, it is not well known how cells dynamically interpret information from multiple extracellular cues. It was earlier proposed that the plausible mechanism of signal integration is through signaling interactions such as additivity, synergy and antagonism among pathways (Borisov et al., 2009; Hsueh et al., 2009; Natarajan et al., 2006). We therefore hypothesized that cells encode signals from multiple extracellular cues through dynamics of signaling network activity and finally decode this information into cell fate decisions. Thus, the aim of this thesis is to identify potential mechanisms of signal integration and processing from multiple cues in living cells that is a physiologically relevant scenario.

In order to unravel the mechanisms underlying the signal integration from multiple cues it is crucial to be able monitoring multiple signaling pathways in living cells. FRET biosensors provide an elegant, non-invasive method to monitor different signaling events with high spatial and temporal precision, permitting the study of many signaling pathways such as Ras/ERK and PI3K/AKT/S6K pathways. However, FRET biosensor imaging is a labor intensive procedure per se. In the first part of the thesis, I therefore will establish the platform allowing imaging of hundreds FRET biosensors in a single experiment. This platform will be proved to be useful to monitor growth factor and lipid signaling as well as its perturbation by functional mutations or therapeutically relevant inhibitors in living cells.

Using the above mentioned high-throughput platform, further insights into mechanisms of signal integration from multiple cues in living cells are expected. To this end, I will focus on the signaling interactions between receptor tyrosine kinases as they signal through shared set of pathways yet can have distinct biological functions *in vivo*. In particular, we will directly compare a single stimulus with their pairwise combinations to reveal signaling interactions at the system level that are difficult to predict from a single treatment. This comprehensive map of dynamic signaling interactions between multiple growth factors and cytokines will help to further explore how gene expression profile depends on the concentration and the ratio of extracellular cues.

Chapter 2 – Experimental methods

2.1 Materials

EGF, TGF- α , IGF-1, PFGF-BB, TNF- α , Trypsin-EDTA and BSA were obtained from Sigma. MEM, fetal calf serum (FBS, Cat.-No. F7524), puromycin, glycerol, Laemmli sample buffer and gelatin from bovine skin were also supplied by Sigma. HGF, Wnt-5A and Gas6 were purchased from R&D systems. The ERK inhibitor (AZD6244, Selumetinib) and PI3K (PI-103) inhibitor were obtained from Selleck Chemicals. DMSO was obtained purchased from Merck KGaA. The β -tubulin (9F3, rabbit), phospho-Erk1/2 (Thr202/Tyr204) antibody, ERK1/2 antibody, phospho-Akt (Ser473) antibody, AKT (pan, 40D4) antibody, anti-rabbit IgG antibody anti-mouse IgG antibody, DRAQ5 and RIPA buffer (10x) were ordered from Cell Signaling Technology. The cOmplete inhibitor cocktail was supplied by Roche. Primocin were purchased from InvivoGen. Lipofectamine 2000, Lipofectamine 3000, L-glutamine and Penicillin Streptomycin (Pen Strep) were supplied by invitrogen. The FuGENE HD transfection reagent was obtained from Promega. The K2, Effectene, ScreenFect A, GenJet and PeqFECT transfection reagents were supplied by BionTex, Qiagen, InCella, SIGnaGen and Peqlab, respectively. The low glucose DMEM was purchased from Life Technologies. The high glucose DMEM with and without phenol red was supplied by Lonza. Sucrose ultrapure was obtained from Affymetrix. The NuPAGE MES SDS running buffer was purchased from Novagen.

Table 2.1: *FRET biosensors used in this work*

Target	Local ization	Provided by	Proteins/protein domains	Named in this work	Ref
ERK	Cyto	Matsuda laboratory	WW (phosphopeptide binding domain)-Substrate domain (PDVPRTPVDKAKLSFQFP)	ERK	(Komat su et al., 2011)
ERK	Cyto	Pertz laboratory	WW (phosphopeptide binding domain) - Substrate domain (PDVPRTPVDKAKLSFQFP)	ERK2G1	(Fritz et al., 2013)
RhoA	Cyto	Pertz laboratory	RhoA-binding domain (RBD) of rhotekin)– RhoA	RhoA2G1	(Fritz et al., 2013)
Ras	PM	Matsuda laboratory	H-Ras domain RafRBD – Ras- binding domain of Raf 1	Ras	(Komat su et al., 2011)
Rac1	PM	Matsuda laboratory	PAK CRIB domain - Cdc42/Rac- interactive binding Rac1 K-Ras CT domain – targeting to plasma membrane	Rac	(Komat su et al., 2011)
RSK	Cyto	Matsuda laboratory	FHA1 domain (phosphopeptide binding Ser-1798 of TSC2) - Substrate domain (GQRKRLITSVDDFTE) NES	RSK	(Komat su et al., 2011)
S6K	Cyto	Matsuda laboratory	FHA1 domain (phosphopeptide binding Thr-1135 of Rictor) - Substrate domain (NRRIRTLTEPDVDFN) NES	S6K	(Komat su et al., 2011)
Akt	Cyto	Matsuda laboratory	Akt PH domain - FHA1 domain (phosphopeptide binding) - Substrate domain (RKRDRLGTLGD) Akt substrate NES	Akt	(Komat su et al., 2011)
PKC	Cyto	Matsuda laboratory	PKC β C1 domain - FHA1 domain (phosphopeptide binding) - Substrate domain (KKKKKRFTFKDSFKL) NES	PKC EV	(Komat su et al., 2011)

JNK	Cyto	Matsuda laboratory	FHA1-EV- Substrate domain (DSVKTPEDEGNPLLEQLEKK)	JNK	(Komatsu et al., 2011)
EGFR/abl	Cyto	Matsuda laboratory	CrkII-SH2-SH3 domain-217–225 residues of CrkII (EPGPYAQPS)	EGFR	(Komatsu et al., 2011)
PIP3/P I(3,4)P₂	Cyto PM	Matsuda laboratory	PH AKT -pseudoligand	PIP3	(Ananthanarayanan et al., 2005)
Src	Cyto	Wang laboratory	CFP-SH2 (Src)- Substrate (synthetic)	Src	(Ouyang et al., 2008)
Cdc42	PM	Matsuda laboratory	PAK1-Cdc42 (EV linker was cloned in between PAK1 and Cdc42)	Cdc42	(Itoh et al., 2002)
PAK1	PM Cyto	Parrini laboratory	human PAK1, Pakabix carries the C-terminal region of Ki-Ras4B	PAK (PM) PAK	(Parrini et al., 2009)
Calcineurin	Cyto	Zhang laboratory	domain of NFAT1	Calcineurin	(Newman and Zhang, 2008)
FAK	Cyto	Wang laboratory	SH2(c-Srk) -substrate	FAK	(Seong et al., 2011)
cRaf	Cyto	Matsuda laboratory	cRaf	cRaf	(Terai and Matsuda, 2005)
bRaf	Cyto	Matsuda laboratory	bRaf	bRaf	(Terai and Matsuda, 2006)
Histone H3-K9 methyl	Cyto	Ting laboratory	HP1 Chromodomain-histone H3	Histone K9 Me	(Lin et al., 2004)

ation					
Histon e H3- K27 methyl ation	Cyto	Ting laboratory	Polycomb (Pc) Chromodomain- histone H3	Histone K27 Me	(Lin et al., 2004)
Histon e H3- S28 phosph orylati on	Nuc	Ting laboratory	14-3-3t – 615-644 residues of Cbl	Histone P	(Lin and Ting, 2004)
Cdk1	Cyto	Pines laboratory	Polo-Box Domain of Plk1-(GGT)5 linker-Cyclin B1 containing the Ser126 autophosphorylation site	Cdk1	(Gavet and Pines, 2010)
PDK1	PM	Zhang laboratory	PDK1	PDK1	(Gao et al., 2011)
Caspas e-3	Cyto	Sorger laboratory	DEVDR	Caspase-3	(Albeck et al., 2008)
Caspas e-8/10	Cyto	Sorger laboratory	IETD2x	Caspase- 8/10	(Albeck et al., 2008)
PKA	Cyto	Matsuda laboratory	FHA1 domain - PKA substrate (LRRATLVD) - NES	PKA	(Komat su et al., 2011)
PKC	ER	Newton laboratory	FHA2 (Rad53P)-Substrate(synthetic)	PKC (ER)	(Violin et al., 2003)
Rap1	PM	Matsuda laboratory	Rap1A-Raf	Rap1	(Mochi zuki et al., 2001)
RalA	PM	Matsuda laboratory	RalA-RalBP1	RalA	(Takay a et al., 2004)
RhoA	PM	Matsuda laboratory	PKN -RhoA	RhoA	(Yoshiz aki et al., 2003)

Ca²⁺	Cyto	Griesbeck laboratory	chicken skeletal muscle TnC	Ca ²⁺ (TNXL)	(Mank et al., 2006)
CaMK II	Cyto	Schultz laboratory	CaMK2 α	Ca ²⁺	(Piljic et al., 2011)
Ca²⁺	Cyto	Griesbeck laboratory	TnC domain	Ca ²⁺ (Twitch)	(Thestrup et al., 2014)
Pickles	Cyto	Ohba laboratory	CrkL	Abl	(Mizutani et al., 2010)
Aurora B	Nuc Cyto Cent	Lampson laboratory	FHA2-substrate(Kif2 57-70)	Aurora B H2B Aurora B Aurora B centro	(Fuller et al., 2008)
Contro l	Cyto	Vogel laboratory	32 amino acids linker	control	(Koushik et al., 2006)
Contro l 2	Cyto	Sorger laboratory	DEVDR mutated to DEVG	DEVG	(Albeck et al., 2008)
Pyruvate	Cyto	Barros laboratory	PdhR protein	Pyruvate	(San Martin et al., 2014)
Glucose	Cyto	Frommer laboratory	Glucose binding domain of MglB protein	Glucose	(Takanaga et al., 2008)
AMPK	PM	Inoue laboratory	FHA (phosphopeptide binding domain)-Substrate domain (GSGEGSTKMRRVATLVDLGTG GSEL)	AMPK	(Miyamoto et al., 2015)
Lactate	Cyto	Barros laboratory	LldR transcription factor from <i>E. coli</i>	Lactate	(San Martin et al.,

					2013)
Zn²⁺	Cyto	Merkx laboratory	Metal binding domains (Atox1 and domain 4 of ATP7B (WD4))	Zn ²⁺	()
DAG	PM	Schultz laboratory	C1B β domain of PKC	DAG	unpubli shed

Abbreviations: Cyto – Cytosole, PM – Plasma Membrane, Cent – Centromere, Nuc - Nucleus

2.2 Buffers and Media

2.2.1 Western Blot Buffers

2x Laemmli buffer

- 4% SDS
- 10% β -mercaptoethanol
- 190 mM glycine
- 20% (v/v) glycerol
- 0.004 % (v/v)

Once prepared, 2x Laemmli buffer was stored at -20 °C.

Transfer buffer

- 25 mM Tris-Cl
- 190 mM glycine
- 20% (v/v) methanol

The transfer buffer was prepared immediately prior use.

10x Tris-Buffered Saline

- 500 mM Tris-Cl
- 1500 mM NaCl

Afterwards, the pH was adjusted to 7.6 using HCl. Once prepared, TBST was stored at 4°C for 3 months.

Tris-Buffered Saline with Tween 20 buffer

TBS buffer supplemented with 0.1% Tween-20. Once prepared, TBST was stored at 4°C for one week.

2.2.2 Bacterial Culture media

LB medium

Autoclaved Luria-Bertani (LB) medium was prepared by the media kitchen at EMBL according to following composition and stored at room temperature.

- 1 % (w/v) bacto trypton
- 0.5 % (w/v) bacto yeast extract
- 170 mM NaCl

Afterwards, the pH was adjusted to 7.6 using NaOH and the medium was supplemented with antibiotics (100 µg/mL ampicillin or 30 µg/mL kanamycin) immediately prior to use.

LB agarose plates

LB agarose plates were prepared by the media kitchen with 1.5 % (w/v) bacto agar in LB, supplemented with antibiotics (100 µg/mL ampicillin or 30 µg/mL kanamycin) and stored at 4 °C.

SOC medium

Super Optimal broth with Catabolite repression (SOC) medium was prepared by the media kitchen according to following composition, pH adjusted to 7.0, autoclaved and stored at 4°C.

- 20 mM glucose
- 10 mM MgCl₂
- 10 mM MgSO₄
- 2.5 mM KCl
- 10 mM NaCl

- 2 % (w/v) bactotryptone
- 0.5 % (w/v) bacto yeast extract

2.2.3 Eukaryotic cell media and solutions

PBS

- 137 mM NaCl
- 2.7 mM KCl
- 2 mM KH₂PO₄
- 10 mM Na₂PO₄
- 1 mM EDTA

PBS was prepared by the media kitchen at EMBL. It was adjusted to pH 7.4 using HCl and sterile filtered. PBS was stored at room temperature.

HeLa cell culture medium

- DMEM (1 g/L glucose, Gibco/Life Technologies)
- 10 % fetal calf serum (Sigma-Aldrich, Lot.-No. 032M3395/ Lot.-No. 014M3395)
- 1 % primocin (InvivoGen)

H838/H1975 cell culture medium

- DMEM (4.5 g/L glucose, Lonza)
- 10 % fetal calf serum (Gibco, Lot.-No. 41965-039)
- 1 % penicillin/streptomycin (Gibco/ Life Technologies)

Min6 cell culture medium

- DMEM (4.5 g/L glucose, w/o pyuvate, Lonza)
- 15 % fetal calf serum (Gibco, Lot.-No. 41965-039)
- 1 % penicillin/streptomycin (Gibco/ Life Technologies)
- 70 mM 2-mercaptoethanol (Pan)

C2BBe1 cell culture medium

- DMEM/F-12 (4.5 g/L glucose, w/o pyruvate, Gibco/ Life Technologies)
- 10 % fetal calf serum (Sigma-Aldrich, Lot.-No. 032M3395/ Lot.-No. 014M3395)
- 1 % penicillin/streptomycin (Gibco/ Life Technologies)

H838-EGFRmut (L858R and resistant T790M) cell culture medium

- DMEM (4.5 g/L glucose, w/o pyruvate, Lonza)
- 10 % fetal calf serum (Sigma-Aldrich, Lot.-No. 032M3395/ Lot.-No. 014M3395)
- 1 % penicillin/streptomycin (Gibco/ Life Technologies)
- 1.5 µg/ml Puromycin

All media were sterile filtered and stored at 4 °C.

2.2.4 Starvation media

HeLa cell starvation medium

- DMEM (1 g/L glucose, Gibco/Life Technologies)
- 1 % primocin (InvivoGen)

H838/H1975/H838-mutEGFR cell starvation medium

- DMEM (w/o phenol red, Lonza)
- Pen/Strep (dilute stock 1:100)
- 1 mg/ml BSA
- 2 mM L-Glutamin

C2BBe1 cell starvation medium

- DMEM (4.5 g/L glucose, Gibco/Life Technologies)
- 1 % penicillin/streptomycin (Gibco/ Life Technologies)

2.2.5 Imaging media and buffers

Cell imaging medium

- MEM (w/o phenol red, Sigma Aldrich)
- 30 mM HEPES

HEPES was added by the media kitchen according to the following concentration, pH adjusted to 7.4, autoclaved and stored at 4°C.

MIN6 cell imaging buffer

- 20 mM HEPES
- 115 mM NaCl
- 1.2 mM MgCl₂
- 1.2 mM K₂HPO₄
- 1.8 mM CaCl₂

The pH of the imaging buffer was adjusted to 7.4 using 1 M NaOH or 1 M HCl solution.

2.3 Cell culture

HeLa (human cervical adenocarcinoma cells, No. Kyoto)

Dr. Rainer Pepperkok (Advanced Light Microscopy Facility, EMBL, Heidelberg, Germany)

MIN6 (mouse pancreatic β -cells)

Dr. Jun-ichi Miyazaki (Department of Stem Cell Regulation Research, Graduate School of Medicine, Osaka University, Japan)

H838 (human lung adenocarcinoma cells derived from metastatic lymph node)

H1975 (human lung adenocarcinoma cells)

H838-mutEGFR (human lung adenocarcinoma cells derived from metastatic lymph node and exogenously expressed EGFR that carries the activating mutation L858R and the resistance mutation T790M)

Prof. Dr. Ursula Klingmueller (Department of Pharmacology, DKFZ, Germany)

C2BBe1 (human colorectal adenocarcinoma cells)

Dr Ultan McDermott (Cancer Genome Project, Wellcome Trust Sanger Institute, Hinxton, UK)

HeLa, H838, H1975, H838-mutEGFR and C2BBe1 cells were kept in appropriate growth medium in a humidified incubator at 37 °C with 5 % CO₂ and were passaged 2 – 3 times per week. Min6 cells were maintained in a humidified incubator at 37 °C with 8 % CO₂. For live-cell imaging experiments, cells were seeded in 8-well Labtek or Mattek dishes (Nunc/Thermo Scientific or Mattek, respectively) 48 h prior to the experiment.

2.4 Methods

2.4.1 Molecular work

Plasmid DNA extraction and concentration determination

Plasmid DNA was isolated from bacteria cultured overnight in LB medium supplemented with suitable antibiotic at 37°C and 230 rpm using the QIAprep Spin Miniprep Kit (Qiagen) or the QIAfilter Plasmid Maxi Kit (Qiagen), depending on the required amount and concentration, according to manufacturer's protocol. DNA concentration was determined by measuring absorption of ultraviolet light of a 260 nm wavelength using a spectrophotometer (Life Technologies, NanoDrop 8000). 1 absorbance unit of light at a wavelength of 260 nm corresponds to a concentration of 50 µg/mL for double-stranded DNA. The ratio of absorbance at 260 nm and 280 nm was used to assess the purity of DNA. The ratio of ~1.8 was accepted as “pure” for DNA. Plasmids for reverse transfection were isolated from *E. coli* using the QIAfilter Plasmid Maxi Kit and diluted to the concentration of 1 mg/mL.

Sequencing of DNA

DNA sequencing was performed by GATC Biotech (Konstanz, Germany).

E. coli transformation

One µg of plasmid DNA or 20 µl of a ligation reaction were added to 50 µl competent *E. coli* DH5α (Life Technologies, 18265-017). After 30 min incubation on ice, samples were heat-shocked at 42°C for 45 sec (Eppendorf, Thermomixer comfort) and then cooled down on ice for

2 min. Afterwards, 1000 µl of SOC medium was added to bacteria and samples were further incubated at 37°C and 500 rpm for 1 h (Eppendorf, Thermomixer comfort). Then cells were centrifuged for at 13000 rpm for 1 min and subsequently supernatant was discarded. The pellet were resuspended in 50 µl of SOC medium followed by plating on LB-agar plates supplemented with suitable antibiotic and overnight incubation at 37°C.

Agarose gel electrophoresis and gel extraction of DNA

DNA fragments after PCR or restriction reaction were mixed with loading dye (Thermo Scientific) and separated by electrophoresis in 1-1.5% (w/v) agarose (Lonza, 50004) gel supplemented with of Redsafe (Intron, 1:2000 dilution) in the TAE buffer (Life Technologies), applying 5 V/cm. DNA fragments were visualized with ultraviolet light on video-based gel documentation system (Intas, GEL Stick "Touch"). As standards for fragment size and DNA amount 100 base pairs (bp) or 1000 bp DNA ladder (Life Technologies, SM0323, SM0313) were used, depending on the expected size of the DNA fragments. When required, DNA fragments were extracted from agarose gels using a gel extraction kit (Qiagen, 28704) according to the manufacturer's protocol.

Molecular cloning

To construct specific plasmids, standard cloning technique employing restriction enzymes was used. All restriction enzymes were purchased from Thermo Scientific. Whenever available, high-fidelity versions of the restriction enzymes were used. Insert was cut out from the donor plasmid or produced by PCR. PCR was conducted with Phusion High-Fidelity DNA Polymerase (Life Technologies, F-530S) according to the enzyme manufacturer's protocol. After each restriction digest and PCR, DNA fragments were isolated by agarose gel electrophoresis and subsequent gel extraction. Ligation of the DNA fragments was performed using T4 DNA ligase (New England Biolabs, M0202S) at 16°C for 16 h, followed by heat shock transformation of *E. coli* and subsequent culturing to obtain the desired plasmid.

RaichuEV-Cdc42: DNA sequence coding for EV linker in pRaichuEV-Ras plasmid was cut out with XhoI and NotI and inserted into the Raichu-Cdc42 sequence that was cut with the same restriction enzymes.

2.4.2 Live-cell microscopy

2.4.2.1 Forward transfection and imaging

For single FRET biosensor imaging experiments, FuGENE HD Transfection reagent (Promega), DMEM and cDNA encoding FRET biosensor was used to transfect cells with following the slightly modified manufacturer's protocol. In this protocol OPTIMEM medium was replaced by DMEM to avoid the influence of cytokines contained in OPTIMEM medium and decrease basal activity of the signaling network. Cells were grown in 8-well LabTek or 1-well Mattek dishes and transfected 16 to 20 hours before imaging. In order to prepare the transfection mixture for a 1-well Mattek, the corresponding amount of cDNA solution (1000 ng of total DNA) was diluted with 50 μ L of FCS free DMEM in an Eppendorf tube. Subsequently, (4 μ L per 1000 ng of total DNA amount) was diluted with 50 μ L of FCS free DMEM in another Eppendorf tube. Then the DNA and FuGENE HD solutions were vortexed for at least 15 seconds and incubated for 10min. In the meantime, cell culture medium was replaced with FCS free DMEM (2 ml). After incubation, transfection mix (100 μ L) was added into a Mattek dish equally distributed and cells were kept growing at 37 °C in the incubator. The response of FRET biosensors was monitored on a Leica AF7000 microscope using a 40x objective with CFP/YFP dual-band beam splitter and two emission filters (470/30 for CFP and 535/50 for YFP) that were controlled by a filter wheel at an interval of 30 s – 2 min per frame. A baseline of at least 10 frames was captured before adding of a stimulus using the Leica software.

2.4.2.2 Solid-phase reverse transfection

In order to achieve better transfection efficacy previously described protocols (Erflé et al., 2007; Piljic et al., 2011) of the solid-phase reverse transection were optimized by varying a transfection reagent and plasmid/transfection reagent ratio in the transfection cocktail (Table 2.2 for details).

Table 2.2: *The optimization of solid-phase reverse transection efficacy*

Transfection reagent (TR) name	Amount of TR, μL	DNA (ERK EV biosensor), μL (conc.= 1 $\mu\text{g}/\mu\text{L}$)	Supplement reagent (depending on the TR)	Sucrose, Conc. (w/v)/ Volume	Gelatine, Conc. (w/v)/ Volume
Lipofectomine 2000	7	2	-	13.7%/3 μL	0.2%/7.25 μL
Lipofectomine 2000	11	3	-	19.9%/3 μL	0.29%/7.25 μL
Lipofectomine 2000	11	5	-	19.9%/3 μL	0.29%/7.25 μL
Lipofectomine 2000	11	3	-	26.1%/3 μL	0.38%/7.25 μL
Lipofectomine 2000	11	6	-	26.1%/3 μL	0.38%/7.25 μL
Lipofectomine 2000	16	4	-	19.9%/3 μL	0.29%/7.25 μL
Lipofectomine 2000	20	3	-	26.1%/3 μL	0.38%/7.25 μL
Lipofectomine 2000	20	5	-	26.1%/3 μL	0.38%/7.25 μL
Lipofectomine 2000	22	3	-	26.1%/3 μL	0.38%/7.25 μL
Lipofectomine 2000	22	6	-	26.1%/3 μL	0.38%/7.25 μL
Lipofectomine 2000	44	6	-	26.1%/3 μL	0.38%/7.25 μL
Lipofectomine 2000	44	12	-	26.1%/3 μL	0.38%/7.25 μL
Lipofectomine 2000	44	18	-	26.1%/3 μL	0.38%/7.25 μL
Lipofectomine 2000	54	12	-	26.1%/3 μL	0.38%/7.25 μL
Lipofectomine 2000	54	18	-	26.1%/3 μL	0.38%/7.25 μL
Lipofectomine 3000	7	2	-	13.7%/3 μL	0.2%/7.25 μL
Lipofectomine 3000	7	2	0.1	13.7%/3 μL	0.2%/7.25 μL
Lipofectomine	7	2	0.5	13.7%/3 μL	0.2%/7.25 μL

3000					
Lipofectomine 3000	7	2	2	13.7%/3 μ L	0.2%/7.25 μ L
Lipofectomine 3000	7	2	4	13.7%/3 μ L	0.2%/7.25 μ L
Lipofectomine 3000	11	3	0.5	19.9%/3 μ L	0.29%/7.25 μ L
Lipofectomine 3000	11	3	0.1	19.9%/3 μ L	0.29%/7.25 μ L
K2	7	2	4	13.7%/3 μ L	0.2%/7.25 μ L
K2	11	3	4	19.9%/3 μ L	0.29%/7.25 μ L
K2	11	5	4	19.9%/3 μ L	0.29%/7.25 μ L
K2	20	3	2	26.1%/3 μ L	0.38%/7.25 μ L
K2	20	3	8	26.1%/3 μ L	0.38%/7.25 μ L
K2	20	6	4	26.1%/3 μ L	0.38%/7.25 μ L
K2	40	3	4	26.1%/3 μ L	0.38%/7.25 μ L
K2	40	6	4	26.1%/3 μ L	0.38%/7.25 μ L
K2	40	6	2	26.1%/3 μ L	0.38%/7.25 μ L
K2	50	6	6	26.1%/3 μ L	0.38%/7.25 μ L
K2	50	6	6	26.1%/3 μ L	0.38%/7.25 μ L
K2	50	6	4	26.1%/3 μ L	0.38%/7.25 μ L
K2	50	12	4	26.1%/3 μ L	0.38%/7.25 μ L
Effectene	7	2	4	13.7%/3 μ L	0.2%/7.25 μ L
ScreenFect A	11	3	-	26.1%/3 μ L	0.38%/7.25 μ L
ScreenFect A	11	6	-	26.1%/3 μ L	0.38%/7.25 μ L
ScreenFect A	22	3	-	26.1%/3 μ L	0.38%/7.25 μ L
ScreenFect A	22	6	-	26.1%/3 μ L	0.38%/7.25 μ L
ScreenFect A	22	12	-	26.1%/3 μ L	0.38%/7.25 μ L
ScreenFect A	44	6	-	26.1%/3 μ L	0.38%/7.25 μ L
ScreenFect A	44	12	-	26.1%/3 μ L	0.38%/7.25 μ L
ScreenFect A	44	18	-	26.1%/3 μ L	0.38%/7.25 μ L
ScreenFect A	54	12	-	26.1%/3 μ L	0.38%/7.25 μ L
ScreenFect A	54	18	-	26.1%/3 μ L	0.38%/7.25 μ L
GenJet	7	2	-	13.7%/3 μ L	0.2%/7.25 μ L
PeqFECT	7	2	-	13.7%/3 μ L	0.2%/7.25 μ L

The following amounts refer to the transfection under conditions optimized for efficacy and toxicity. Briefly, plasmids for reverse transfection were diluted to concentration of 1 mg/mL. The transfection mixture were prepared by mixing 9 μ L of a 0.4 M sucrose solution in DMEM, 9 μ L of DNA and 33 μ L of lipofectamine 2000 mixed in a 96-well plate and incubated for 20 min at room temperature. Subsequently, 21.75 μ L of 0.29% gelatin solution in water was added to the transfection mixture. The transfection cocktail was distributed in 384-well plates (24 μ L per well). The plates were stored at 4°C. In order to print Labteks the 384-well plate was thawed at room temperature and centrifuged briefly up to 54 g to straighten the surface of the samples. Afterwards, residual bubbles were removed by a 10 μ L tip and placed immediately in the contact printer. Before printing, LabTek dishes were washed with 70% ethanol increasing hydrophobicity of the LabTek surface and, accordingly, improving the shape of the spots. 1-well LabTek dishes were printed with a “ChipWriter” contact printer equipped with solid pins. Using PTS 600 pins, the diameter of printed spots was about 400 μ m and the spot-to-spot distance was 1125 μ m. Printed 1-well LabTek dishes were stored at room temperature in a gel drying box in the presence of drying pearls.

2.4.2.3 Cell microarray imaging

For live cell microarray imaging, 65×10^4 cells suspended in a culture media were seeded onto a printed glass coverslip 1-well LabTek chamber and kept growing at 37 °C in an incubator for 24 – 48 h. Afterwards, the culture media were changed to starvation media (see above) at least 12-17 h prior to imaging. Prior to microscopy experiment, transfected cells were incubated with 7.5 nM DRAQ5 according to manufacturer’s protocol to improve cellular segmentation. During imaging, cells were kept in imaging medium at 37°C without CO₂. All microscopy experiments were carried out on an Olympus IX83 microscope under constant conditions (at 37°C without CO₂) in the imaging medium. The imaging buffer was used for MIN6 cells. The microscope was equipped with a Hamamatsu Image EM CCD camera and an environmental chamber. Time-lapse imaging was performed with 20X 0.70 NA or 10X 0.40 NA and 436/20 excitation filter, a CFP/YFP dual-band beam splitter (51017bs; Chroma) and two emission filters (470/30 for CFP and 535/50 for YFP) that were controlled by a filter wheel. Before the time-lapse imaging, the DRAQ5-stained nuclei of the cells were imaged. Typically, ten frames were recorded as a

baseline before stimulation in order to estimate signal stability and to normalize single cell traces. The xCELLence software was used to carry out time-lapse imaging with 3 min interval over 5 hours.

2.4.2.4 Cross-contamination assay

In order to evaluate the cross-contamination between spots in close proximity that might be due to the diffusion of DNA-lipofectamin 2000 transfection complex or cell migration, microarrays were printed with two plasmids encoding ECFP and EGFP in an alternating pattern and dried in a gel drying box in the presence of drying pearls at room temperature. Afterwards, 65×10^4 cells suspended in a culture media were seeded onto a printed glass coverslip 1-well LabTek and kept growing at 37 °C in an incubator for 48 h. Prior to microscopy experiment, transfected cells were incubated with 7.5 nM DRAQ5 according to manufacturer's protocol to improve cellular segmentation. The transfected cells were monitored on an Olympus IX83 microscope using a 10x objective, two excitation filter (436/20 for CFP and 492/18 for YFP), a CFP/YFP dual-band beam splitter (51017bs; Chroma) and two emission filters (470/30 for CFP and 535/50 for YFP). For DRAQ5-stained nuclei imaging I used the excitation filter 635/20 and emission filter 6654LP.

2.4.3 Image processing

2.4.3.1 FRET quantification

The single image of a nuclei channel and the time-lapse series of CFP and FRET channels acquired from different positions were exported as separate TIFF files. The images were analyzed with FIJI (Schindelin et al., 2012) and FluoQ (Stein et al., 2013). The FIJI-based macro developed in-house was used to preprocess and multiply nuclei image and subsequently concatenate all channels together. This macro produced a single tiff file containing three channels: binary mask of nuclei (repeated 100 times), FRET and CFP channels obtained from the same position. The file containing three channels was further analyzed with the FIJI-based macro FluoQ as illustrated in Figure 2.1. Although cells express different amount of FRET biosensors I used image analysis pipeline that automatically account for a low expressing cells that are close to background cellular fluorescence. In order to subtract background I used a histogram-based “Triangle” algorithm to calculate the mean of the thresholded background that was subsequently

subtracted from each pixel. Next, image smoothing with a median filter (radius size = 2) was applied and the images were transformed to a 32-bit float. Cells were automatically segmented by using binary mask created by Huang's fuzzy thresholding method. The signal intensity that was equal or close to intensity of the background was set as NaN value due to Huang's fuzzy thresholding. This image analysis pipeline automatically accounts for a very low expressing cells and avoided erroneous FRET ratios. The nuclear binary mask was used to for cell segmentation by the voronoi algorithm. In order to define ROIs the particle analyzer, a build-in FIJI plugin, was applied to the binary image of segmented cells. Although acquired images contain information of the subcellular activity I simplified image analysis pipeline in order be able to analyze 13900 images (more than 5000 cells) from a single experiment in a reasonable time window by averaging the intensity of FRET, CFP and FRET ratio over each ROI. However, significant compartmentalized signaling fluctuations might be averaged out. In all experiments, single-cell traces were normalized to the of the FRET ratio from before stimulation. The output file in a text format that was produced by FluoQ contained all measured parameters, statistical summaries.

2.4.3.2 Automated cell counting

In order to count transfected cells FIJI-based macro were developed. Briefly, All channels were smoothed applying the median filter (radius = 3). Subsequently, the local maxima in nuclear images were determined with output type set as a point selection (noise tolerance = 3). Next, the CFP and GFP channel images were thresholded (min = 33050, max = 36863) and converted to the binary mask. Afterwards, the *build in command* imageCalculator (“AND create”) was used to find the maxima in the nuclear channel corresponding to the area of transfected cells. Finally, the macro provided the text file that contained the number of detected cells in nuclear, CFP and GFP channels. The further data and statistical analysis were performed using the R software for statistical computing and graphics (Team, 2012).

2.4.4 Western blotting

To determine the phospho-AKT and phospho-ERK dynamics, I seeded the HeLa Kyoto cells on 60 mm dishes (5×10^5 /dish). After 24 hours, the culture media were changed to starvation media

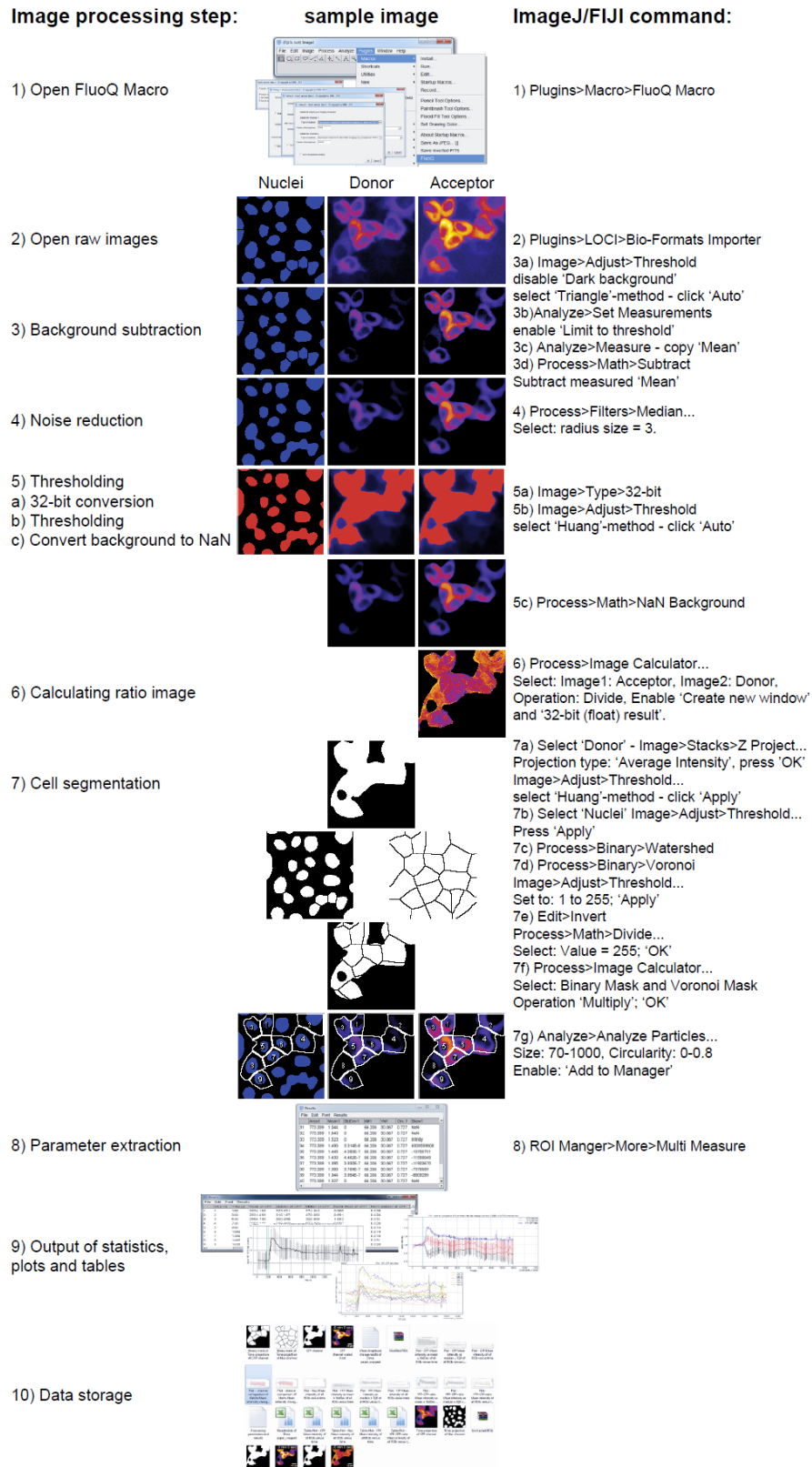


Figure 2.1 Image analysis pipeline of an in-house developed macro FluoQ.

(see above) at least 12-17 h prior to the beginning of the experiment. The cells were next treated with 100 ng/ml EGF. At the indicated time points, the plates were washed two times with ice cold PBS and the cells were lysed in RIPA buffer supplemented with protease inhibitors and 5 % (v/v) β -mercaptoethanol. The cell lysates were immediately boiled on a preheated block at 95 °C for 5 min and cooled down at room temperature (RT). Afterwards, the cell lysate was treated with the Benzonase Nuclease (1:100 dilution) and incubate at RT for 20 min. The clarified lysates were diluted in Laemmli sample buffer and proteins were separated by sodium dodecyl sulfate polyacrylamide gel electrophoresis (SDS-PAGE), using the Mini-Cell electrophoresis system (Thermo Fisher), 12% resolving gel (Novex/Thermo Fisher) and voltage of 50 V for 30 min followed by 100V for 2h in SDS running buffer (Novex/Thermo Fisher). Separated proteins were transferred to a polyvinylidene fluoride (PVDF) membrane in mini trans-blot cell (BIO-RAD) filled with ice-cold transfer buffer using voltage of 100 V for 90 min. The membrane was blocked in TBST buffer containing 5 % (w/v) skim milk for 1 h at RT. Subsequently the membrane was incubated with specific primary antibodies from rabbit or mouse overnight at 4 °C and washed three times in TBST for 10 min. For detection, the membrane was then stained with respective secondary antibodies conjugated with horse peroxidase and washed again two times in TBST for 10 min and once in TBS for 10 min. The electrochemiluminescence (Pierce ECL Plus) method were used according to the manufacturer's instructions to visualize the protein of interest.

2.4.5 RNA extraction, evaluation and sequencing

Hela cells were seeded in 60 mm dishes pre-coated with gelatin to reproduce conditions similar to microarrays. Prior to stimulation cells were starved in the absence of serum overnight. Afterwards, cells were incubated with GFs for four hours. I lysed cells by the direct addition of 3 ml of TRIzol (Life Technologies) after media removal. For RNA extraction lysates were treated with 0.6 ml chloroform (Sigma-Aldrich) for 3 min and centrifuged at 12,500 g for 15 min at 4 °C. Aqueous supernatant was collected and diluted 1:1 with 70% ethanol. Total RNA was extracted from solution using RNeasy Mini Kit (Qiagen), following the manufacturer's instructions and quantified using a NanoDrop spectrophotometer. RNA was used with $A(260/280) \text{ nm} \geq 1.8$ and $A(260/230) \text{ nm} \geq 2.0$. RNA quality was assessed using RNA 6000 Nano chips on the Agilent 2100 Bioanalyzer. The library preparation, RNA sequencing and

reads alignment were performed by a Genomics Core Facility at EMBL. Sequencing was performed on Illumina NextSeq-500 instruments.

2.4.6 Statistical and data analysis

2.4.6.1 Outliers removal

In each independent experiment, single-cell traces were cautiously examined for artificial intensity spikes in the CFP and FRET channels. Those spikes were due to lamp intensity fluctuation, cell division, cell movement and, in rare cases, cell death. Therefore, we have developed the automated algorithm that detected artificial intensity spikes and removed cell traces containing those spikes from further data analysis. First, the baseline and response values were smoothed by running median (width of median window = 5). Subsequently, the difference between real values and smoothed values was used to calculate sample quantiles. The quantile mean and standard deviation for baseline and response was calculated from the values belonging to the interval lying between 5th and 95th quantiles. Afterward, the z-score was calculated for each value of the baseline and response using quantile mean and standard deviation. Single cell traces containing z-score in the experimentally defined range ($z\text{-score} \geq 40$ or $z\text{-score} \leq -40$) were automatically removed. After removal single cell traces containing spikes, the mean baseline (formula 2.1), the standard deviation of the baseline (formula 2.2), the slope of the baseline (formula 2.3), the mean (formula 2.4), maximum (formula 2.5) and minimum (formula 2.6) response were calculated for each single-cell trace. Those features were subjected to the

$$\bar{x}_{baseline} = \frac{1}{n_{baseline}} \sum_{t=0}^{t_{stim}} x_t \quad (2.1)$$

$$s_{baseline} = \sqrt{\frac{1}{n_{baseline} - 1} \sum_{t=0}^{t_{stim}} (x_t - \bar{x}_{baseline})^2} \quad (2.2)$$

$$slope_{baseline} = \frac{\sum_{i=0}^{t_{stim}} ((t - \bar{t}_{baseline})(x_t - \bar{x}_{baseline}))}{\sum_{i=0}^{t_{stim}} (t - \bar{t}_{baseline})} \quad (2.3)$$

$$\bar{x}_{response} = \frac{1}{n_{resp}} \sum_{t=t_{stim}}^{t_{resp}} x_t \quad (2.4)$$

$$Max_{response} \frac{\max(x_{response} - \bar{x}_{baseline})}{S_{baseline}} \quad (2.5)$$

$$Min_{response} \frac{\min(x_{response} - \bar{x}_{baseline})}{S_{baseline}} \quad (2.6)$$

algorithm that classifies an outlier if it falls outside the interval defined in the following formula:

$$[\tilde{x}_{0.25} - 2(\tilde{x}_{0.5} - \tilde{x}_{0.05}), \tilde{x}_{0.75} - 2(\tilde{x}_{0.95} - \tilde{x}_{0.50})]$$

Once any feature of a particular single-cell trace was detected as an outlier, the cell was excluded from the analysis.

2.4.6.2 Synergy score

In order to calculate an interaction mode between two stimuli for each signaling molecule (or FRET biosensor), single-cell traces first were normalized by dividing each time point with the mean baseline ($\bar{x}_{baseline}$) and with the mean value of untreated cells (x_{mock}) at each time point followed by a subtraction of 1. Afterwards, area under the curve (AUC) was computed for each single-cell trace (formula 2.7). In order to determine if the data is well modeled by a normal

$$AUC_{cell} = \sum_{t=0}^{t=end} \left(\frac{\tilde{x}_t}{x_{mock_t}} - 1 \right), \text{ where } \tilde{x}_t = \frac{x_t}{\bar{x}_{baseline}} \quad (2.7)$$

distribution this data normality was analyzed using Shapiro-Wilks test and Q-Q-plots. Then, the area under the curve was averaged for the corresponding sensor and stimulus. The error for

calculated additive response was estimated by computing standard error of the mean. The expected response upon co-stimulation was calculated by the simple addition of the AUC mean of individual treatments. The combined error was estimated by an error propagation of the individual standard errors of the mean applying a Variance formula (Ku, 1966). In order compare the experimental and expected (calculated) additivity the means of two groups were subjected to Student's two sample t-test and subsequently obtained P-values were corrected for multiple testing (Benjamini and Hochberg, 1995). I defined the 'synergy score' as the difference between the experimental and expected (calculated) additivity. In order to simplify visualization, the synergy score was scaled to the maximum synergy score observed for a FRET biosensor, giving a value that ranges from -1 (antagonism) to +1 (synergy).

2.4.6.3 Analysis of RNA-Seq data

The count matrix was generated by a Genomics Core Facility at EMBL using STAR software (Dobin et al., 2013). Mapping rate was more than 70% for all samples. DESeq2 package (Love et al., 2014) was used to perform differential expression analysis of the treated cells vs. untreated cells comparison. A Wald test was used to determine the significance of fold change between experimental groups for the genes of interest. To analyze KEGG pathway enrichment, the R packages org.Hs.eg.db (Carlson, 2017) and gage (Luo et al., 2009) were used.

2.4.6.4 General statistical analyses and data visualization

Unless otherwise stated, a FRET biosensor response is represented as normalized FRET ratio mean of all individual cells from identical conditions +/- SEM where the SEM is calculated from all cells in all experiments with identical conditions. In order to compare and cluster FRET biosensor dynamics the maximum observed FRET ratio value of each biosensor were additionally used for normalization.

Data visualization

The data was visualized using the R package 'ggplot2' (Wickham, 2009) or the heatmap2 function of the R package 'gplots' (Warnes et al., 2012).

Clustering

Hierarchical clustering was performed using the heatmap2 function of the R package ‘gplots’. The R package ‘kml’ (Genolini et al., 2015) was utilized to perform k-means clustering with $k = 6$ or 4. The synergy score matrix was hierarchically clustered with the Euclidean metric and the Ward linkage.

Principal component analysis (PCA)

The prcomp function with centering and scaling of the program R was used to perform PCA analysis. PCA was performed on $X \times Y$ matrix, where Y is different FRET biosensors each with X that included: a) time points and cell lines; b) time points, stimuli and stimuli doses.

Chapter 3 – Results and discussions

3.1 FRET-based multi-parameter imaging platform (FMIP) as a tool to study intracellular signaling networks

Intracellular signaling networks are formed by the interplay of hundreds of proteins and second messengers. They are able to reliably receive and process information from extracellular environment to adjust a cellular state appropriately. The investigation of signal encoding and decoding mechanisms by a signaling network is hampered by dynamic features of distinct signaling events, the diverse forms of signals (molecular interactions, post-translational modifications (PTMs), subcellular localization) and the complexity of signaling network architecture (chapter 1.3). Only the simultaneous quantitative monitoring of a large number of the signaling events in a single living cell with high temporal resolution will allow us to understand signal transduction mechanisms and the function of a living cell. Following this evident need, several high-throughput approaches have been developed to measure the diverse set of signals at a single-cell level including flow (Bendall et al., 2012) and mass cytometry (Giesen et al., 2014), microfluidics (Cheong et al., 2009), single-cell Western blot (Hughes et al., 2014) and fluorescence lifetime imaging microscopy on cell arrays (CA-FLIM) (Grecco et al., 2010). Although these single cell assays provide advantages including multiplexed quantification, most of the methods are based on endpoint measurement resulting in limited information on dynamic changes. Importantly, these assays are focused on a collection of signals

of a particular form such as the protein-protein interaction, the phosphorylation state or the subcellular localization. While powerful, such system-level methods require assumptions and approximations to interpret the acquired data. For example, a single phosphorylation state or another PTM approximation is used to estimate protein activity, which is not necessarily valid in every case (de la Cruz-Herrera et al., 2015; Liu et al., 2014). One way to overcome this problem would be to use several high-throughput approaches and combine different types of information together. However, such experimental design would dramatically increase the total cost of the experiments as well as raise the issue of data integration from diverse assays that is not always computationally trivial.

Another way to rapidly measure signaling dynamics inside living cells is to use FRET biosensors. Since FRET efficiency strongly depends on the distance between and relative orientation of two fluorophores, the FRET biosensor methodology is very successful at monitoring conformational change of the protein under observation (chapter 1.5). The synthetic design of a FRET biosensor is therefore able to report on different types of signaling events including protein-protein interactions, PTMs, concentration of second messengers and, most importantly, protein activities (not merely abundance at the single live cell level) in real-time (Newman et al., 2011). Additionally, a single FRET biosensor can be successfully used in high-throughput experiments in combination with siRNA screening (Bakal et al., 2008). Thus, FRET biosensors are a toolset that in principle permits the activity of multiple signaling pathways to be followed over time at the single-cell level.

However, the number of FRET biosensors that can be used in the same cell is limited by their extended occupation of the available spectral regions and cell tolerance to the expression of many exogenous genes that prohibits extensive multiplexing at the single cell level (Miyawaki, 2003; Welch et al., 2011). To overcome those limitations and increase high-throughput capacity we have devised a method for imaging a large number of FRET biosensors in a single experiment. This platform described here is based on reverse transfection microarrays that allow collecting quantitative information in real time with high reliability and sensitivity (Kuchenov et al., 2016; Neumann et al., 2006; Ziauddin and Sabatini, 2001). The FRET-based multi-parameter imaging platform (FMIP) employs LabTek chambers printed with library of plasmids encoding

various FRET biosensors along with the transfection agent lipofectamine 2000 (Figure 3.1). All spots were equally spaced with a distance between spot centres of 1125 μm . Each spot contains a single plasmid encoding one FRET biosensor. Although seeded cells are able to attach to the whole surface of a glass slide only cells attached to the printed spots are transfected with a FRET biosensor. In principle this design allows fabricating a cell microarray transfected with up to 384 plasmids encoding distinct FRET biosensors.

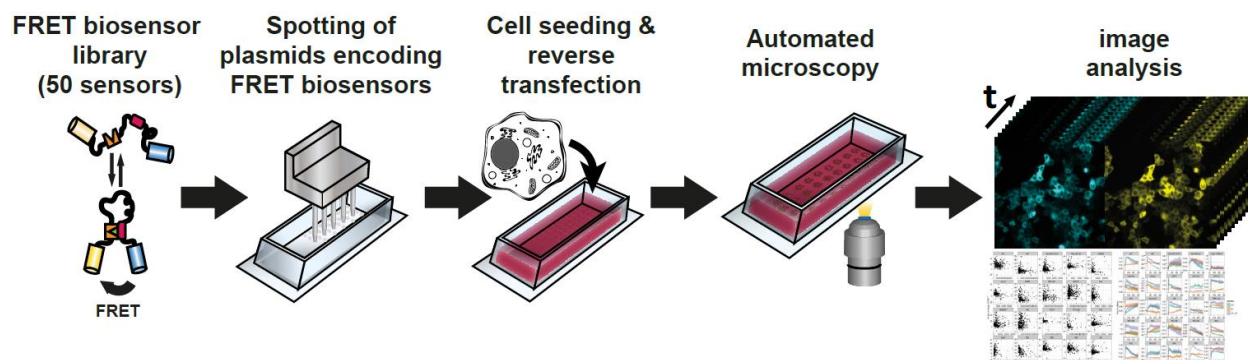


Figure 3.1 FRET-based multi-parameter imaging platform (FMIP). Figure is adapted from (Kuchenov et al., 2016)

By combining microarray technology with time-lapse imaging of FRET biosensors I was able to analyze the dynamics of multiple signaling pathways in living HeLa, MIN6, H838 and H195 cells. Use of an automated microscope equipped with a filter wheel allows images of the CFP and FRET channels to be acquired from one spot in about 1.3 s. Therefore the temporal resolution can be adjusted by the number of spots. Typically, 40 spots were imaged every 50 sec or 140 spots were imaged every 3 min over 2 or 5 hours, respectively. However, various imaging and cellular parameters such as light intensity, exposure time, FRET biosensor expression, photo toxicity, cell type determine the temporal resolution and duration of imaging. Therefore imaging settings have to be optimized for each particular experimental design and cell line. Details of the optimization are described in the next sections.

3.1.1 Transfection optimization

The previously described transfection mixture for microarrays containing Opti-MEM (Piljic et al., 2011) might perturb the signaling network under observation due to the presence of

biologically active compounds such as insulin, transferrin, hypoxanthine, thymidine, and other trace elements. Therefore I first tested whether imaging buffer or DMEM that have a defined chemical composition are able to substitute Opti-MEM in the transfection mixes. Surprisingly, substitution of Opti-MEM with imaging medium or DMEM significantly increased the efficacy of reverse transfection that was observed after 24 hours (figure 3.2). These results indicate that DMEM is a very efficient Opti-MEM substitute suitable for reverse transfection. Therefore, DMEM was used as a substitute of Opti-MEM in the process of reverse transfection optimization.

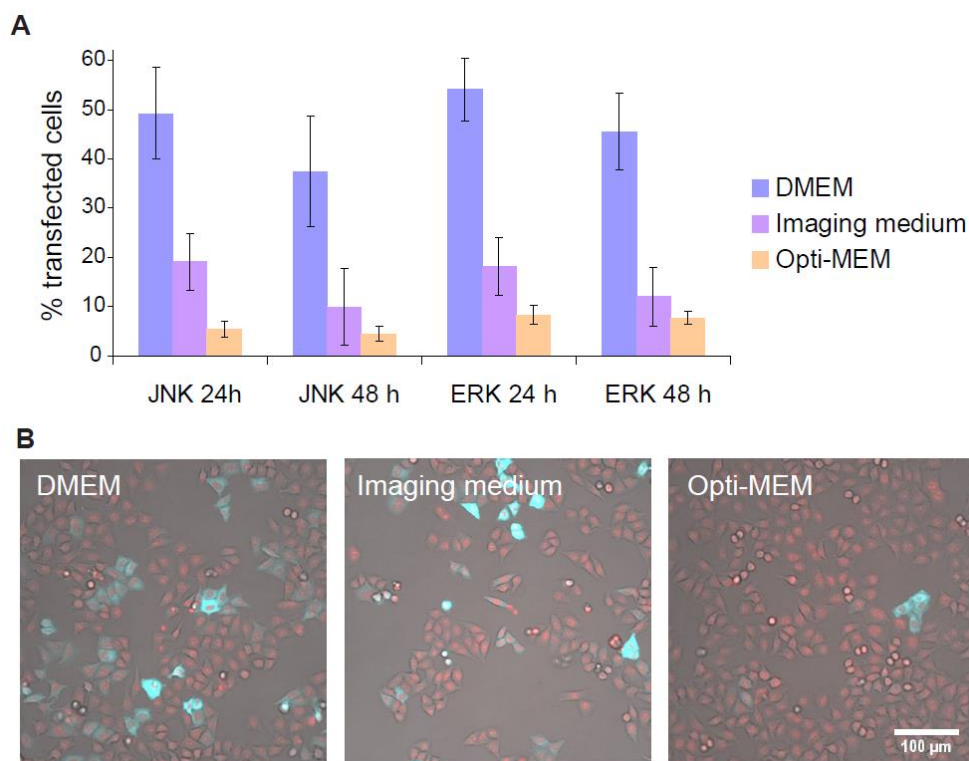


Figure 3.2 Substitution of Opti-MEM with DMEM or imaging buffer. (A) The reverse transfection efficacy in HeLa cells with the JNK and ERK FRET biosensors. Cells were observed 24 and 48 hours after transfection. Data represent mean \pm SEM ($n = 4$). (B) Representative images of HeLa cells transfected with the JNK FRET biosensor for 48 hours from (A). FRET biosensor is visualized with CFP channel (blue) and nuclei were stained with DRAQ5 (red).

Single-cell studies clearly indicate that cell-to-cell heterogeneity plays an important role in diverse biological processes such as early embryo development (Ohnishi et al., 2014) and cancer progression (Brock et al., 2009). Recently it was also suggested that signal transduction might not be uniform and coherent in cell populations, which also increases the complexity of the

system (Frechin et al., 2015; Tay et al., 2010; Yuan et al., 2011). In order to address this complexity by performing single cell variation analysis, large numbers of cell observations are needed in each experiment. Therefore I tested different spot surfaces such as gelatin, fibronectin, collagen and poly-L-lysine to define the best candidate for reverse transfection (figure 3.3). This experiment showed that “collagen-only” and “Poly-L-lysine (PLL)-only” transfection mixtures were unable to form spots on the surface of a glass slide, leading to the absence of transfected cells. Although fibronectin has been reported as a potent accelerator of reverse transfection (Miyake et al., 2009) it only slightly facilitated the DNA delivery. Interestingly, gelatin mixed with collagen or fibronectin slightly decreased transfection efficacy. Overall, no considerable improvement of transfection efficacy was observed. Because gelatin is a mixture of different water-soluble proteins and other protein surfaces did not strongly increase transfection efficacy it was decided that gelatin would be the best matrix for a wide variety of cell types.

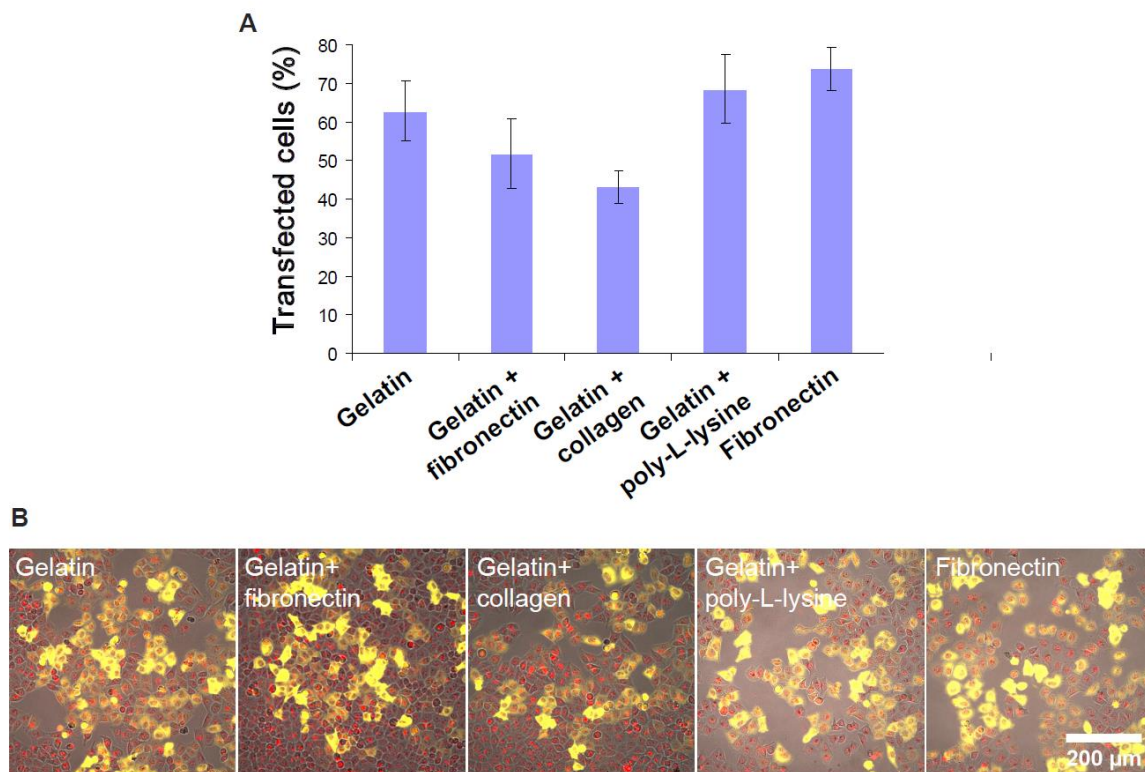


Figure 3.3 The substitution of gelatin in transfection mixes. (A) Reverse transfection efficacy in HeLa cells expressing the JNK FRET biosensors. Cells were observed 48 hours after transfection. Data represent mean \pm SEM (n = 4). (B) Representative images of HeLa cells transfected with the JNK FRET biosensor for 48 hours from (A). Fret biosensor is visualized with YFP channel (yellow) and nuclei were stained with DRAQ5 (red).

As our final goal was to develop an assay that is suitable for distinct cell lines, reverse transfection efficacy was optimized by spotting transfection cocktails that contained different transfection reagents and plasmid/transfection reagent ratios in cell-imaging chambers (figure 3.4).

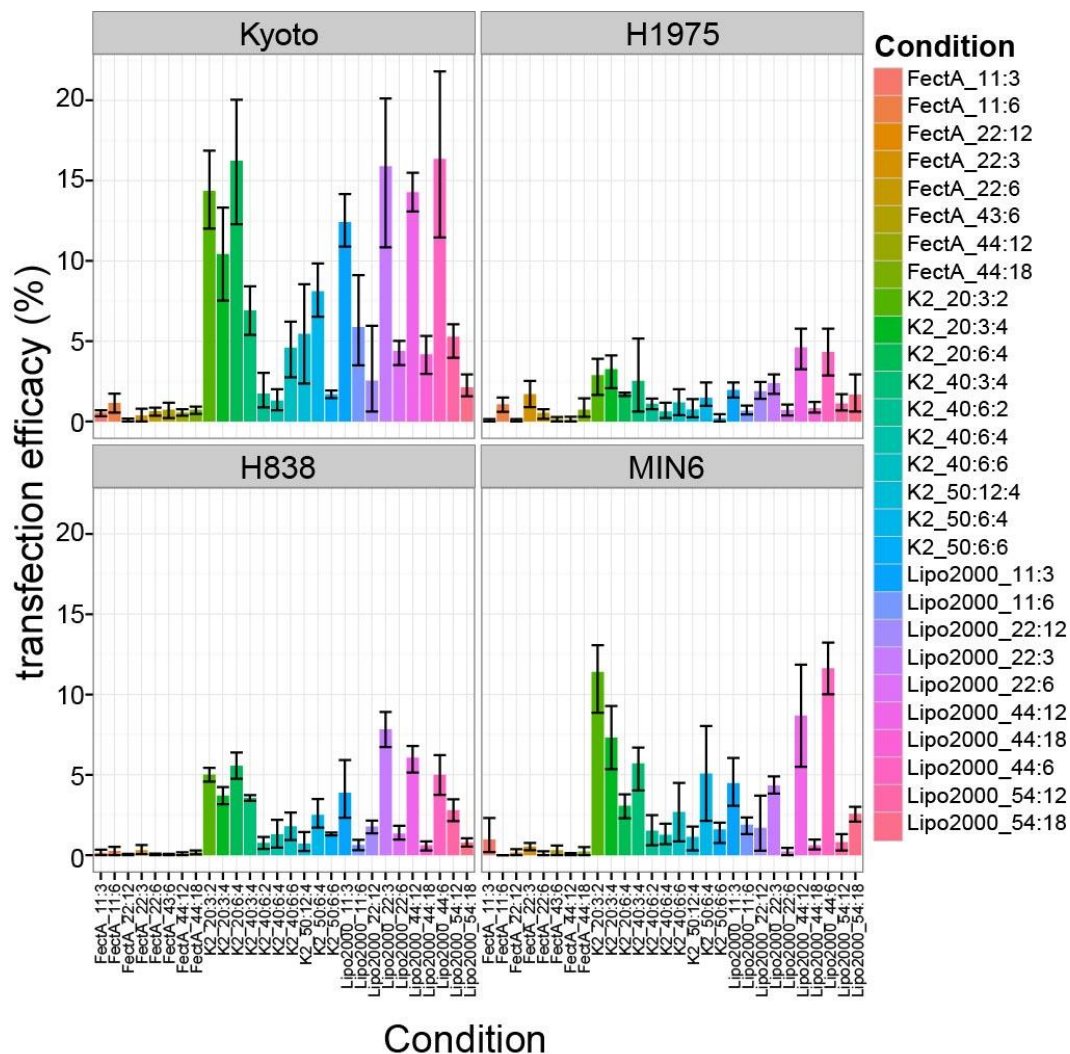


Figure 3.4 Transfection optimization. The reverse transfection efficacy in HeLa, H838, H1975 and MIN6 cells expressing the ERK FRET biosensor. Cells were observed 48 h hours after transfection. Data represent mean \pm SEM (n = 4).

Although efficacy varied strongly between cell lines, the K2 and Lipofectamine 2000 transfection agents showed the best transfection efficacy in all tested cell lines. Interestingly, increasing concentrations of both the K2 transfection agent and the plasmid encoding the ERK FRET sensor led to a decline in the transfection efficacy. In contrast, an important parameter for the lipofectamine 2000 is the transfection reagent/plasmid ratio. Overall, I did not observe a

significant difference between Lipofectamine 2000 and K2 transfection reagents whereas ScreenFect A demonstrated much less transfection efficacy. The combination of 11 μL of Lipofectamine 2000 with 3 μg of DNA demonstrated high transfection efficacy with moderate toxicity for most cell lines that were tested. Unexpectedly, I also noticed that transfection efficacy was 20 % - 30 % lower on cells that had been split earlier in comparison to other experiments when cell splitting was performed 24h before reverse transfection. I therefore tested whether splitting cells 24 hours before reverse transfection increases transfection efficacy. Indeed, I observed a significant increase in transfection efficacy if cells were trypsinized and seeded 24 hours before starting reverse transfection (figure 3.5). This step most probably helps to avoid cell aggregation (or clumps) and enriches cells that are in the active proliferative state.

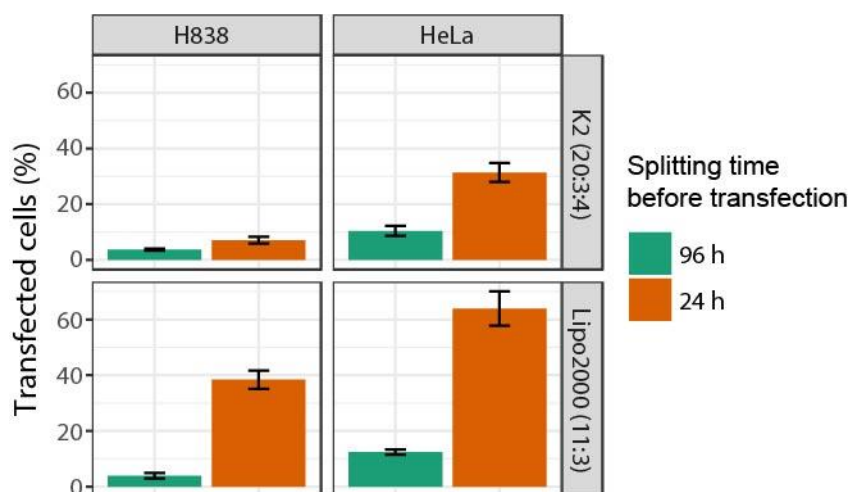


Figure 3.5 The influence of the splitting time before reverse transfection on efficacy. The reverse transfection efficacy in HeLa and H838 cells expressing the ERK FRET biosensor. Data represent mean \pm SEM (n = 4).

With this information in hand, I further determined the optimal transfection conditions when cells were split 24 hours before reverse transfection. Several liposomal-based reagents were compared for their transient transfection efficiency of H838 and HeLa cells (figure 3.6 A). Among these transfection reagents, lipofectamine 2000 achieved higher transfection efficiency than the other liposomal reagents tested. Although transfection efficacy using 20 μL of lipofectamine 2000 and 5 μg of DNA was slightly higher in HeLa cells, H838 cells did not show this improvement in comparison to transfection mixture containing 11 μL of lipofectamine 2000. Moreover, by using 11 μL of lipofectamine 2000 and 3 μg of DNA, I achieved the transfection rate that allowed monitoring an average of 27-150 cells (depending on the cell line and FRET

biosensor) in a single experiment (figure 3.6 C). Interestingly, counting the total number of cells indicated low variability in the number of attached H838 cells between conditions (figure 3.6 B). However, HeLa cells were more sensitive to reverse transfection conditions.

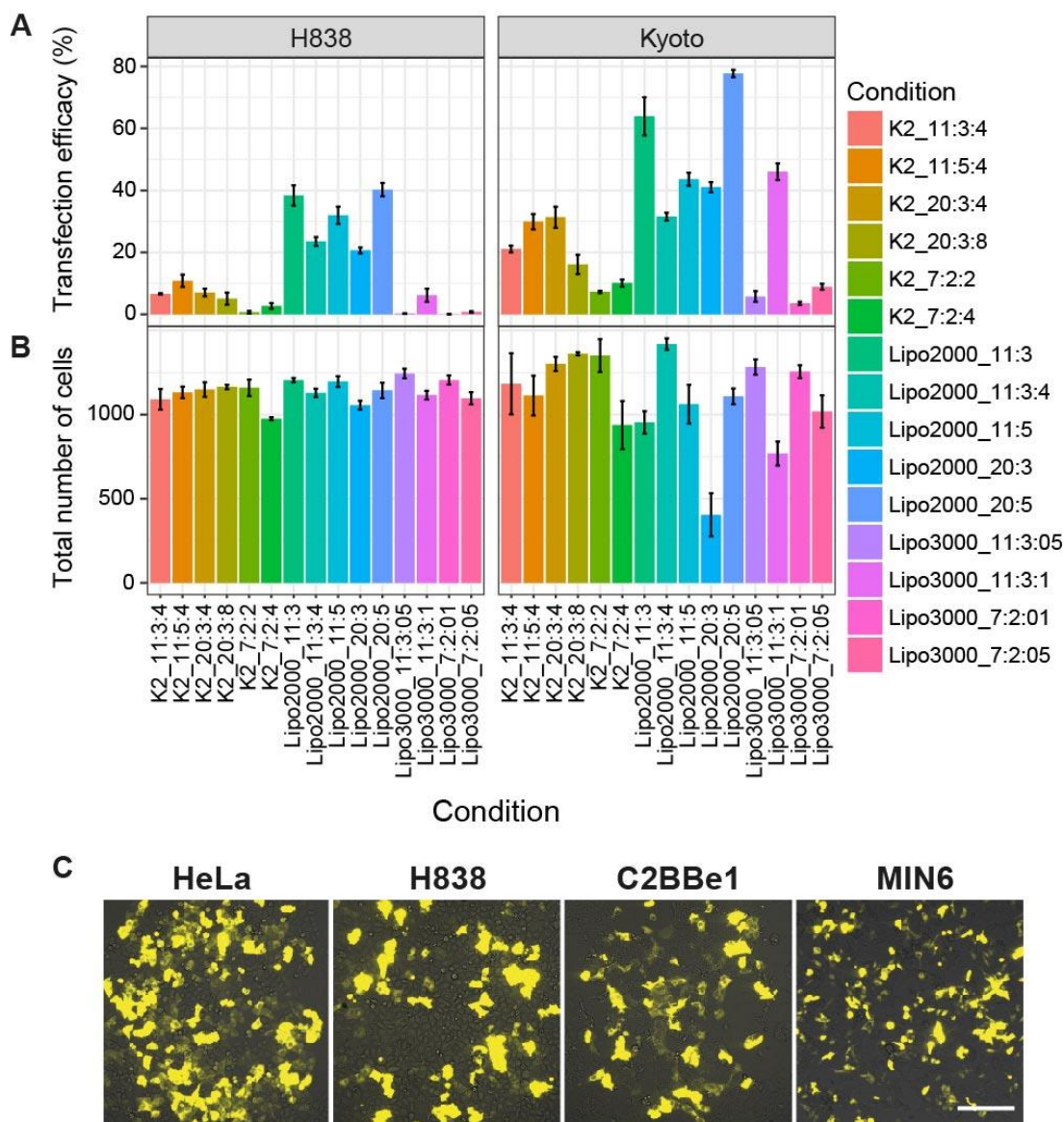


Figure 3.6 Efficacy optimization when cells were split 24 hours before reverse transfection. (A) Transfection efficacy in HeLa and H838 cells expressing the ERK FRET biosensor. Data represent mean \pm SEM (n = 4). (B) Total number of cells attached to a spot. Data from (A) represent mean \pm SEM. (n = 4) (C) Images showing the compatibility of the chosen transfection conditions with a variety of adherent cells. Cells were transfected with the ERK FRET biosensor using 11 μ L of lipofectamine 2000 and 3 μ g of DNA. Scale bar, 200 μ m.

Thus, this method is applicable to various cultured cell lines and suitable to perform single cell variation analysis. Importantly, it is highly advisable to optimize reverse transfection for a

particular cell line by seeding cells on the microarrays with various transfection conditions. For these experiments, seeding cells 24 hours in advance of transfection, culturing on gelatin, using 11 μL of lipofectamine 2000 and 3 μg of DNA and using DMEM instead of OptiMEM were considered the best conditions to achieve an adequate number of transfected cells.

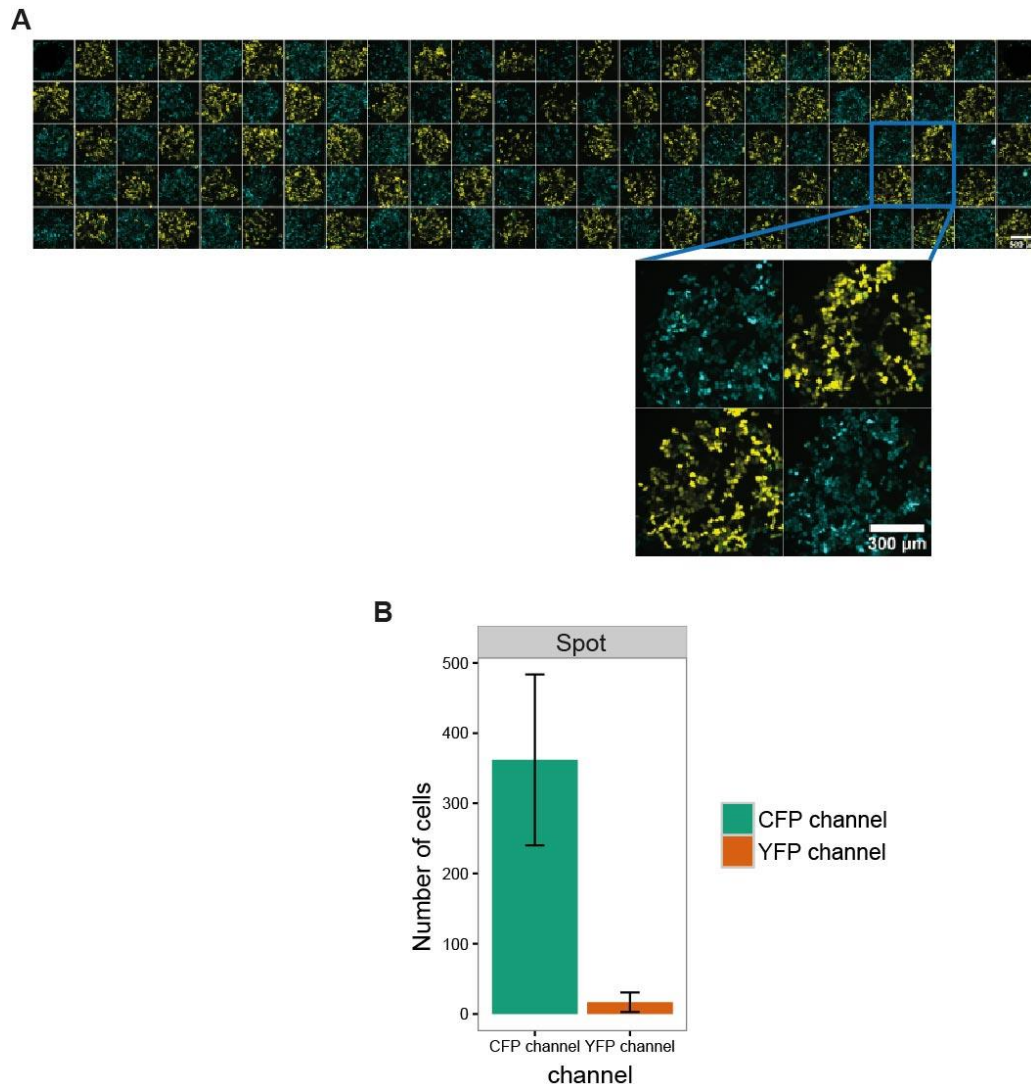


Figure 3.7 Cross-contamination analysis. (A) Microarray of HeLa cells printed with plasmids expressing either CFP (blue) or GFP (yellow) in an alternating pattern (scale bar, 500 μm). Bottom, higher magnification image of four spots from the array (scale bar, 300 μm). (B) Quantification of cells expressing CFP and/or YFP on a spot containing CFP plasmid from (A). Data represent mean of all spots \pm SD. (180 spots, three independent experiments). Figure is adapted from (Kuchenov et al., 2016).

Because printed spots in cell-microarrays are not physically separated, the microarrays may suffer from spot-to-spot contamination due to lateral diffusion of the spotted test compounds or

cell migration upon reverse transfection. By modifying the transfection protocol we might influence parameters facilitating cross-contamination. In order to examine whether cells within one spot would become contaminated with plasmids or cells from spots in vicinity, we printed imaging chambers with two plasmids encoding ECFP and EGFP in an alternating pattern (Figure 3.7 A).

Upon seeding HeLa cells on these microarrays we observed a high level of green fluorescence on EGFP-transfected spots and vice versa high level of cyan fluorescence on ECFP-transfected spots (Figure 3.7 A). The number of cells with blue fluorescence was eighteen times greater than the number of cells expressing EGFP on spots printed with the plasmid encoding ECFP (Figure 3.7 B). Therefore, we demonstrated that under our optimized transfection conditions good local segregation of transfected cells to the original spot was achieved.

3.1.2 Monitoring EGF signaling network activity and platform validation

In order to validate whether the FMIP was able to reliably report the time-dependant activity of the signaling network under observation we focused on the well-characterized epidermal growth factor (EGF) signaling (Lemmon and Schlessinger, 2010; Wagner et al., 2013). In these experiments HeLa or H838 cells were seeded on Labteks printed with plasmids each encoding one of the 58 previously described FRET biosensors (table 2.1). The transfected cells were observed using a wide field microscope by acquiring sequential images of the CFP and FRET channels for 30 min (a baseline) before and for over 4 hours after stimulation with EGF. The microscope setup allowed capturing the fluorescence of both channels every three minutes from 140 spots. As expected, treatment with EGF induced signaling through Ras/ERK and PI3K/Akt pathways in HeLa cells (Figure 3.8 A). Although we observed the activation of Ras/ERK and PI3K/Akt signaling pathways in H838 cells, the dynamics of RSK, PDK1 and S6K activity were altered in comparison to HeLa cells, most probably due to difference in the cell line specific gene expression (Figure 3.8 B). Upon subjecting dynamics of protein activity to hierarchical clustering, we identified at least 3 classes of response patterns: strong, moderate and weak (Figure 3.8 C). Interestingly, the dynamics of Ras, ERK and RSK (the Ras\ERK pathway) were clustered together whereas the PDK1, Akt and S6K (the PDK1/Akt/S6K pathway) dynamics belonged to clusters with weak, moderate and strong responses, respectively. These results show

that information within the same pathway may encode distinct dynamics. With our platform we also showed that EGF-induced signaling is concentration dependent (Figure 3.8 D). We observed that different doses of EGF influenced not only the amplitude but also the signaling dynamics. For example, 100 ng/mL EGF induced strong sustained activation of PKA whereas cells stimulated with 50 ng/mL EGF responded with transient dynamics of PKA activity. In contrast, the RhoA 2G FRET biosensor showed different correlation to the concentration of EGF: a strong sustained response was induced by 100 ng/mL EGF whereas RhoA was transiently active after treatment with 50 ng/mL EGF (Figure 3.8 D).

One of the key advantages of the FMIP is that it produces data with single cell resolution. Analysis of single cell trajectories revealed pulsatile activity of ERK (12.5 ng/mL EGF) and Src (100 ng/mL EGF) that would not be possible to observe using other methods measuring responses at the population level (Figure 3.9 A). In recent studies it was reported that ERK can show such pulsatile activity depending on the concentration of EGF or confluences from the environment (Albeck et al., 2013; Aoki et al., 2013). Also, it was shown that local mechanical forces induced a wave of Src activity in live cells (Wang et al., 2005). Moreover, a theoretical study suggests that under certain parameters Src can have pulsatile and oscillatory activity, explaining the results observed by Wang et al. (Kaimachnikov and Kholodenko, 2009). In our study, we observed pulsatile activity of ERK and Src in a fraction of cells and under certain conditions, suggesting that the variations are of biological relevance and not due to technical reasons.

In order to estimate the reproducibility of the data generated with our platform, we calculated the coefficient of variation. The average coefficient of variation (CV) of spots over all time points after stimulation was 5.5%; the average CV of replicate spots over time was 6.5%; and the average CV across replicate experiments over time was 7.3%. The low value of CV confirmed the very high data reproducibility between independent experiments. As expected, single cell responses have increased CV ($CV < 30\%$) due to heterogeneous responses of cells in the same experiment (Figure 3.9 B and C).

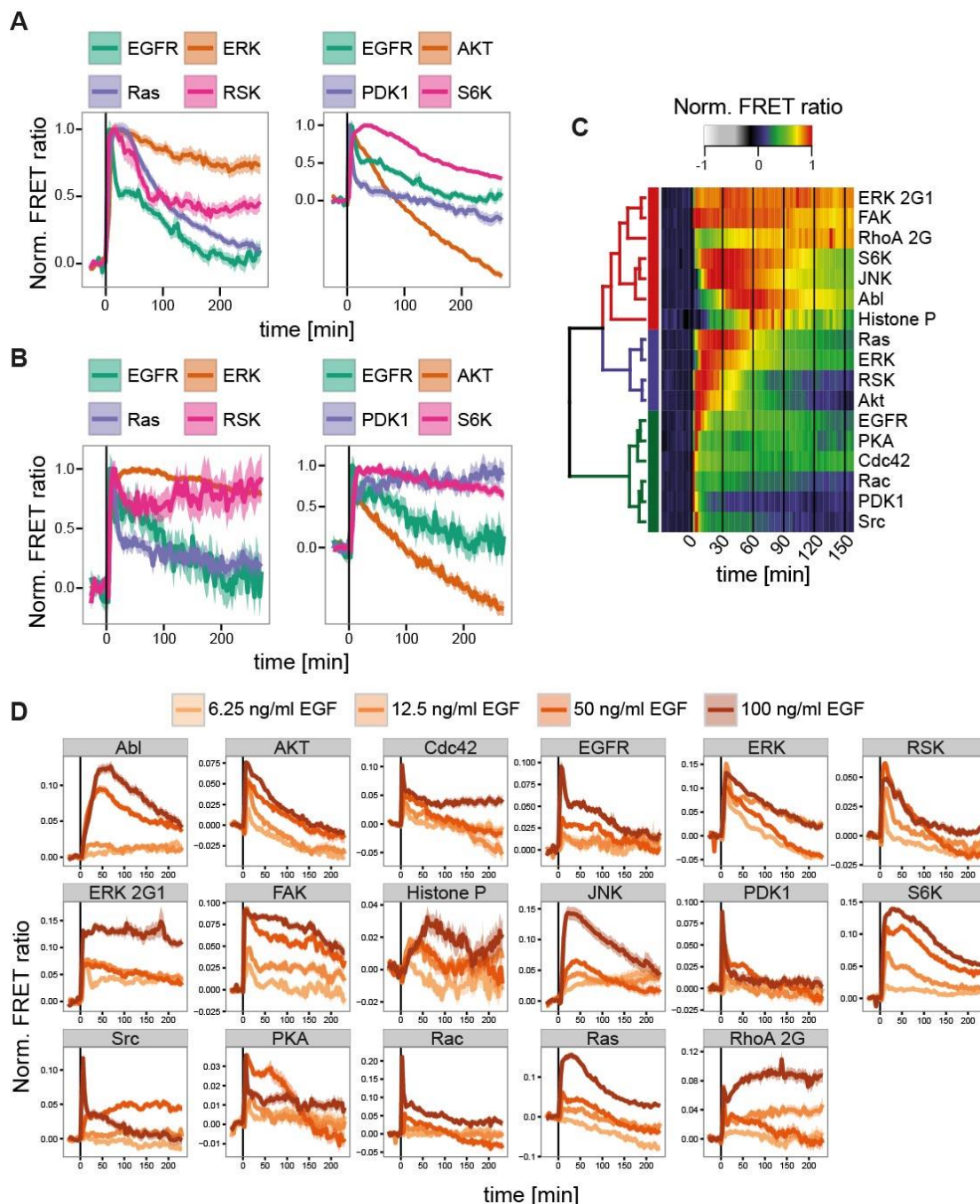


Figure 3.8 EGF-induced signaling in HeLa and H838 cells. (A) EGF activates Ras/ERK and PI3K/Akt signaling in HeLa cells. Cells were treated with 100 ng/mL EGF. (B) EGF induced Ras/ERK and PI3K/Akt signaling in H838 cells. Cells were treated with 50 ng/mL EGF. Cells in (A) and (B) were stimulated at time 0. Data represent mean \pm SEM of four (HeLa) and three (H838) independent experiments. C) Hierarchical clustering of EGF-induced signaling dynamics in HeLa cells. Dynamic responses are clustered into 3 groups: weak (green), moderate (blue), and strong (red). Data from (A) is normalized to non-treated cells and represent a mean response. D) Concentration dependent EGF signaling in HeLa cells. Figure is adapted from (Kuchenov et al., 2016)

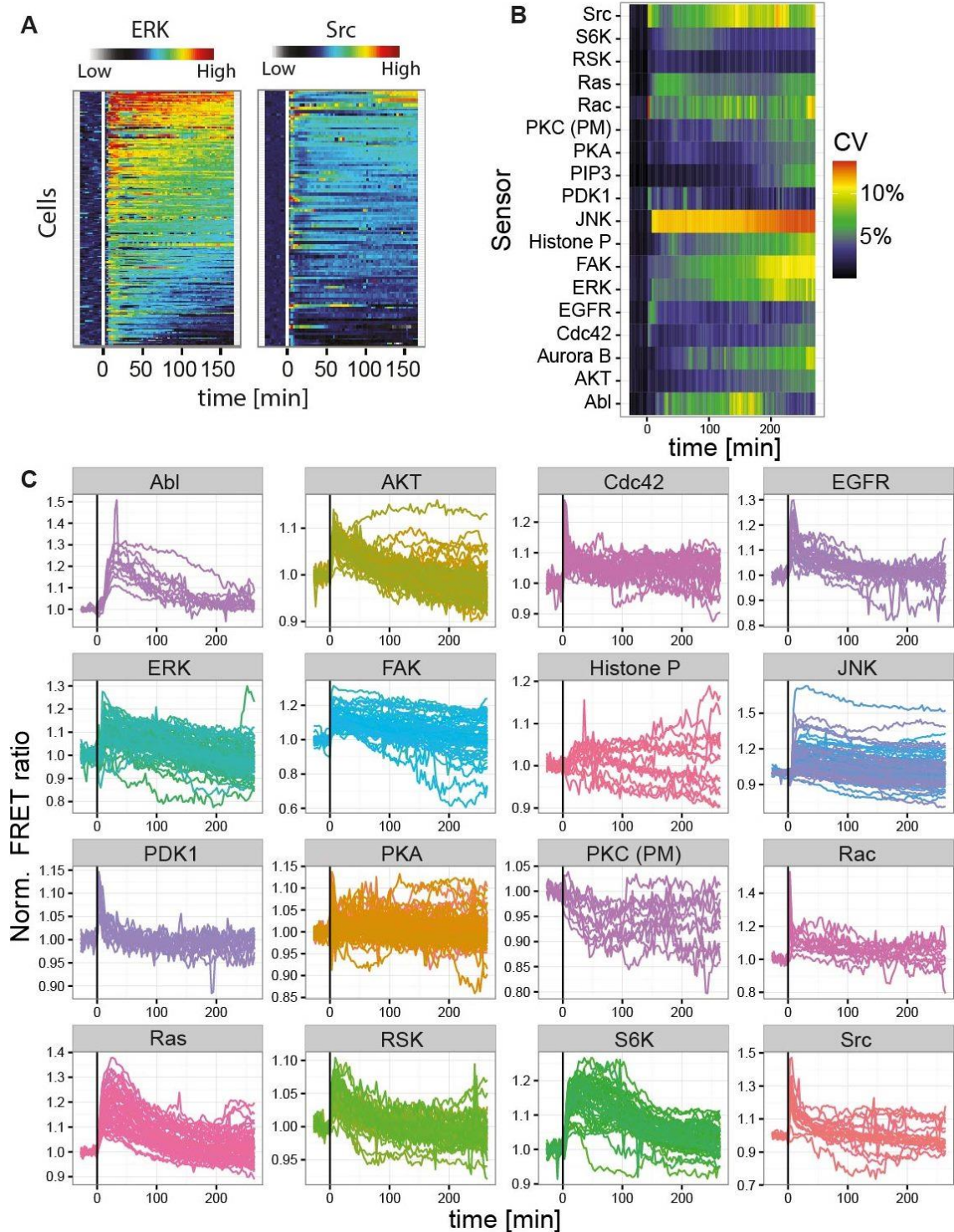


Figure 3.9 Heterogeneous cellular responses. (A) Pulsatile activity of ERK and Src after treatment with 12.5 ng/ml (left) and 100 ng/ml EGF (right), respectively. (B) Coefficient of variation of HeLa cell responses in a single experiment. Cells were stimulated with 100 ng/mL at time 0. (C) Single cell responses from (B). Figure is adapted from (Kuchenov et al., 2016).

The heterogeneous cellular response might be due to differential expression of FRET biosensors. I therefore estimated the changes in the expression by observing CFP intensity as the approximation of biosensor expression over the course of imaging. In most cases fluorescent intensity increased in both CFP and FRET channels, indicating changes in the expression of FRET biosensors (Figure 3.10 A). However, as previously described, the FRET/CFP ratio is more stable in comparison to CFP and FRET channels, demonstrating an advantage of using FRET biosensors that provide internal control for the expression level over translocation or *intensiometric* sensors (Thestrup et al., 2014). In order to estimate the influence of biosensor expression on the signaling responses I further compared maximum responses between individual cells that differently expressed the amount of a biosensor. The scatter plots and the Kendal's tau correlation coefficient (Figure 3.10 B and C) strongly demonstrate a weak or no correlation between the maximum of FRET/CFP ratio value and expression of FRET biosensor after EGF stimulation, except the Ras FRET biosensor (Kendal's tau correlation coefficient $r = 0.33$, $p < 0.0001$). Overall, the data suggest that the FMIP assay is able to monitor multiple signaling events without significant perturbation by FRET biosensor overexpression in a single experiment.

3.1.3 FMIP applied to various experimental designs

Potentially the FMIP allows monitoring of intracellular signaling with different experimental designs and under various conditions of physiological relevance. We also believe that our platform is suitable for the screening of therapeutic targets or drug candidates to profile and evaluate potency as well as off-target effects. Although we explicitly demonstrated the ability to monitor growth factor signaling network after stimulation with EGF, one might speculate this was possibly due to the downstream amplification of the signal. We therefore confirmed the ability of the platform: (i) to profile the perturbation of EGF signaling caused by constitutively active EGFR harbouring L858R/T790M double mutation and by the MEK inhibitor (AZD6244, Selumetinib); (ii) to monitor fatty acids dependent DAG signaling.

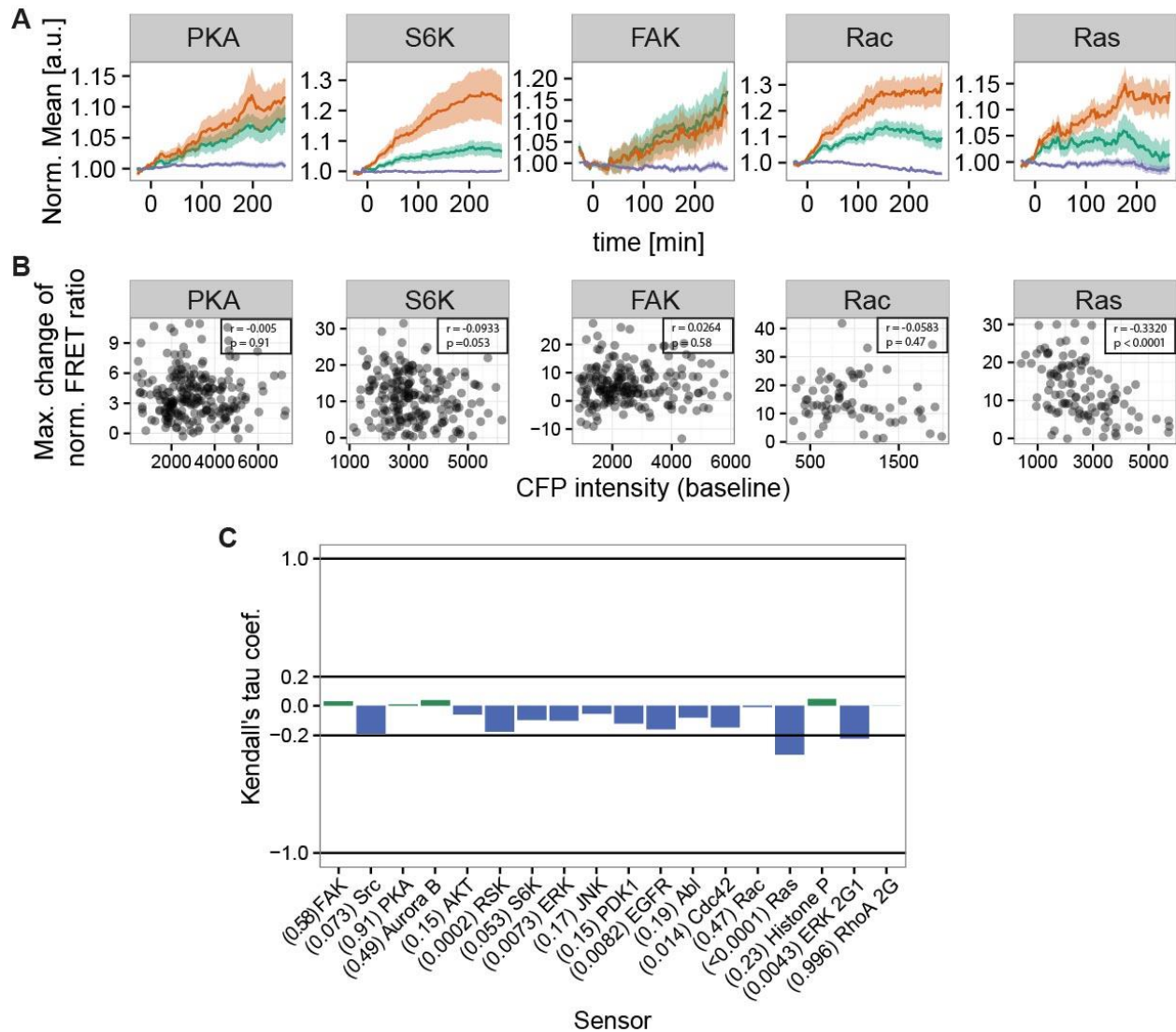


Figure 3.10 The impact of the FRET biosensor expression level on cellular signaling. (A) Examples of FRET biosensor expression dynamics. Color reflects the channel: CFP, red; FRET, green; and CFP/FRET ratio, blue. Cells were treated with imaging medium at time 0. Data represent mean \pm SEM ($n = 3$) (B) Examples of scatter plots comparing the expression and maximum response in each cell. HeLa cells were stimulated with 100 ng/mL EGF ($n > 65$, depending on the FRET biosensor). Expression levels were approximated by averaging donor channels (CFP) before stimulation. r : Kendall's correlation coefficient. p : p-value. (C) Kendall's tau coefficients between FRET biosensor expressions and the maximum of normalized response to EGF in HeLa cells. Brackets show p-value.

3.1.3.1 Monitoring EGF signaling perturbations caused by EGFR mutations and a clinically relevant inhibitor

The development of cancer involves protein mutations that cause aberrant signaling supporting the proliferation and survival of cancer cells. Proper therapeutic intervention into cancer cell signaling may reverse the course of the disease or prevent its further progression. Therefore measuring the signaling state across multiple disease settings will open the possibility to study aberrant signaling and to improve current as well as the development of novel therapies. In order to challenge our platform in such an application we first tested the ability of the FMIP to detect perturbations in EGFR signaling network activity caused by the clinically relevant MEK inhibitor (AZD6244) (Bekaii-Saab et al., 2011). In these experiments microarrays with HeLa cells were pre-stimulated with 100 ng/mL EGF and after 69 min of imaging the cells were treated with 5 μ M AZD6244. As expected, we observed a strong decrease in ERK and RSK activity after the MEK inhibitor was added in comparison to DMSO-treated cells (Figure 3.11 A). In contrast, we did not observe significant changes in the activity of EGFR, Ras, Cdc42, FAK, Rac or Abl between AZD6244 and DMSO treated cells (Figure 3.11 C). Unpredictably, we also observed a strong decrease in the activity of PKA activity and a significant increase in JNK activity after the MEK inhibitor AZD6244 was added to the cells (Figure 3.11 B). Whereas it was earlier shown that ERK inhibition causes activation of JNK (Monick et al., 2006), the decrease in PKA activity cannot be readily explained. Although we cannot rule out potential off-target effects of the inhibitor, we found in the literature that RSK is able to interact with the catalytic subunit of PKA and decreases the ability of cAMP to activate PKA (Gao and Patel, 2009). In contrast, our data suggest a more complex interplay between PKA and RSK such as mutual regulation of RSK and PKA by the Ras/ERK signaling pathway or potentiation of one signaling molecule by the other in the presence of EGF.

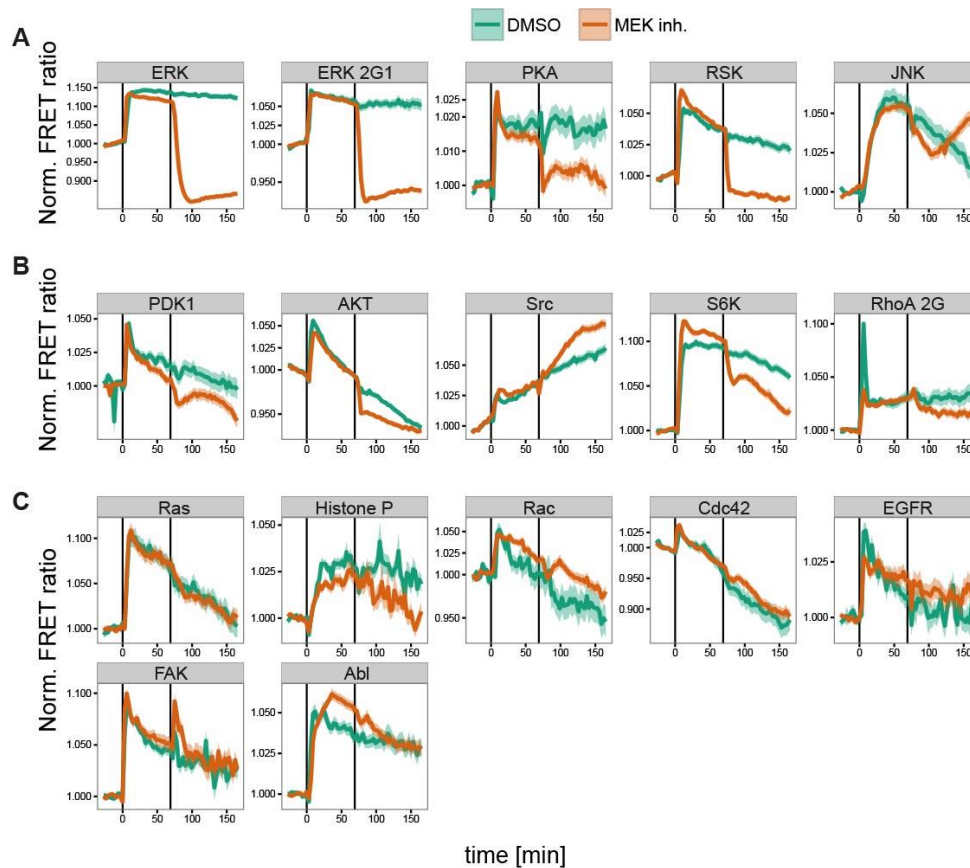


Figure 3.11 Perturbation of EGF signaling network by the MEK inhibitor AZD6244. Examples of (A) strong, (B) moderate and (C) no effect on the EGF signaling are shown. Cells were pre-stimulated with 100 ng/mL EGF at time 0 and treated with DMSO or MEK inhibitor (5 μ M) after 69 min. Data represent mean \pm SEM ($n = 3$). Figure is adapted from (Kuchenov et al., 2016)

Activating RTK mutations are often associated with cancer development. To further test whether the FMIP is able to detect signaling perturbations caused by pathophysiologically relevant RTK mutations, we profiled EGF signaling in cell lines derived from adenocarcinoma (H1975) or its metastatic variety (H838) of patients with non-small cell lung cancer. H1975 cells express EGFR carrying the activating mutation L858R and the resistance mutation T790M. In order to characterize perturbations initiated by the EGF receptor carrying constitutively active (L858R) and erlotinib-resistant (T790M) mutations, we also profiled EGF signaling in H838-EGFRmut cells that exogenously express EGFR derived from H1975 cells. We observed that H838-EGFRmut cells failed to activate Src, PKA, AKT and RSK in response to EGF stimulation whereas ERK, S6K, and Abl were activated with much lower amplitude compared to wild type H838 cells (Figure 3.12 A).

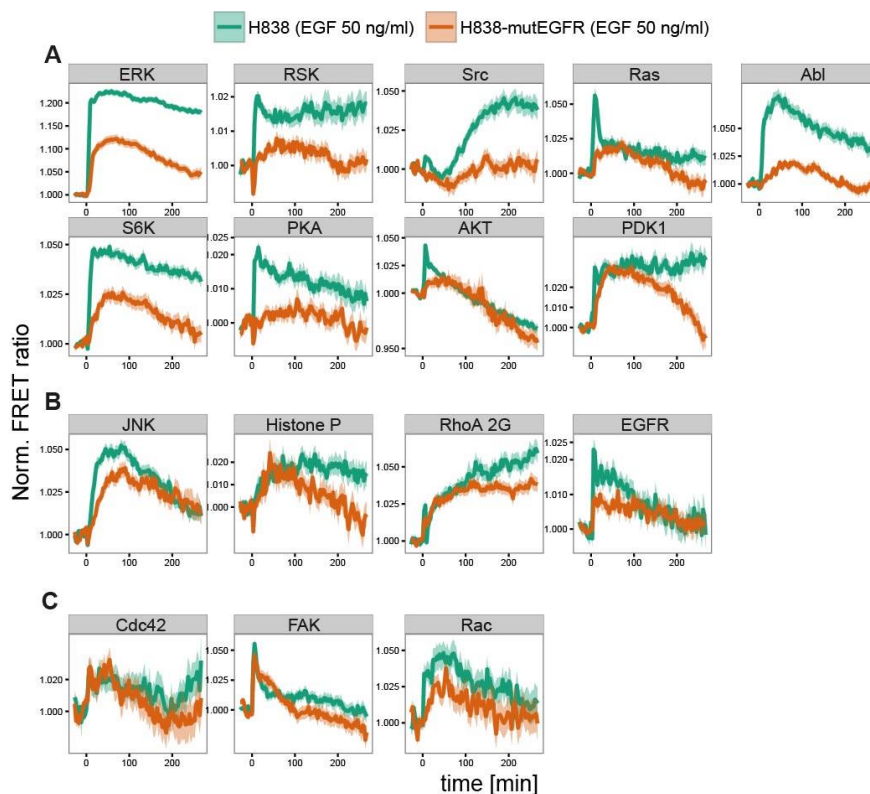


Figure 3.12 Changes of the EGF signaling network by constitutively active EGFR carrying L858R and T790M mutations. Examples of (A) strong, (B) moderate and (C) no effect on the EGF signaling are shown. Cells were stimulated with 50 ng/mL EGF at time 0. Data represent mean \pm SEM ($n = 3$). Figure is adapted from (Kuchenov et al., 2016)

Interestingly, exogenously expressed constitutively active EGFR altered the dynamics of PDK1, RhoA and JNK activation as well as the dynamics of histone phosphorylation (Figure 3.12 A and B). In contrast, the responses of Cdc42, FAK and Rac to EGF treatment were not significantly changed in H833-EGFRmut cells (Figure 3.12 C). By subjecting the generated signaling data to principal component analysis (PCA), we further compared the global response after 50 ng/mL EGF treatment in H838 and HeLa cells expressing wild type EGFR as well as in H1975 and H838-EGFRmut cells expressing constructively active EGFR (Figure 3.13).

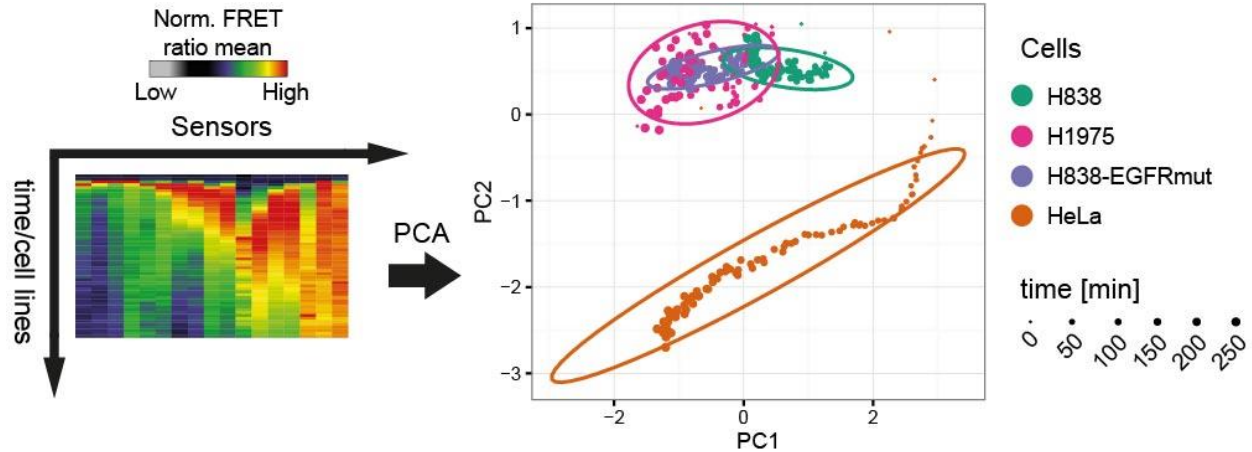


Figure 3.13 Comparison of global signaling responses. H838, H838-EGFRmut, H1975 and HeLa cells were treated with 50ng/mL EGF. The matrix with 340 rows (85 time points, and 4 cell lines) and 14 columns (FRET biosensors) was subjected to PCA. Each dot represents a time point and ovals indicate 90 % of time points of the same cell line. Figure is *adapted from (Kuchenov et al., 2016)*

Interestingly, the PCA in figure 3.13 shows that global EGF signaling in HeLa cells is localized far apart from H838, H838-EGFRmut and H1975 cells, which indicates strong cell line dependent differences. As expected, time points of EGF-stimulated H1975 and H838-EGFRmut cells were clearly clustered together suggesting that EGF signaling in exogenously (H838-EGFRmut) and endogenously (H1975) expressing constitutively active EGFR cells have a high degree of similarity in comparison to H838 cells expressing wild type EGFR (Figure 3.13). Overall, the EGFR activation in H838-EGFRmut and H1975 cells after stimulation with 50 ng/mL EGF gave rise to lower signaling amplitudes or much altered dynamics compared to control H838 cells expressing wild type EGFR. Although the same signaling molecules were activated in HeLa and H838 cells, their dynamics were significantly different most probably due to altered gene expression. In general, using the FMIP we demonstrated that unbiased profiling of global signaling network activity offers quantitative information to assess the degree of perturbation induced by clinically relevant mutations.

3.1.3.2 Monitoring fatty acid dependent diacylglycerol induced signaling

Diacylglycerols (DAGs) are second messengers consisting of two fatty acids that are covalently attached through an ester bond to glycerol. DAGs are important for the signaling of different RTK including EGFR (Crotty et al., 2006; Wang et al., 2006). Recent studies in the Schultz group showed that the fatty acid composition in DAGs can modulate the local Ca^{2+} signaling response (Nadler et al., 2013). We therefore hypothesised that the fatty acid composition of DAG could also affect the downstream DAG signaling. Taking advantage of our platform, we profiled a large portion of the RTK signaling network upon treatment of HeLa cells with DAGs containing various fatty acids: stearyl-linoenyl glycerol (SLG), stearyl-arachidonyl glycerol (SAG), and 1,2-di-O-octanoyl glycerol (1,2-DOG) (Figure 3.14 A).

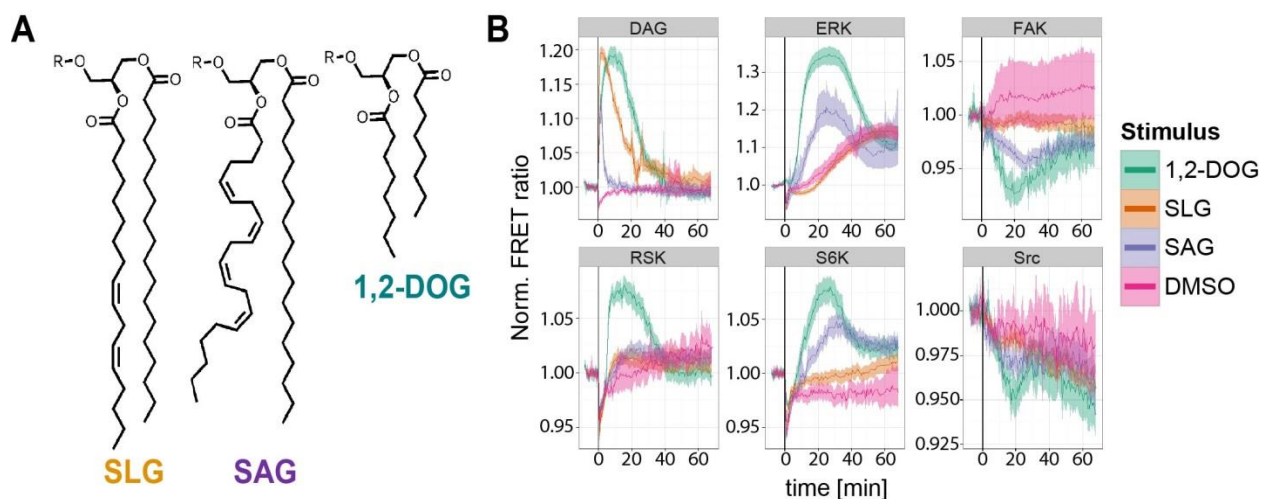


Figure 3.14 Fatty acid composition dependent DAG signaling. (A) Structures of DAGs used in this work. (B) Signaling dynamics induced by DAGs.

Importantly, a FRET biosensor based on the C1 β domain of PKC β enables quantification of the amount of DAG on the inner leaflet of the plasma membrane (Stein, 2014). This sensor strongly responded to all DAGs albeit with distinct dynamics that were transient and dependent on the specific fatty acid composition. The DAG biosensor indicates the prolonged presence of 1,2-DOG with short unnatural fatty acids in comparison to other DAGs containing long natural fatty acids (Figure 3.14 B). In contrast, SLG induced a highly transient response of the DAG biosensor (Figure 3.14 B).

The observed difference in the dynamics of the DAG biosensor could be caused by two scenarios: 1) fatty acid dependant membrane permeability of DAGs; or 2) differences in the metabolic rate of the different DAGs. Using the C1-GFP biosensor, previous studies demonstrated that responses induced by the uncaging of protected 1,2-DOG and SLG were slightly different from responses upon adding free 1,2-DOG and SLG to the medium (Stein, 2014). Although slight differences between caged and free SAG were observed, aforementioned study suggests that there is an effect of fatty acid composition on the permeability of DAGs detected in the first 2 min. Indeed, Figure 3.14 shows that FRET/CFP-ratio maximum for all DAGs is achieved within a few minutes after free lipids were added to the medium, indicating quick diffusion and cell penetration for all DAGs, so scenario 1) above can be ruled out. Thus, use of the DAG FRET biosensor demonstrated that there is a different rate of metabolism depending on the fatty acid composition of diacylglycerols that is in a good agreement with a previous study from our group (Nadler et al., 2013).

We also observed a strong difference between SAG, SLG and 1,2-DOG in downstream signaling. The most potent signaling was initiated by unnatural 1,2-DOG that strongly activated ERK, RSK, FAK and S6K (Figure 3.14 B). In contrast, while SLG concentration was clearly increased, we did not detect the activation of downstream signaling in HeLa cells treated with this diacylglycerol (Figure 3.14 B). Moreover, although SAG induced the most transient response of the DAG FRET biosensor among all DAGs tested, SAG treatment led to the stronger activation of ERK, FAK and S6K in comparison to SLG (Figure 3.14 B). Together, this data strongly suggest that the fatty acid composition of DAGs modulates the rate of metabolism and downstream signaling.

3.1.4 Conclusions and Outlook

A GF signaling network is one of the cellular machineries that constantly encode information from extracellular cues and decodes it into specific cellular responses (Lemmon and Schlessinger, 2010). In order to reliably perform this essential task, a signaling network that consists of chemically diverse molecules utilizes signals of a distinct nature such as

concentration, chemical modifications, binding, subcellular localization and enzymatic activity (Landry et al., 2015). Importantly, dynamic properties including delay, duration, amplitude or fold change of these signaling events are also employed to transmit information along signaling pathways (Purvis and Lahav, 2013). Understanding of signaling network operation is impeded by the lack of approaches enabling the simultaneous detection of chemically diverse molecules and signaling events at the systems level. In this work, we have developed a FRET-based multi-parameter imaging platform (FMIP) that allows monitoring signaling events of diverse nature at the single cell level with high-temporal resolution in a single experiment. The unique combination of reverse transfection microarrays and FRET biosensor technologies allowed monitoring the activity of many signaling molecules in living cells that are under identical conditions. The latter led to higher reproducibility in comparison to a single FRET biosensor experiments. As a proof of principle we imaged 40 FRET biosensors over 5 hours with the help of this platform. To acquire the same data from a single FRET biosensor experiments it would take 200 hours of imaging on a microscope, which is also labor-intensive. Although each FRET biosensor is expressed in different cells, we were able to perform multidimensional analysis of the signaling network activity in different cell lines with statistically significant cell numbers. We believe that this platform will prove to be a useful tool for investigating diverse signaling networks including growth factors, cytokines, hormones and GPCRs.

To highlight the utility of the FMIP we experimentally demonstrated the potential application of the FMIP for the characterization of targets and off-targets of the clinically relevant MEK inhibitor (AZD6244). Our approach recapitulated known AZD6244 effects on EGF signaling and identified novel signaling interplay. For example, AZD6244 dramatically abrogated the ERK and RSK signaling as well as unexpectedly inhibiting PKA activity. One possible explanation is that the PKA activity is regulated by RSK. In support of this notion, it was previously shown that RSK is able to directly bind to PKA (Chaturvedi et al., 2006). However, later the same research group reported that RSK attenuated PKA activity (Gao and Patel, 2009). Although we are not able to exclude effects due to the signaling network architecture and/or the level of gene expression between HeLa and B82L cells, we believe that the observed differences might be explained by the experimental design. Whereas we detected PKA activation upon EGF stimulation, in the aforementioned studies the PKA activity is observed in the presence of slowly

metabolized cAMP analogue (8-pCPT-cAMP) (Gao and Patel, 2009) suggesting a low sensitivity of the assay. We therefore suspect that the experimental design in our study is relevant to physiological conditions. Thus, our observation suggesting a complex interplay between RSK, ERK and PKA upon EGF stimulation raises two important questions: (1) how does RSK potentiate PKA activity, and (2) is this complex interplay between RSK and PKA common for other cell types. Such questions will be investigated in future experiments.

Furthermore, using the FMIP we were able to profile perturbation caused by the constitutive active EGF receptor (EGFRmut) carrying clinically relevant mutations (L858R and T790M). We demonstrated much decreased responses in cells expressing EGFRmut in comparison to wild type cells, most probably due to increased basal activity. Our platform in combination with PCA allowed the multidimensional analysis of the signaling network activity. This analysis revealed the strong similarity between exogenously and endogenously EGFRmut-expressing cells. Surprisingly, the FMIP coupled to PCA could also visualize cell line dependent differences between non-small cell lung cancer cell lines and the cervical adenocarcinoma cell line. We believe that such largely unbiased profiling of signaling network activity in living cells will be a valuable approach to characterize and study disease-causing and network-perturbing mutations.

Receptor activation leads to the multiple amplification steps of downstream signaling. One might argue that the platform would fail to detect immediate signaling events without an amplification step. To test the FMIP under such conditions we investigated how the fatty acid composition of diacylglycerols (DAGs) affected downstream signaling. The platform was able to detect not only different dynamics of DAG metabolism but also a dramatic diversity in downstream signaling response depending on the fatty acid composition. Our data suggest that fatty acid composition might modulate DAG signaling at three related yet conceptually different levels: 1) regulating the rate of metabolism; 2) tuning signaling by DAG metabolites such as free fatty acids and 3) tuning the affinity to direct DAG effectors including PKC. Further investigations and experiments are needed to decouple the relative contribution of each level into DAG signaling and to study their downstream effects on the signaling network activity.

In the future, this platform can be extended further by coupling it with any assay that can be detected by fluorescence microscopy. For example, FRET biosensors could be combined with translocation probes to multiplex the detection of several signaling events in the same cell (Regot et al., 2014). Additionally, the unique design of the FMIP enables its integration with recently developed techniques for signaling manipulation such as perfusion systems, optogenetics or caged molecules that allows precise control over extracellular environment and protein or lipid activity, respectively (Nadler et al., 2013; Toettcher et al., 2013). Moreover, our platform can be used in combination with siRNA libraries, which unlocks the possibility for kinome- or genome-wide perturbation of the signaling network. Thus, further development of this platform by expanding its functionality will enable deeper insights into the basic principles of signal transduction.

Our approach has several limitations. First, we expect low transfection efficacy for most primary cells that, generally, are difficult to transfect. However, the platform can be improved employing lentivirus-based plasmid delivery which has demonstrated high rates of transfection for hard-to-transfect cells (Bailey et al., 2006). Second, all results in this platform rely on FRET biosensors; for this work, we utilized FRET biosensors that were previously published and characterized. We believe that novel biosensors covering additional signaling parameters as well as new generations of existing sensors with improved dynamic range, sensitivity and selectivity will further advance the overall performance of the FMIP in the near future.

3.2 Signaling network integration and processing of multiple extracellular cues

Cells have an amazing ability to monitor and adapt to environmental changes, continuously deciding whether they survive, differentiate, undergo apoptosis or migrate. Although individual cytokine, growth factor and hormone signaling networks have been characterized in detail, the understanding how cells, using a limited number of signaling components, integrate and process information from numerous external cues is one of the major challenges of cell biology. This question is also relevant for clinical research since overexpression or spontaneous activation of various receptors as well as perturbations of downstream signaling components due to mutations

are well-known mechanisms for the development of cancer and drug resistance (Arteaga and Engelman, 2014; Duncan et al., 2012; Pazarentzos and Bivona, 2015). Additionally, it has been shown that complex tumor micro-environments could influence therapeutic response (Junttila and de Sauvage, 2013; Straussman et al., 2012). Therefore, the understanding of basic principles of processing multiple extracellular cues and their dysregulation in diseases will expand and improve current therapeutic strategies for intervention in various diseases including cancer.

We hypothesized that cells encode signals from multiple extracellular cues through the dynamics of signaling network activity and later decode this information into gene expression and, finally, cell fate decisions. It was earlier proposed that a plausible mechanism of signal transduction is through signaling interaction among pathways such as synergy and antagonism (Chatterjee et al., 2010; Hsueh et al., 2009; Natarajan et al., 2006). Those regimes are unique and are not predictable from the individual components of a signaling network and/or the individual treatments with a single cue (Chatterjee et al., 2010). Only the combinatorial stimulation with simultaneous quantitative monitoring of signaling network events will allow us to understand the integration of information from multiple cues and the function of signaling networks in living cells. Such extended data sets will reflect the complexity of the cellular signaling networks, but are labor-intensive to generate in a comprehensive fashion by conventional approaches.

3.2.1 Overview of the approach

We sought to study the processing of multiple extracellular cues in a biologically relevant context. In this thesis, I considered the signaling interaction between RTK networks for the following reasons: (1) individual RTK signaling networks (or GF signaling networks) are relatively well-studied (Hill et al., 2016; Wagner et al., 2013), (2) RTKs signal through a shared set of signaling molecules yet can have distinct biological functions *in vivo* (Vasudevan et al., 2015), and (3) aberrant RTK signaling is involved in various diseases including cancer (Verstraete and Savvides, 2012; Wilson et al., 2012). I applied the FRET-based multi-parameter imaging platform (FMIP, see chapter 3.1) to monitor key RTK signaling network components

with high temporal resolution in living cells. This unique experimental system is able to monitor multiple RTK-induced signaling pathways including survival (PI3K/AKT/S6K), mitogenic (EGFR/Ras/Raf/ERK), calcium (PKC, CaMKIIa, Calcineurin) and migratory (FAK, Src, Cdc42, Rac1, RhoA) signaling over 5 hours in a single experiment. As an experimental model we chose HeLa cells that are easily transfected and most importantly express the receptors of interest including EGFR, IGF-1R, c-Met, TNFR. We also believe that signaling characterization of HeLa cells will be valuable for the scientific community since these cells are relatively often utilized in signaling studies. In typical experiments HeLa cells were serum starved for 12-16 hours and then at time $t = 0$ min stimulated with one of 5 growth factor/cytokines or their combination. In order to study signaling network activity at the single cell level we typically identify four representative dynamic patterns for each FRET biosensor separately. To this end we pulled single cell traces from across all treatments together and subjected them to K-means clustering (Figure 3.15). We used the cell proportions in those clusters as signatures of dynamic activity.

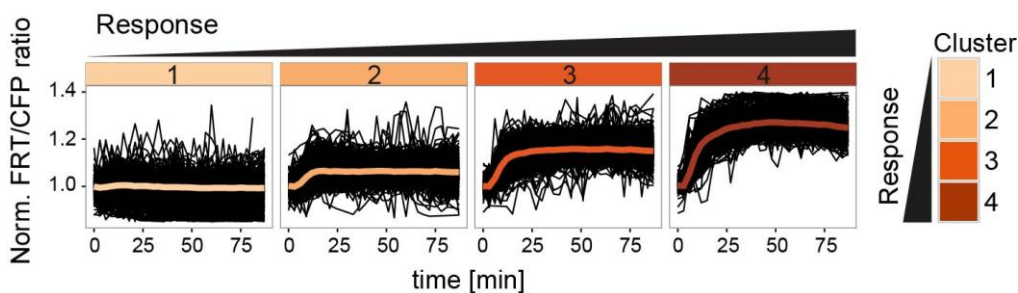


Figure 3.15 K-means clustering of single cell S6K activation as representative example of 4 clusters.

Such a single-cell approach enables all-or-nothing or graduated responses to be distinguished. PCA was also used to decrease the dimensionality of the average data generated by the FMIP and to compare global signaling changes in an unbiased manner. One of the unique features of the PCA coordinate system is linearity that allows signaling interactions (synergy, additivity and antagonism) to be visualized. In addition, the unique combination of multi-parameter signaling data with PCA increases sensitivity to detect signaling perturbation in comparison to a single-signaling event approaches. This is achieved because PCA coordinates are composed of linear combinations of multiple signaling network activity measurements. Thus, we were able to

characterize the signaling network activity at the single cell (K-means clustering) and population (PCA) levels.

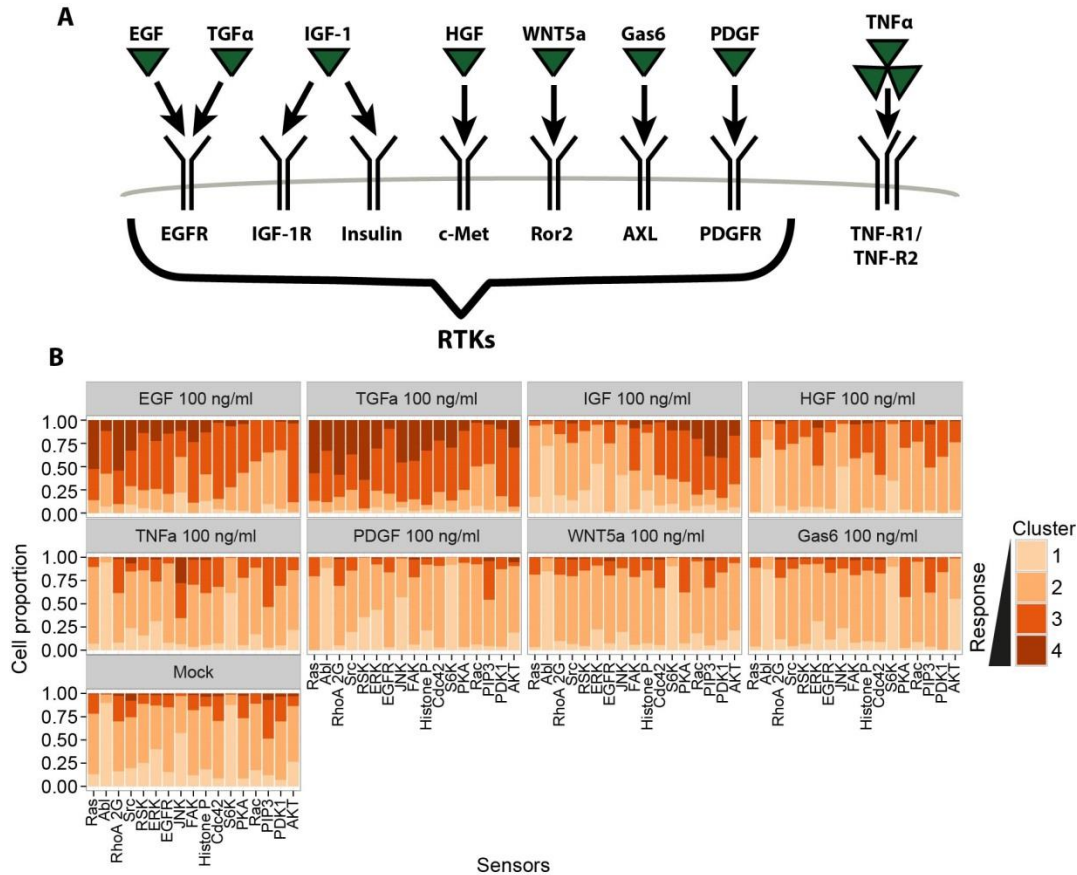


Figure 3.16 The identity of the extracellular cues specifies characteristic dynamic signaling responses in living HeLa cells. (A) Overview of GFs and cytokines signaling studied in this work. The Binding of EGF, TGF α , IGF-1, HGF, WNT5a, Gas6, PDGF and TNF α to their respective receptors is shown. **(B)** Distribution of FRET biosensors time series in response to various stimuli. HeLa cells were treated with 100 ng/ml EGF, 100 ng/ml TGF α , 100 ng/ml IGF-1, 100 ng/ml HGF, 100 ng/ml WNT5a, 100 ng/ml Gas6, 100 ng/ml PDGF or 100 ng/ml TNF α . $n > 50$ cells for each sensor/stimulus pair.

3.2.2 Single stimulus treatment experiments

In order to select stimuli for combinatorial screening, we first performed single-stimulus experiments in which HeLa cells were stimulated with 100 ng/ml of PDGF, EGF, TGF α , IGF-1, HGF, Gas6 or WNT5a (Figure 3.16A). In order to verify that the signaling interaction is common mechanism of signal integration we also included TNF α which binds to the receptor of different protein family. Each of these signaling molecules binds to well-known receptors that

induce signaling that has been intensively characterized (Figure 3.16 A). Although PDGF, Gas6 and WNT5a did not induce reliable signaling changes we detected strong responses upon stimulation with EGF, TGF α , IGF-1, HGF and TNF α (Figure 3.16 B). We observed a unique signaling network activity that was characteristic for each stimulus. For example, IGF-1 strongly activated the PI3K/AKT/S6K signaling pathway whereas EGF and TGF α induced stronger signaling through the Ras/ERK/RSK and Src/FAK pathways. Importantly, we could also detect dramatic signaling induced differences between EGF and TGF α that act through the same receptor, EGFR. In good agreement with previous studies, TGF α induced much stronger signaling responses in comparison to EGF (Ebner and Derynck, 1991; Francavilla et al., 2016; Scholler et al., 2017). Using PCA we were able to efficiently visualize the differential activation of signaling pathways as well as distinct signaling dynamics (Figure 3.17). The PCA clearly indicates that time points belonging to the same treatment are clustered together. Thus the GFs and cytokines are able to induce the specific responses that are efficiently visualized and distinguished in the PCA space.

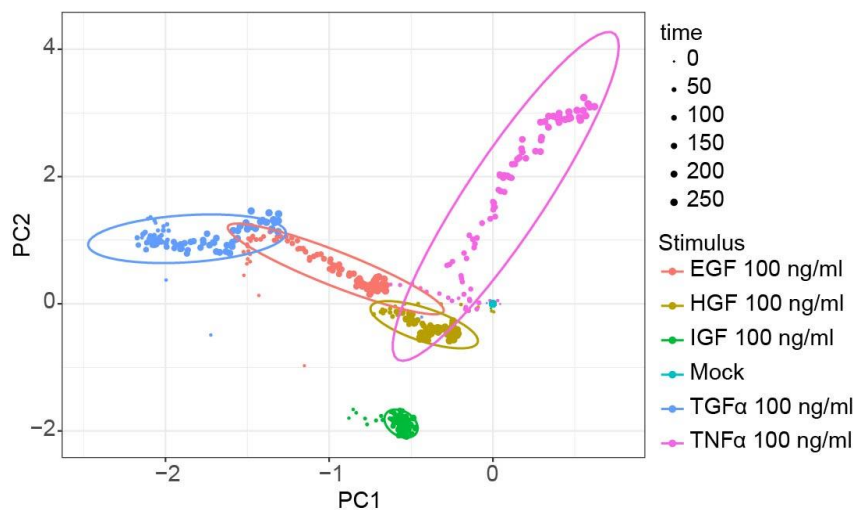


Figure 3.17 The identity of the extracellular cues specifies their location in PCA space.

3.2.3 Pairwise treatment experiments

We hypothesized that the cross-talk (signaling interaction) between GFs is not only dependent on identity of the GFs but most importantly on their concentration and/or ratio (relative amounts). To evaluate the signaling interactions we carried out pairwise treatment experiments using

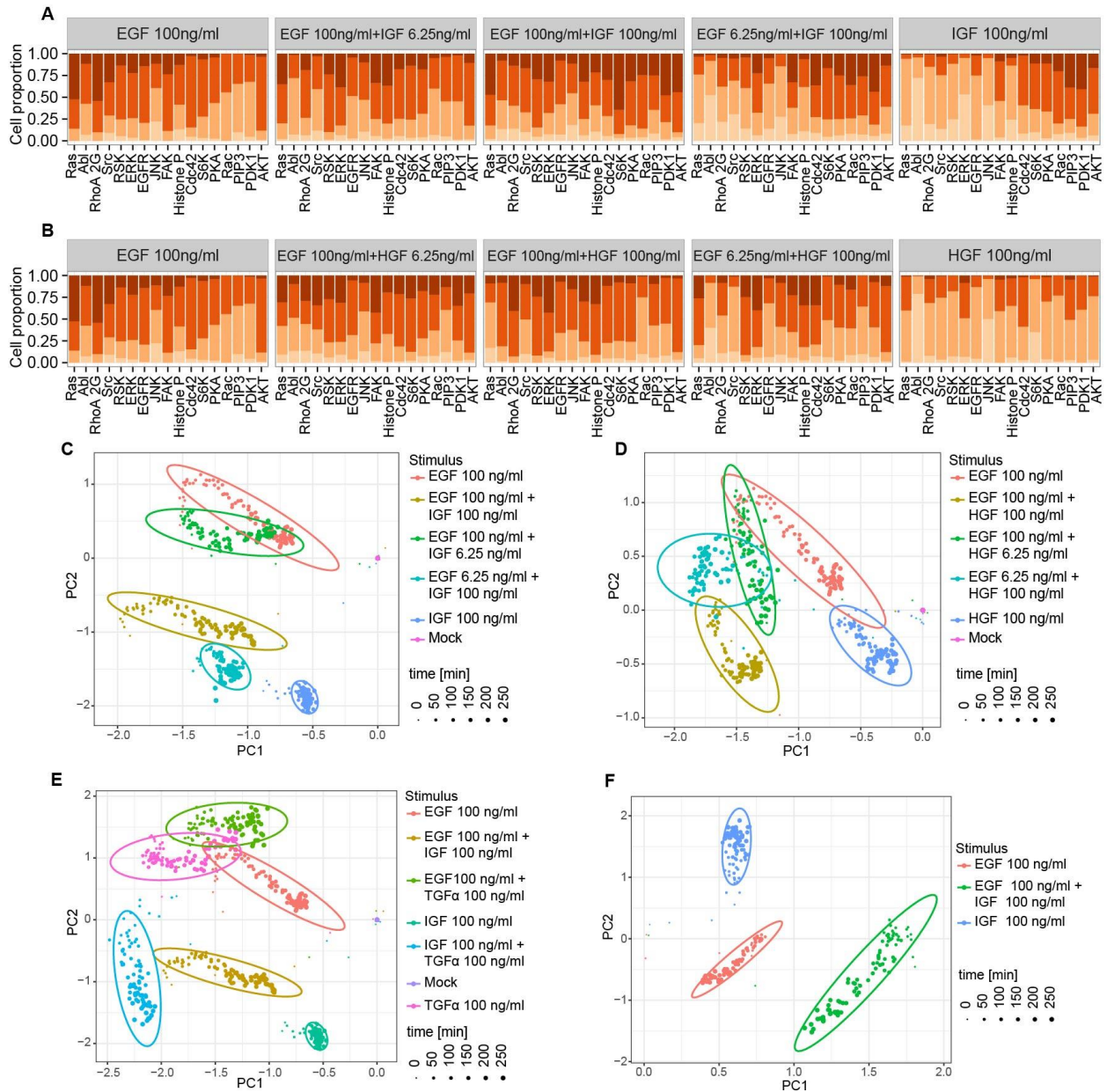


Figure 3.18 Crosstalk of two growth factors shapes signaling dynamics. (A) Cross-talk between EGF and IGF-1 signaling networks. (B) Cross-talk between EGF and HGF signaling networks. (C) PCA of the average EGF and IGF-1 signaling interaction. (D) PCA of the average EGF and HGF signaling interaction. (E) PCA of the average EGF, TGF α , and IGF-1 signaling interaction. (F) PCA of the average EGF and IGF-1 signaling interaction in H838 cells. Each dot in PCA represents a single time point while the ovals indicate 95 % of time points of the same treatment.

different concentrations of GFs. The co-stimulation of HeLa cells with two growth factors showed concentration dependent features that are the combination of the signatures characteristic for individual treatments (Figure 3.18 A and B).

A concentration dependent interaction was observed between EGF and IGF-1 as well as between EGF and HGF, indicating that this mechanism of signaling network tuning is a general way of signal integration from multiple growth factors in HeLa cells. Moreover, using PCA it can be seen that condition-specific network activity occupies a unique position in the PCA space (Figure 3.18 C and D). Surprisingly, the PCA clearly illustrates that the shift of time points belonging to the same combinatorial treatment is not proportional to the concentration or to the ratio of GFs (Figure 3.18 C and D). Importantly, although EGF and TGF α bind to the same RTK, EGFR, they have slightly different profiles of signaling interaction with IGF-1 suggesting that the interaction is also tuned by the identity of the stimuli that have unique signaling characteristics (Figure 3.18 E). We also demonstrated that signaling interaction between EGF and IGF-1 occurs in H838 cells (Figure 3.18 F). Overall, the data strongly suggest that signaling interactions (antagonism, additively and synergy) are a common mechanism of a single system integration from multiple extracellular cues.

3.2.4 Signal integration from the pair of extracellular cues.

We hypothesized that the observed signaling interaction between two stimuli might be due to receptor cross-reactivity, downstream signaling amplification and/or inhibition as well as autocrine signaling. To study the integration mechanisms from two extracellular cues on the molecular level we calculated a synergy score (Ss) according to the following equation:

$$\text{Synergy score (Ss)} = \frac{\sum A+B - (\sum A + \sum B)}{\max|\sum A+B - (\sum A + \sum B)|}$$


Ss > 0, synergy
Ss = 0, additivity
Ss < 0, antagonism

The synergy score demonstrates the relative difference between the area under the curve for the combined response to stimuli A and B versus the area under the curve for both individual stimuli responses added together, normalized to the maximum absolute Ss for each FRET sensor

(Chatterjee et al., 2010; Kuchenov et al., 2016). This means that the synergy score is able to detect non-additive signaling interactions: namely synergy and antagonism. A positive S_s value indicates synergistic behavior between stimuli A and B whereas a negative S_s value suggests antagonistic or saturating behavior. At the same time $S_s = 0$ represents a purely additive response or the absence of response.

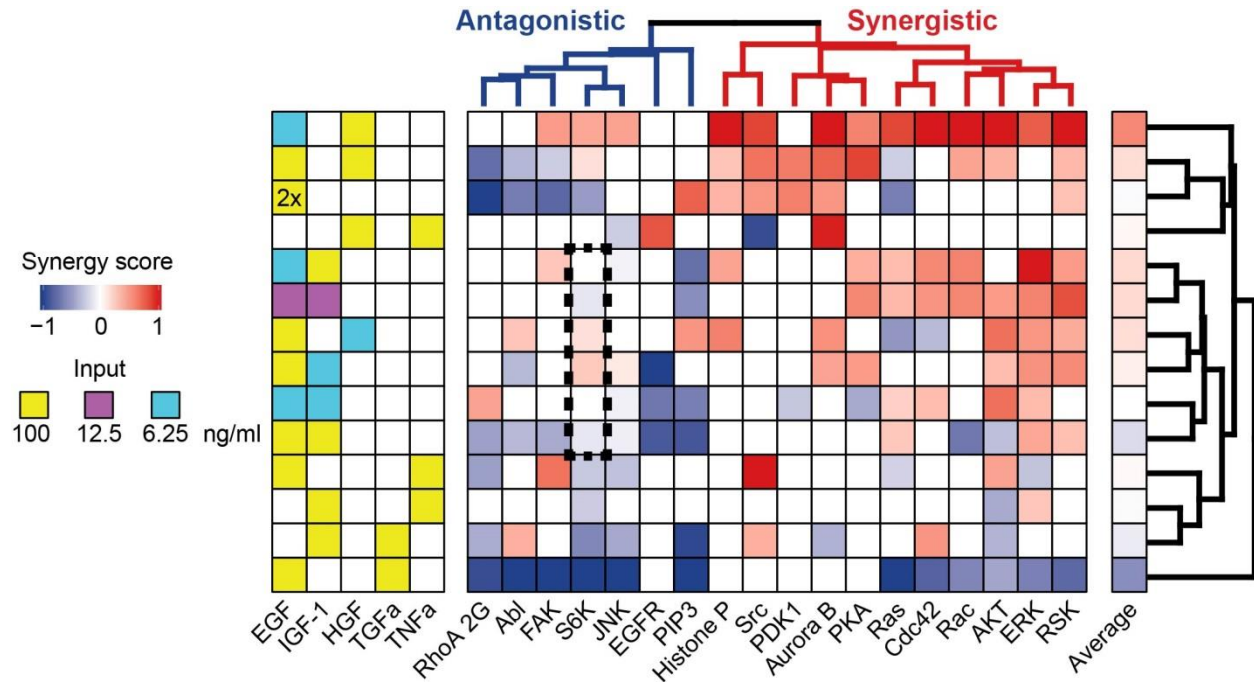


Figure 3.19 Composite interaction map reflecting antagonism, additivity and synergy due to GFs signaling interaction. The matrix of synergy scores was hierarchically clustered with the Euclidean metric and the Ward linkage. All insignificant values (P value ≥ 0.05) are colored white.

We created a composite interaction map to visualize signaling interaction modes between two stimuli (Figure 3.19 B). Interestingly, we observed that the interaction between 100 ng/mL EGF and 6.25 ng/mL HGF induced the strongest synergy in our data set (Figure 3.19 B). The strongest antagonistic affect was achieved between 100 ng/mL EGF and 100 ng/mL TGF α , most probably due to saturation of the signaling network activity. The hierarchical clustering of the map suggests that the signaling events can be clearly segregated in to at least two groups by synergy properties: synergistic and antagonistic responses. Surprisingly, the signaling interaction mode was dependent on the concentration of two stimuli that clearly explains the non-proportional shift in the PCA space (Figure 3.19 B, dashed line selected area). For example, 100 ng/ml EGF and 100 ng/ml IGF-1 strongly activate S6K although with distinct dynamics, but the

combined action of the two is lower than that expected for their additive effect (antagonism). However, a decrease of either EGF or IGF-1 concentration induces the additive or synergistic effect in the S6K activation, respectively. In contrast, the interaction between 12.5 ng/ml EGF and 12.5 ng/ml IGF-1 induced a slightly antagonistic effect in S6K activation. Thus, the interaction modes shape the response of each signaling component individually that in turn allows tuning global signaling responses.

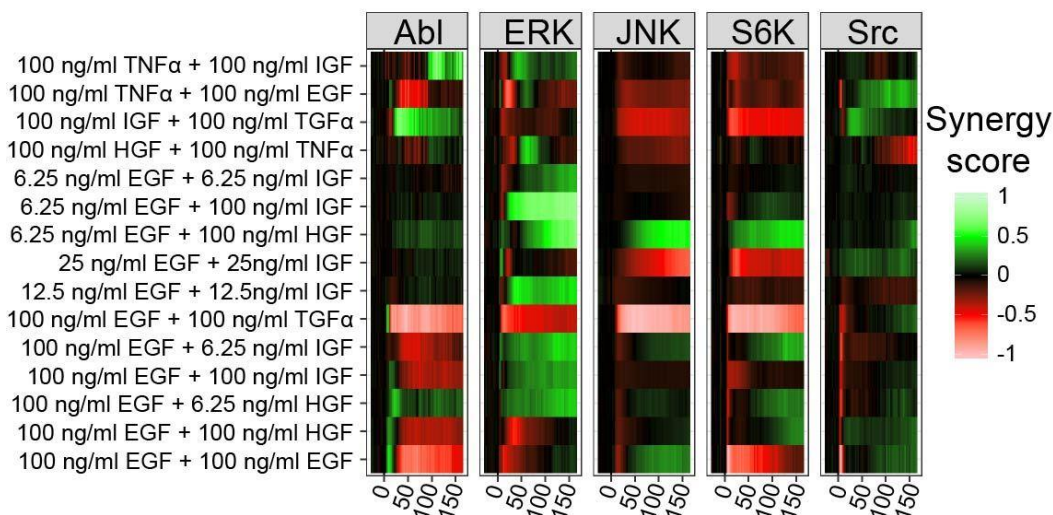


Figure 3.20 The dynamics of signaling interactions. HeLa cells were stimulated at time 0. Synergy score was computed for each time point and normalized to the maximum observed absolute value for each sensor separately.

It is well-known that one of the characteristic features of cellular signaling is dynamics. It is therefore plausible that a signaling interaction between two stimuli would be highly dynamic as well. Thus we were anxious to use our data to evaluate the dynamic properties of signaling interactions. We calculated a synergy score for each time point separately and plotted it over time (Figure 3.20). Indeed, we observed highly dynamic properties of the signaling interactions. Surprisingly, the synergy score may change interaction mode over time illustrating a new level of complexity that has to be taken under consideration in future studies. For example, JNK activated by 100 ng/ml EGF + 100 ng/ml IGF-1 shows gradual decrease from negative to positive interaction mode. In contrast, under the same conditions Abl changes the synergy score from positive to negative.

3.2.5 Signaling interactions tune gene expression profile

We next explored how paired signaling interactions may change gene expression profile in cells by focusing on the interaction between EGF and IGF-1 because (1) EGF and IGF-1 differentially activated signaling pathways (chapter 3.2.2) and (2) strong synergistic as well as antagonistic signaling interactions were also identified (chapter 3.2.4). Figure 3.21 shows the workflow of the mRNA sequencing (mRNA-seq) screen as it was performed. Briefly, HeLa cells were seeded on 6 cm dishes previously covered with gelatin. Prior to stimulation cells were starved in the absence of serum overnight. Afterwards, cells were incubated under ten different conditions for 4 hours: (1) untreated (Mock), (2) 6.25 ng/ml EGF, (3) 6.25 ng/ml IGF-1, (4) 12.5 ng/ml EGF, (5) 12.5 ng/ml IGF-1, (6) 100 ng/ml EGF, (7) 100 ng/ml IGF-1, (8) 12.5ng/ml EGF + 12.5ng/ml IGF-1, (9) 6.25 ng/ml EGF + 100 ng/ml IGF-1, (10) 100 ng/ml EGF + 6.25 ng/ml IGF-1, (11) 100 ng/ml EGF + 100 ng/ml IGF-1 (figure 3.21). These conditions were used to profile signaling interactions between EGF and IGF-1 in chapter 3.2.4. Afterwards, the cells were harvest by the direct addition of Trizol to the cells after media removal. DNase digestion was followed by total RNA isolation using the RNeasy Mini Kit. The total mRNAs library were purified and then subjected to the next-generation sequencing pipeline.

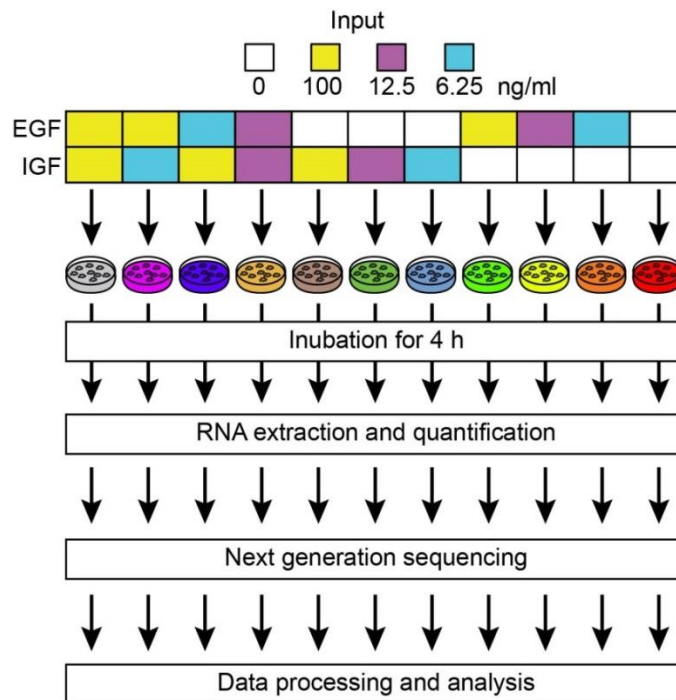


Figure 3.21 Schematic overview of the RNA-seq screen performed with GFs.

The mRNA-seq screen was performed in independent triplicates and yielded a total of 11787 differentially expressed genes (DEGs) compared to untreated cells (Mock) that have adjusted P value <0.05 . The reproducibility of the screens was visualized by subjecting of the data to the PCA. Replicates of the same condition were clearly clustered together suggesting a good reproducibility between independent screens (Figure 3.22 A). PCA of gene expression also revealed pronounced changes between cells treated with low and high concentration of growth factors. As expected, the tendencies depicted by PCA of gene expression data are similar to PCA of signaling data (Figure 3.22 A and B). For example, “100 ng/ml EGF only” and “100 ng/ml IGF-1 only” treatments are clearly separated whereas the combinatorial treatment, 100 ng/ml EGF + 100 ng/ml IGF-1, is placed in between. However, we did not observe clear segregation of “100 ng/ml EGF only” and “100 ng/ml EGF + 6.25 ng/ml IGF-1” as well as “100 ng/ml IGF-1 only” and “6.25 ng/ml EGF + 100 ng/ml IGF-1” conditions, most probably, due to low number of unique and/or differentially expressed genes under those conditions.

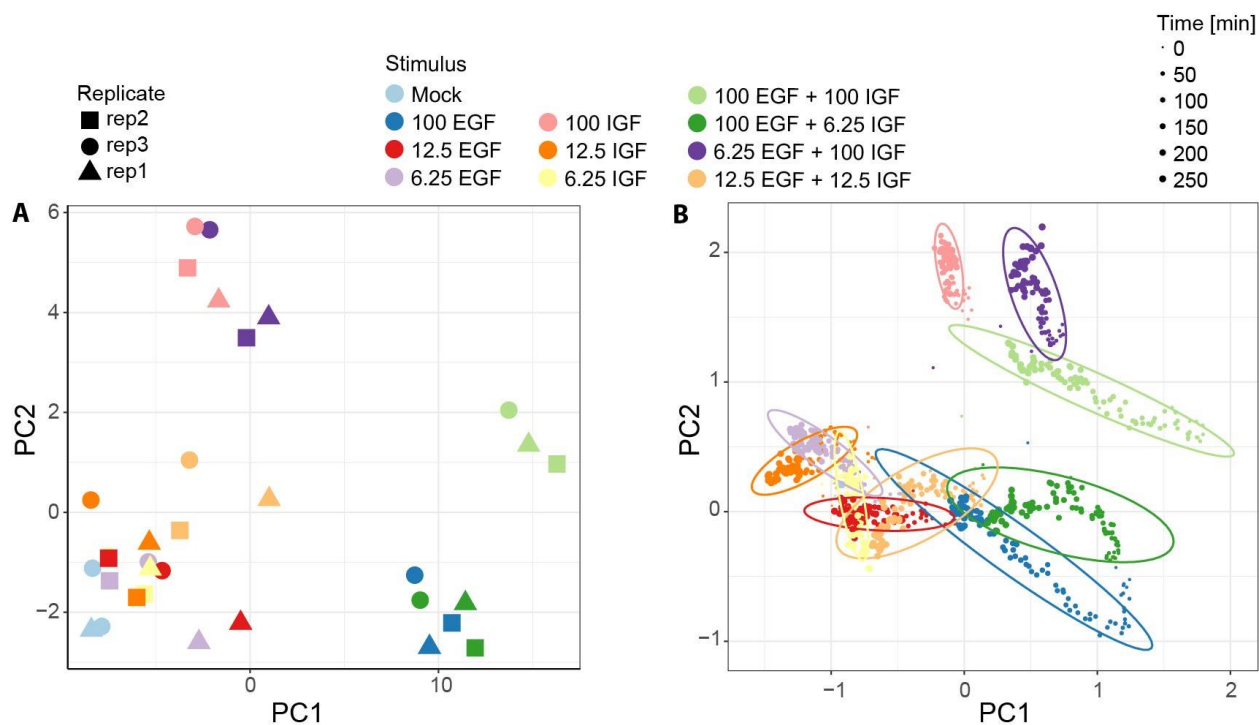
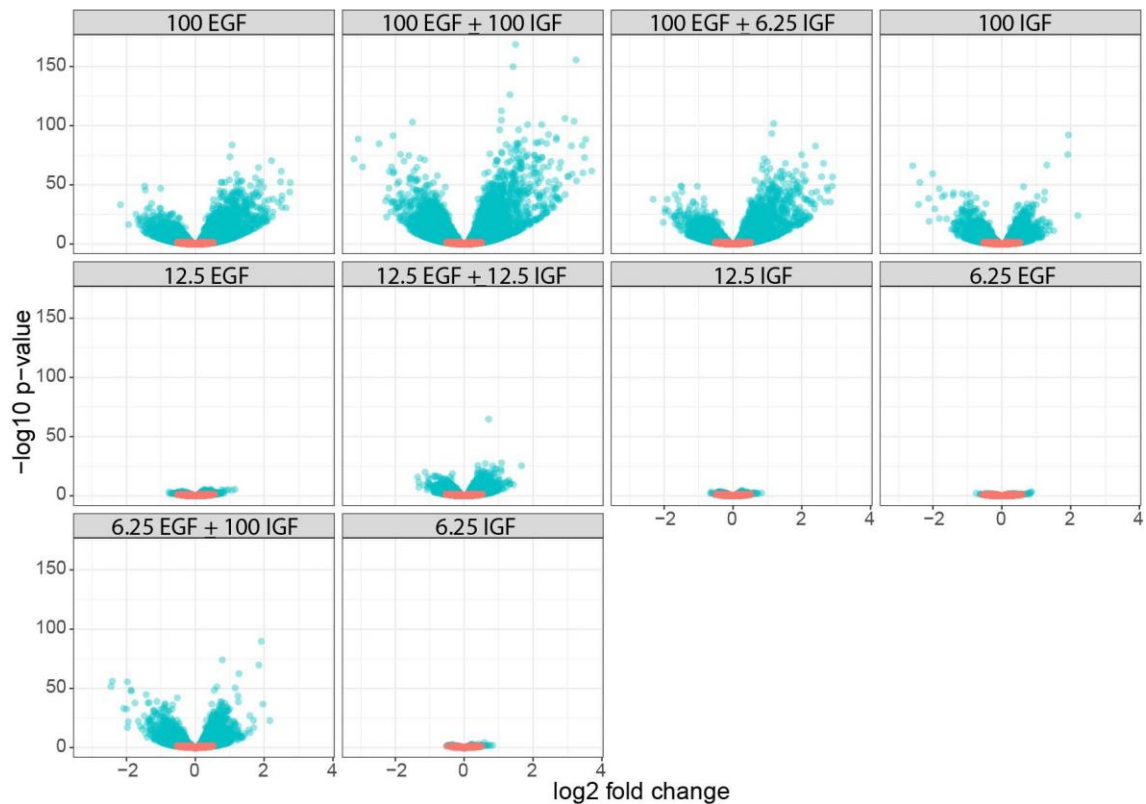


Figure 3.22 Gene and signaling response dynamics after single or pairwise stimulation. (A) Principal component analysis (PCA) of the HeLa cell transcriptomes. **(B)** PCA of the HeLa cell signaling response.

Table 3.1: *The DEGs identified for each condition vs Mock cells*

Condition	Up-regulated	Down-regulated	Unique up-regulated	Unique down-regulated	total
100 ng/ml EGF + 100 ng/ml IGF	4895	4235	567	615	9130
100 ng/ml EGF + 6.25 ng/ml IGF	4196	3421	206	247	7617
6.25 ng/ml EGF + 100 ng/ml IGF	3423	2617	88	73	6040
100 ng/ml EGF	3945	3113	105	119	7058
100 ng/ml IGF	3401	2589	254	212	5990
12.5 ng/ml EGF + 12.5 ng/ml IGF	2707	1824	167	186	4531
12.5 ng/ml EGF	701	293	8	1	964
12.5 ng/ml IGF	380	218	5	2	598
6.25 ng/ml EGF	58	52	0	0	110
6.25 ng/ml IGF	123	36	0	0	159

**Figure 3.23** Volcano plots of differentially expressed genes (DEGs). Genes at $p < 0.01$ are colored with blue.

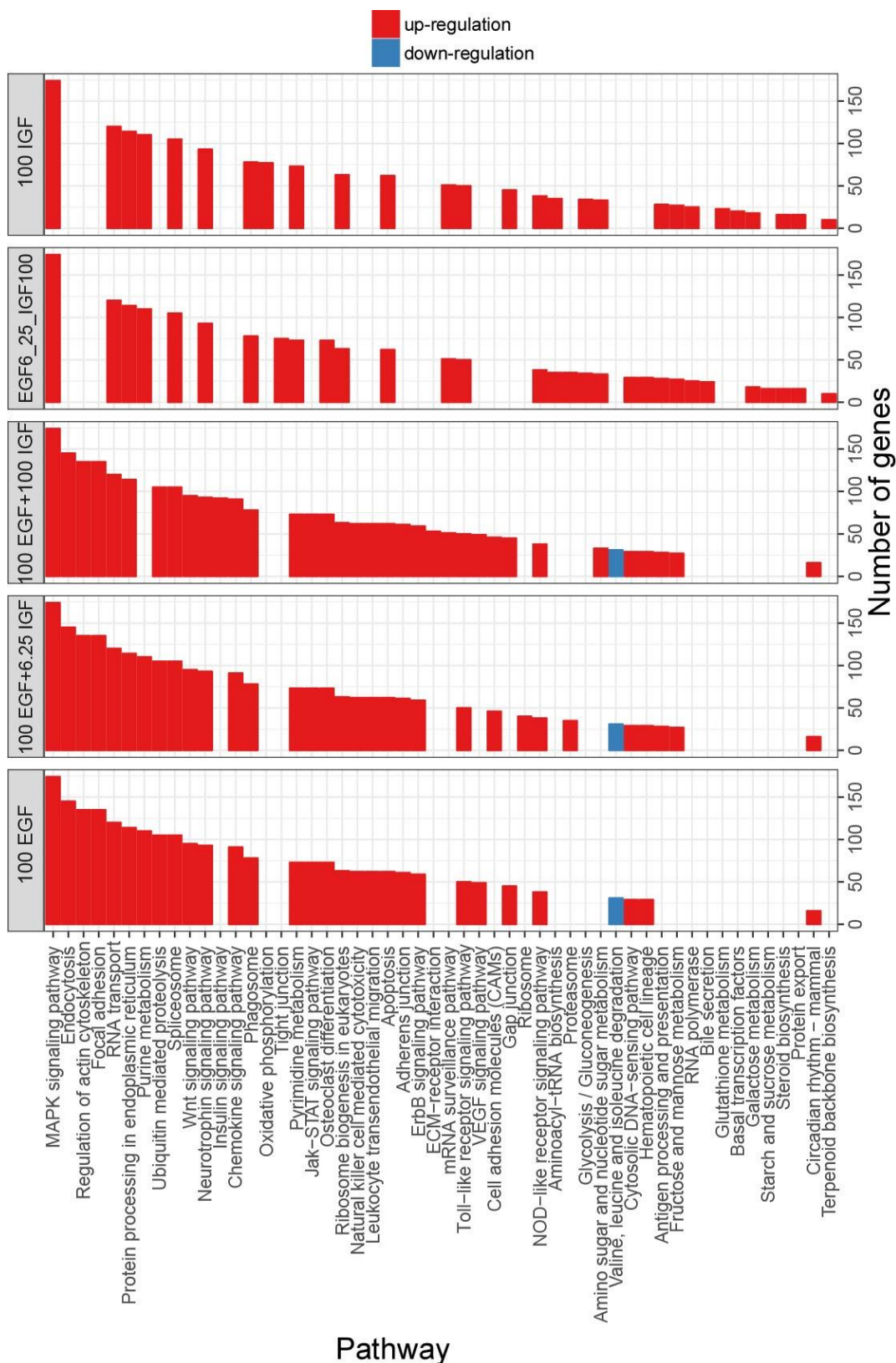


Figure 3.24 Signaling pathway enrichment analysis of DEGs. Pathways at $p < 0.01$ are depicted.

In order to visualize the difference between those conditions we identified condition specific genes. Interestingly, I was not able to achieve significant enrichment of unique genes under “EGF only” and “IGF-1 only” conditions of low concentrations (≤ 12.5 ng/ml) (Table 3.1). However, “12.5 EGF ng/ml + 12.5 ng/ml IGF-1” condition increased the number of condition specific genes (Table 3.1). Importantly, we also observed the boost of total differentially expressed genes upon co-treatment with EGF and IGF-1 of suboptimal concentration (12.5 ng/ml) in comparison to individual GFs of the same concentration (Figure 3.23) suggesting strong interaction of EGF and IGF-1 under sub-optimal concentrations on the level of gene expression. In addition, analysis of biological process enrichment for genes that are differentially expressed after stimulation showed overrepresentation of signaling pathways common for all experimental conditions such as MAPK, neurotrophin and Toll-like receptor signaling pathways. In contrast, we were able to identify overexpression of signaling pathways under few conditions, for example VEGF signaling pathway is overexpressed after stimulation with 100 ng/ml EGF or co-stimulation 100 ng/ml EGF + 100 ng/ml IGF-1. A unique signaling pathway overexpression was also identified under one condition (ECM-receptor interaction pathway, 100 ng/ml EGF + 100 ng/ml IGF-1). The comparison of gene expression profiles of cells treated with single and combined growth factors allowed us to define genes poised for expression in a condition-specific manner. Moreover, our data indicate that concentration and/or ratio of growth factors tune signaling network state through differential expression of genes involved into specific signaling pathways and cellular processes. Overall, these data suggest that the signaling interactions between EGF and IGF-1 that are of sub-optimal physiologically relevant concentrations potentiate responsiveness of the cells on the level of gene expression and also shape the signaling network state.

3.2.6 Signaling interactions shape signaling response under quasi-physiological conditions

The physiological levels of GFs are much lower than the concentrations that are typically used in cellular signaling studies (Francavilla et al., 2016; Hill et al., 2016; Sigismund et al., 2005). A potential reason might be that the protocol usually used by the scientific community implements non-physiological procedures potentially influencing cellular signaling. For example, in the

majority of signaling studies, cells are starved overnight in the absence of fetal bovine serum (FBS) (Francavilla et al., 2016; Hill et al., 2016). It is broadly believed that the starvation of cells reduces basal activity, supports uniform cellular responses and is also dissecting for cue-specific signaling. At the same time our data strongly suggest that depending on the extracellular environment, the signaling network activity is tuned and in turn specifies the responses of cells to the GF treatment. Notably, we observed stronger response induced by pairwise treatment indicating higher responsiveness under such conditions. The responding FRET biosensors in our library are sensitive enough to monitor signaling in a single cell. We therefore reasoned that our FRET biosensor-based platform is overall more sensitive to changes in the activity of a signaling network over time in comparison to standard end-point population approaches such Western Blot and mass spectrometry. Thus, we hypothesized that under physiological condition when cells are exposed to the many extracellular cues of low concentrations, we would observe dramatically different signaling responses.

To study the signaling under quasi-physiological conditions we focused on a suboptimal concentration of EGF. We used our platform to monitor EGF signaling in overnight serum starved and non-starved HeLa cells. As expected, non-starved HeLa responded with dramatically distinct dynamics (Figure 3.25 A). Surprisingly, the signaling response was much stronger in the presence 10% of FBS in comparison to starved HeLa cells. For example, we observed stronger activation of AKT, Cdc42, EGFR, ERK, JNK, PDK1, PIP3, Rac1, Ras and Src in non-starved cells. In contrast, we observed inhibition of RhoA in the presence of 10% FBS. Although RSK and S6K did not show stronger activation, their overall dynamics were distinct between starved and non-starved cells. This experiment suggests that supplementing with 10% of FBS tunes the signaling network state to achieve higher responsiveness of the cells to physiological levels of EGF.

Next, using PCA we analyzed the global signaling response in starved and non-starved cells. PCA showed a clear separation between starved cells treated with range of EGF concentrations and non-starved cells, indicating that the presence of 10% FBS results in unique features of EGF signaling (Figure 3.25 B). Collectively, these data suggest that the molecular composition of

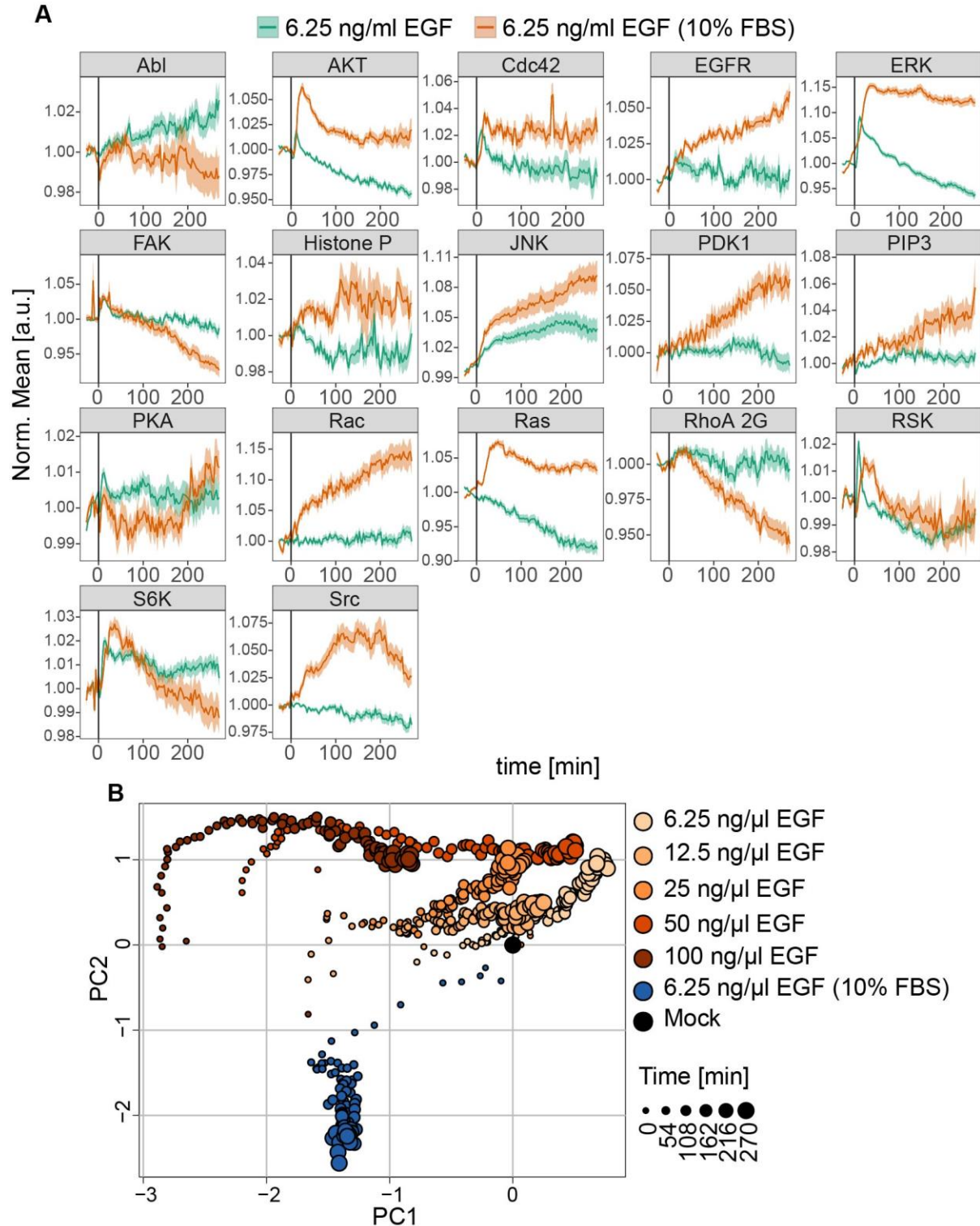


Figure 3.25 Quasi-physiological condition shape EGFR response. (A) Signaling responses to 6.25 ng/ml EGF in the presence or absence of 10% FBS. HeLa cells were stimulated at time 0. (B) PCA of the average EGF response in HeLa cells. Each dot represents a single time point.

10% FBS potentiates responsiveness of the cells and most importantly shapes the EGF-induced signaling response under sub-optimal physiologically relevant concentration.

3.2.7 Conclusions and Outlook

Under physiological conditions mammalian cells are constantly exposed to numerous extracellular signals such as growth factors, cytokines and hormones. They are able to constantly monitor the identity and the concentration of extracellular cues and adapt their cellular state to the sudden physiological changes accordingly. This adaptation to the environmental changes is achieved through an intertwined signaling network that is composed of a limited number of components. The dynamic interplay between components of this signaling machinery is able to encode the extracellular information and regulate the specific cellular responses. Although individual cytokine, growth factor and hormone signaling networks have been characterized in detail, the understanding how cells, using the limited number of signaling components, integrate and process information from the numerous extracellular cues is not completely understood. In this work, we investigated the tuning of signaling network activity by multiple growth factors in living cells.

Using our FRET-based multi-parameter imaging platform we profiled temporal changes in signaling network activity induced by the five ligands EGF, TGF α , IGF-1, HGF and TNF α . As expected, monitoring distinct signaling pathways including those relevant for survival (PI3K/AKT/S6K), mitogenesis (EGFR/Ras/Raf/ERK/RSK) and migration (FAK/Src; Cdc42/Rac1/RhoA), we detected unique signaling network activity dynamics that were characteristic to specific extracellular cues (Ronan et al., 2016; Wagner et al., 2013). We also confirmed that although EGF and TGF α bind to the same receptor, EGFR, they induce distinct dynamic signaling through a network (Francavilla et al., 2016). Importantly, we observed different signaling dynamics between different epithelial cancer cells, HeLa and H838, treated with the same stimuli and concentration. This is consistent with previous work in which it has been shown that different epithelial cells have distinct cellular outcomes to the same combinatorial treatment (Miller-Jensen et al., 2007). The data supports the concept that each ligand-receptor

pair differently controls a dynamic signaling program. In addition, we illustrated that a signaling response is unique for each cell line and is adjusted by internal cellular parameters such as protein abundance and/or signaling network connectivity.

We further showed signaling cross-talk between two extracellular stimuli in HeLa cells. To this end we treated cells with two stimuli simultaneously to reveal crosstalk. Similar non-additive interactions between pairwise combinations of ligands have previously been observed in distinct human cells (Beyer and MacBeath, 2012; Borisov et al., 2009; Natarajan et al., 2006). Those interactions are crucial for the regulation of distinct cellular process such as proliferation, apoptosis and cytokine secretion (Janes et al., 2005; Martin et al., 2009). As expected, pairwise treatment induced combinations of dynamic signaling features that were characteristic of each individual combination of stimuli. Importantly, by employing PCA we observed non-linear global signaling responses that were clearly explained by three signaling interactions modes: additivity, antagonism or synergy. Altogether we observed about 52% of non-additive signaling interactions within the whole landscape of measured signaling parameters. Closely related receptors had a higher order of interaction compared to receptors belonging to more distant families. For instance, in our data set 56% of interactions between RTKs were non-additive whereas unpredicted signaling interactions between RTKs and TNFRs were about 35% non-additive indicating that evolutionary closely related receptors employ highly overlapped downstream signaling effectors. The combinatorial extracellular code raises distinct dynamic signaling responses through signaling interaction modes. The identification of these signaling interaction modes raises important questions such as what is their physiological significance and how is the signaling interaction code interpreted or decoded on the level of gene expression?

In good agreement with a previous study focused on the interaction of the single protein kinase ERK (Borisov et al., 2009), we showed for the first time at the systems-level that those interaction modes were stimulus concentration and/or ratio dependent across many signaling nodes. We propose that those concentration- and ratio-dependent signaling interactions are crucial for signal transduction under physiological conditions when cells are exposed to many extracellular signaling cues. The extracellular environment that is defined by the identity of the cues and their concentrations specifies the signaling network activity state. In support of this

hypothesis we showed the potentiation and, most importantly, the tuning of dynamic EGF signaling under quasi-physiological concentration in non-starved cells. Overall the present results suggest that under physiological conditions, in the presence of multiple signaling cues of low concentrations, the cellular signaling network is pre-activated and tuned to achieve specific strong responses to low concentrations of ligands. This is in contrast to the common use of high ligand concentrations in cellular signaling studies that rely on long term serum starvation. The underlying mechanism controlling the signaling activity state by multiple cues is not fully clear but it is linked to two coupled but conceptually distinct levels working at the different time scales: (1) protein abundance and network topology is controlled by gene expression and/or protein degradation that works in the order of hours and (2) the signaling activity as well as network connectivity is regulated through signaling cross-talk emerging in the order of seconds or minutes (Figure 3.26).

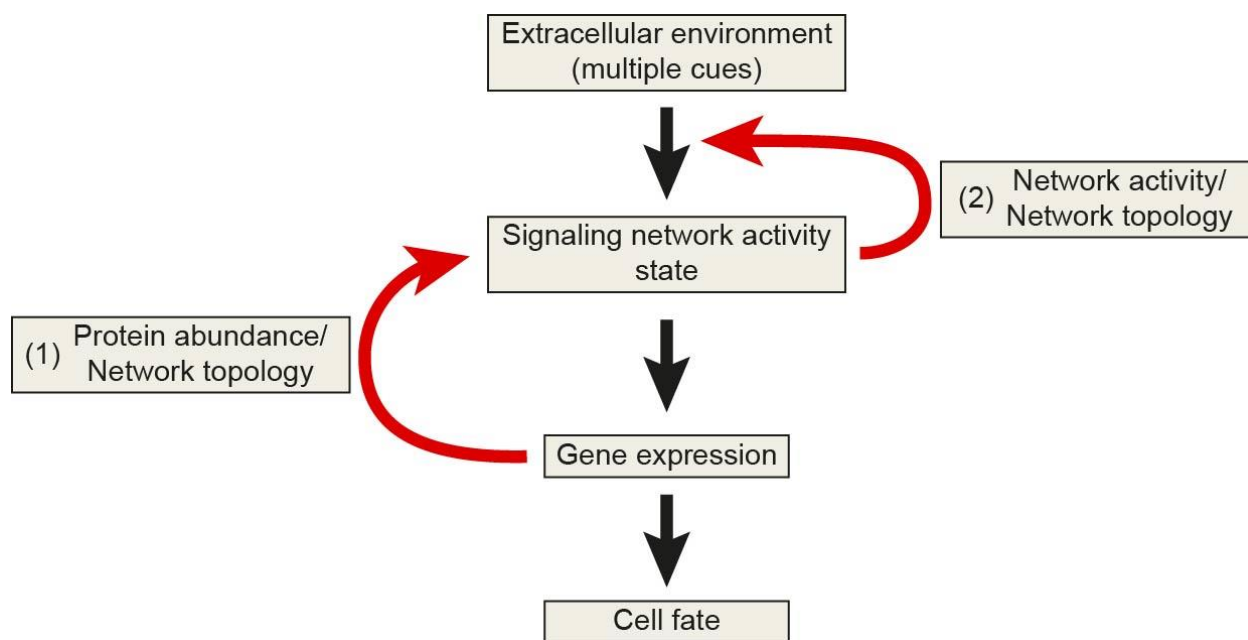


Figure 3.26 Intracellular information processing from multiple cues. Two feedback loops acting at different time scales are highlighted in red. (1) The expression of signaling network components is regulated in the order of hours. (2) Signaling network activity is regulated in the order of seconds and minutes.

The former mechanism of signaling network state regulation is relatively well studied in the context of protein overexpression and/or mutational status (Adlung et al., 2017; Hill et al., 2016; Li et al., 2017; Lun et al., 2017). However, the molecular mechanisms of signaling network

tuning and pre-activation by multiple extracellular cues in the order of minutes have not been clearly identified yet. In all likelihood, the tuning of the signaling network state by cross-talk is determined by kinetic parameters of the reactions (or network activity) and network component interactions (or network topology) (Kolch et al., 2015; Kuchenov et al., 2016; Purvis and Lahav, 2013). It was also proposed that high rates of activation/deactivation cycle may increase sensitivity and kinetic proofreading (Lemmon et al., 2016). It therefore is plausible that similar mechanisms of increased sensitivity may occur under exposure to multiple cues of low concentrations. Thus it will be enlightening to determine whether similar mechanisms of increased sensitivity and proof reading occurs under exposure to multiple cues of low concentrations and further, how the feedback loops work together to shape the cellular response. The better understanding of signaling response tuning under physiologically relevant conditions may lead to the development of new pharmacological strategies for altering cell fate.

Bibliography

Adlung, L., Kar, S., Wagner, M.C., She, B., Chakraborty, S., Bao, J., Lattermann, S., Boerries, M., Busch, H., Wuchter, P., *et al.* (2017). Protein abundance of AKT and ERK pathway components governs cell type-specific regulation of proliferation. *Molecular systems biology* *13*, 904.

Ahmad, T., Farnie, G., Bundred, N.J., and Anderson, N.G. (2004). The mitogenic action of insulin-like growth factor I in normal human mammary epithelial cells requires the epidermal growth factor receptor tyrosine kinase. *The Journal of biological chemistry* *279*, 1713-1719.

Albeck, J.G., Burke, J.M., Spencer, S.L., Lauffenburger, D.A., and Sorger, P.K. (2008). Modeling a snap-action, variable-delay switch controlling extrinsic cell death. *PLoS biology* *6*, 2831-2852.

Albeck, J.G., Mills, G.B., and Brugge, J.S. (2013). Frequency-modulated pulses of ERK activity transmit quantitative proliferation signals. *Molecular cell* *49*, 249-261.

Alessi, D.R., Saito, Y., Campbell, D.G., Cohen, P., Sithanandam, G., Rapp, U., Ashworth, A., Marshall, C.J., and Cowley, S. (1994). Identification of the sites in MAP kinase kinase-1 phosphorylated by p74raf-1. *The EMBO journal* *13*, 1610-1619.

Alon, U. (2007). Network motifs: theory and experimental approaches. *Nat Rev Genet* *8*, 450-461.

Ananthanarayanan, B., Ni, Q., and Zhang, J. (2005). Signal propagation from membrane messengers to nuclear effectors revealed by reporters of phosphoinositide dynamics and Akt activity. *Proceedings of the National Academy of Sciences of the United States of America* *102*, 15081-15086.

-
- Anido, J., Scaltriti, M., Bech Serra, J.J., Santiago Josef, B., Todo, F.R., Baselga, J., and Arribas, J. (2006). Biosynthesis of tumorigenic HER2 C-terminal fragments by alternative initiation of translation. *The EMBO journal* 25, 3234-3244.
- Aoki, K., Kumagai, Y., Sakurai, A., Komatsu, N., Fujita, Y., Shionyu, C., and Matsuda, M. (2013). Stochastic ERK activation induced by noise and cell-to-cell propagation regulates cell density-dependent proliferation. *Molecular cell* 52, 529-540.
- Arteaga, C.L., and Engelman, J.A. (2014). ERBB receptors: from oncogene discovery to basic science to mechanism-based cancer therapeutics. *Cancer cell* 25, 282-303.
- Azeloglu, E.U., and Iyengar, R. (2015). Signaling networks: information flow, computation, and decision making. *Cold Spring Harbor perspectives in biology* 7, a005934.
- Bailey, S.N., Ali, S.M., Carpenter, A.E., Higgins, C.O., and Sabatini, D.M. (2006). Microarrays of lentiviruses for gene function screens in immortalized and primary cells. *Nat Methods* 3, 117-122.
- Baird, G.S., Zacharias, D.A., and Tsien, R.Y. (1999). Circular permutation and receptor insertion within green fluorescent proteins. *Proceedings of the National Academy of Sciences of the United States of America* 96, 11241-11246.
- Bajar, B.T., Wang, E.S., Lam, A.J., Kim, B.B., Jacobs, C.L., Howe, E.S., Davidson, M.W., Lin, M.Z., and Chu, J. (2016). Improving brightness and photostability of green and red fluorescent proteins for live cell imaging and FRET reporting. *Scientific reports* 6, 20889.
- Bakal, C., Linding, R., Llense, F., Heffern, E., Martin-Blanco, E., Pawson, T., and Perrimon, N. (2008). Phosphorylation networks regulating JNK activity in diverse genetic backgrounds. *Science* 322, 453-456.
- Balana, M.E., Labriola, L., Salatino, M., Movsichoff, F., Peters, G., Charreau, E.H., and Elizalde, P.V. (2001). Activation of ErbB-2 via a hierarchical interaction between ErbB-2 and type I insulin-like growth factor receptor in mammary tumor cells. *Oncogene* 20, 34-47.
- Bekaii-Saab, T., Phelps, M.A., Li, X., Saji, M., Goff, L., Kauh, J.S., O'Neil, B.H., Balsom, S., Balint, C., Lierseemann, R., *et al.* (2011). Multi-institutional phase II study of selumetinib in patients with metastatic biliary cancers. *Journal of clinical oncology : official journal of the American Society of Clinical Oncology* 29, 2357-2363.
- Bendall, S.C., Nolan, G.P., Roederer, M., and Chattopadhyay, P.K. (2012). A deep profiler's guide to cytometry. *Trends in immunology* 33, 323-332.
- Benjamini, Y., and Hochberg, Y. (1995). Controlling the false discovery rate: A practical and powerful approach to multiple testing. *J R Stat Soc* 57, 289-300.
- Beyer, E.M., and MacBeath, G. (2012). Cross-talk between receptor tyrosine kinase and tumor necrosis factor-alpha signaling networks regulates apoptosis but not proliferation. *Molecular & cellular proteomics : MCP* 11, M111 013292.

Bibliography

Boggon, T.J., and Eck, M.J. (2004). Structure and regulation of Src family kinases. *Oncogene* 23, 7918-7927.

Bolbat, A., and Schultz, C. (2017). Recent developments of genetically encoded optical sensors for cell biology. *Biology of the cell / under the auspices of the European Cell Biology Organization* 109, 1-23.

Borisov, N., Aksamitiene, E., Kiyatkin, A., Legewie, S., Berkhout, J., Maiwald, T., Kaimachnikov, N.P., Timmer, J., Hoek, J.B., and Kholodenko, B.N. (2009). Systems-level interactions between insulin-EGF networks amplify mitogenic signaling. *Molecular systems biology* 5, 256.

Brennan, J.A., Volle, D.J., Chaika, O.V., and Lewis, R.E. (2002). Phosphorylation regulates the nucleocytoplasmic distribution of kinase suppressor of Ras. *The Journal of biological chemistry* 277, 5369-5377.

Brock, A., Chang, H., and Huang, S. (2009). Non-genetic heterogeneity--a mutation-independent driving force for the somatic evolution of tumours. *Nat Rev Genet* 10, 336-342.

Bromann, P.A., Korkaya, H., and Courtneidge, S.A. (2004). The interplay between Src family kinases and receptor tyrosine kinases. *Oncogene* 23, 7957-7968.

Buchler, N.E., Gerland, U., and Hwa, T. (2003). On schemes of combinatorial transcription logic. *Proceedings of the National Academy of Sciences of the United States of America* 100, 5136-5141.

Burger, H., van Tol, H., Brok, M., Wiemer, E.A., de Bruijn, E.A., Guetens, G., de Boeck, G., Sparreboom, A., Verweij, J., and Nooter, K. (2005). Chronic imatinib mesylate exposure leads to reduced intracellular drug accumulation by induction of the ABCG2 (BCRP) and ABCB1 (MDR1) drug transport pumps. *Cancer biology & therapy* 4, 747-752.

Cabodi, S., del Pilar Camacho-Leal, M., Di Stefano, P., and Defilippi, P. (2010a). Integrin signalling adaptors: not only figurants in the cancer story. *Nature reviews Cancer* 10, 858-870.

Cabodi, S., Tinnirello, A., Bisaro, B., Tornillo, G., del Pilar Camacho-Leal, M., Forni, G., Cojoca, R., Iezzi, M., Amici, A., Montani, M., *et al.* (2010b). p130Cas is an essential transducer element in ErbB2 transformation. *FASEB journal : official publication of the Federation of American Societies for Experimental Biology* 24, 3796-3808.

Carlson, M. (2017). org.Hs.eg.db: Genome wide annotation for Human. R package version 341.

Carriere, A., Romeo, Y., Acosta-Jaquez, H.A., Moreau, J., Bonneil, E., Thibault, P., Fingar, D.C., and Roux, P.P. (2011). ERK1/2 phosphorylate Raptor to promote Ras-dependent activation of mTOR complex 1 (mTORC1). *The Journal of biological chemistry* 286, 567-577.

Carrillo, L.D., Krishnamoorthy, L., and Mahal, L.K. (2006). A cellular FRET-based sensor for beta-O-GlcNAc, a dynamic carbohydrate modification involved in signaling. *Journal of the American Chemical Society* 128, 14768-14769.

- Chandarlapaty, S., Sawai, A., Scaltriti, M., Rodrik-Outmezguine, V., Grbovic-Huezo, O., Serra, V., Majumder, P.K., Baselga, J., and Rosen, N. (2011). AKT inhibition relieves feedback suppression of receptor tyrosine kinase expression and activity. *Cancer cell* 19, 58-71.
- Chatterjee, M.S., Purvis, J.E., Brass, L.F., and Diamond, S.L. (2010). Pairwise agonist scanning predicts cellular signaling responses to combinatorial stimuli. *Nature biotechnology* 28, 727-732.
- Chaturvedi, D., Gao, X., Cohen, M.S., Taunton, J., and Patel, T.B. (2009). Rapamycin induces transactivation of the EGFR and increases cell survival. *Oncogene* 28, 1187-1196.
- Chaturvedi, D., Poppleton, H.M., Stringfield, T., Barbier, A., and Patel, T.B. (2006). Subcellular localization and biological actions of activated RSK1 are determined by its interactions with subunits of cyclic AMP-dependent protein kinase. *Molecular and cellular biology* 26, 4586-4600.
- Chen, T.W., Wardill, T.J., Sun, Y., Pulver, S.R., Renninger, S.L., Baohan, A., Schreiter, E.R., Kerr, R.A., Orger, M.B., Jayaraman, V., *et al.* (2013). Ultrasensitive fluorescent proteins for imaging neuronal activity. *Nature* 499, 295-300.
- Cheong, R., Wang, C.J., and Levchenko, A. (2009). High content cell screening in a microfluidic device. *Molecular & cellular proteomics : MCP* 8, 433-442.
- Cohen-Saidon, C., Cohen, A.A., Sigal, A., Liron, Y., and Alon, U. (2009). Dynamics and variability of ERK2 response to EGF in individual living cells. *Molecular cell* 36, 885-893.
- Costantini, L.M., Baloban, M., Markwardt, M.L., Rizzo, M., Guo, F., Verkhusha, V.V., and Snapp, E.L. (2015). A palette of fluorescent proteins optimized for diverse cellular environments. *Nature communications* 6, 7670.
- Cranfill, P.J., Sell, B.R., Baird, M.A., Allen, J.R., Lavagnino, Z., de Gruiter, H.M., Kremers, G.J., Davidson, M.W., Ustione, A., and Piston, D.W. (2016). Quantitative assessment of fluorescent proteins. *Nat Methods* 13, 557-562.
- Crotty, T., Cai, J., Sakane, F., Taketomi, A., Prescott, S.M., and Topham, M.K. (2006). Diacylglycerol kinase delta regulates protein kinase C and epidermal growth factor receptor signaling. *Proceedings of the National Academy of Sciences of the United States of America* 103, 15485-15490.
- Cui, X., Kim, H.J., Kuiatse, I., Kim, H., Brown, P.H., and Lee, A.V. (2006). Epidermal growth factor induces insulin receptor substrate-2 in breast cancer cells via c-Jun NH(2)-terminal kinase/activator protein-1 signaling to regulate cell migration. *Cancer research* 66, 5304-5313.
- de la Cruz-Herrera, C.F., Campagna, M., Lang, V., Del Carmen Gonzalez-Santamaria, J., Marcos-Villar, L., Rodriguez, M.S., Vidal, A., Collado, M., and Rivas, C. (2015). SUMOylation regulates AKT1 activity. *Oncogene* 34, 1442-1450.
- Depry, C., Allen, M.D., and Zhang, J. (2011). Visualization of PKA activity in plasma membrane microdomains. *Molecular bioSystems* 7, 52-58.

Bibliography

Deribe, Y.L., Pawson, T., and Dikic, I. (2010). Post-translational modifications in signal integration. *Nat Struct Mol Biol* *17*, 666-672.

Dobin, A., Davis, C.A., Schlesinger, F., Drenkow, J., Zaleski, C., Jha, S., Batut, P., Chaisson, M., and Gingeras, T.R. (2013). STAR: ultrafast universal RNA-seq aligner. *Bioinformatics* *29*, 15-21.

Dougherty, M.K., Muller, J., Ritt, D.A., Zhou, M., Zhou, X.Z., Copeland, T.D., Conrads, T.P., Veenstra, T.D., Lu, K.P., and Morrison, D.K. (2005). Regulation of Raf-1 by direct feedback phosphorylation. *Molecular cell* *17*, 215-224.

Douville, E., and Downward, J. (1997). EGF induced SOS phosphorylation in PC12 cells involves P90 RSK-2. *Oncogene* *15*, 373-383.

Duncan, J.S., Whittle, M.C., Nakamura, K., Abell, A.N., Midland, A.A., Zawistowski, J.S., Johnson, N.L., Granger, D.A., Jordan, N.V., Darr, D.B., *et al.* (2012). Dynamic reprogramming of the kinome in response to targeted MEK inhibition in triple-negative breast cancer. *Cell* *149*, 307-321.

Ebner, R., and Derynck, R. (1991). Epidermal Growth-Factor and Transforming Growth Factor-Alpha - Differential Intracellular Routing and Processing of Ligand-Receptor Complexes. *Cell Regul* *2*, 599-612.

Erfle, H., Neumann, B., Liebel, U., Rogers, P., Held, M., Walter, T., Ellenberg, J., and Pepperkok, R. (2007). Reverse transfection on cell arrays for high content screening microscopy. *Nature protocols* *2*, 392-399.

Ermakova, Y.G., Bilan, D.S., Matlashov, M.E., Mishina, N.M., Markvicheva, K.N., Subach, O.M., Subach, F.V., Bogeski, I., Hoth, M., Enikolopov, G., *et al.* (2014). Red fluorescent genetically encoded indicator for intracellular hydrogen peroxide. *Nature communications* *5*, 5222.

Esposito, C.L., D'Alessio, A., de Franciscis, V., and Cerchia, L. (2008). A cross-talk between TrkB and Ret tyrosine kinases receptors mediates neuroblastoma cells differentiation. *PLoS one* *3*, e1643.

Ferrell, J.E., Jr., and Machleder, E.M. (1998). The biochemical basis of an all-or-none cell fate switch in *Xenopus* oocytes. *Science* *280*, 895-898.

Förster, T. (1948). Zwischenmolekulare Energiewanderung und Fluoreszenz. *Ann Phys* *437*, 55-75.

Frame, M.C., Patel, H., Serrels, B., Lietha, D., and Eck, M.J. (2010). The FERM domain: organizing the structure and function of FAK. *Nature reviews Molecular cell biology* *11*, 802-814.

- Francavilla, C., Papetti, M., Rigbolt, K.T., Pedersen, A.K., Sigurdsson, J.O., Cazzamali, G., Karemore, G., Blagoev, B., and Olsen, J.V. (2016). Multilayered proteomics reveals molecular switches dictating ligand-dependent EGFR trafficking. *Nat Struct Mol Biol* 23, 608-618.
- Frechin, M., Stoeger, T., Daetwyler, S., Gehin, C., Battich, N., Damm, E.M., Stergiou, L., Riezman, H., and Pelkmans, L. (2015). Cell-intrinsic adaptation of lipid composition to local crowding drives social behaviour. *Nature* 523, 88-91.
- Fritsche-Guenther, R., Witzel, F., Sieber, A., Herr, R., Schmidt, N., Braun, S., Brummer, T., Sers, C., and Bluthgen, N. (2011). Strong negative feedback from Erk to Raf confers robustness to MAPK signalling. *Molecular systems biology* 7, 489.
- Fritz, R.D., Letzelter, M., Reimann, A., Martin, K., Fusco, L., Ritsma, L., Ponsioen, B., Fluri, E., Schulte-Merker, S., van Rheenen, J., *et al.* (2013). A versatile toolkit to produce sensitive FRET biosensors to visualize signaling in time and space. *Science signaling* 6, rs12.
- Fuller, B.G., Lampson, M.A., Foley, E.A., Rosasco-Nitcher, S., Le, K.V., Tobelmann, P., Brautigan, D.L., Stukenberg, P.T., and Kapoor, T.M. (2008). Midzone activation of aurora B in anaphase produces an intracellular phosphorylation gradient. *Nature* 453, 1132-1136.
- Ganley, I.G., Lam du, H., Wang, J., Ding, X., Chen, S., and Jiang, X. (2009). ULK1.ATG13.FIP200 complex mediates mTOR signaling and is essential for autophagy. *The Journal of biological chemistry* 284, 12297-12305.
- Gao, X., Lowry, P.R., Zhou, X., Depry, C., Wei, Z., Wong, G.W., and Zhang, J. (2011). PI3K/Akt signaling requires spatial compartmentalization in plasma membrane microdomains. *Proceedings of the National Academy of Sciences of the United States of America* 108, 14509-14514.
- Gao, X., and Patel, T.B. (2009). Regulation of protein kinase A activity by p90 ribosomal S6 kinase 1. *The Journal of biological chemistry* 284, 33070-33078.
- Garrenton, L.S., Young, S.L., and Thorner, J. (2006). Function of the MAPK scaffold protein, Ste5, requires a cryptic PH domain. *Genes Dev* 20, 1946-1958.
- Gavet, O., and Pines, J. (2010). Progressive activation of CyclinB1-Cdk1 coordinates entry to mitosis. *Developmental cell* 18, 533-543.
- Genolini, C., Alacoque, X., Sentenac, M., and Arnaud, C. (2015). kml and kml3d: R Packages to Cluster Longitudinal Data. *J Stat Softw* 65, 1-34.
- Giesen, C., Wang, H.A., Schapiro, D., Zivanovic, N., Jacobs, A., Hattendorf, B., Schuffler, P.J., Grolimund, D., Buhmann, J.M., Brandt, S., *et al.* (2014). Highly multiplexed imaging of tumor tissues with subcellular resolution by mass cytometry. *Nat Methods* 11, 417-422.
- Goedhart, J., von Stetten, D., Noirclerc-Savoie, M., Lelimosin, M., Joosen, L., Hink, M.A., van Weeren, L., Gadella, T.W., Jr., and Royant, A. (2012). Structure-guided evolution of cyan fluorescent proteins towards a quantum yield of 93%. *Nature communications* 3, 751.

Bibliography

Goh, L.K., and Sorkin, A. (2013). Endocytosis of receptor tyrosine kinases. *Cold Spring Harbor perspectives in biology* 5, a017459.

Good, M., Tang, G., Singleton, J., Remenyi, A., and Lim, W.A. (2009). The Ste5 scaffold directs mating signaling by catalytically unlocking the Fus3 MAP kinase for activation. *Cell* 136, 1085-1097.

Good, M.C., Zalatan, J.G., and Lim, W.A. (2011). Scaffold proteins: hubs for controlling the flow of cellular information. *Science* 332, 680-686.

Grecco, H.E., Roda-Navarro, P., Girod, A., Hou, J., Frahm, T., Truxius, D.C., Pepperkok, R., Squire, A., and Bastiaens, P.I. (2010). In situ analysis of tyrosine phosphorylation networks by FLIM on cell arrays. *Nat Methods* 7, 467-472.

Grecco, H.E., Schmick, M., and Bastiaens, P.I. (2011). Signaling from the living plasma membrane. *Cell* 144, 897-909.

Guan, K.L., Figueroa, C., Brtva, T.R., Zhu, T., Taylor, J., Barber, T.D., and Vojtek, A.B. (2000). Negative regulation of the serine/threonine kinase B-Raf by Akt. *The Journal of biological chemistry* 275, 27354-27359.

Hagiwara, A., Cornu, M., Cybulski, N., Polak, P., Betz, C., Trapani, F., Terracciano, L., Heim, M.H., Rugg, M.A., and Hall, M.N. (2012). Hepatic mTORC2 activates glycolysis and lipogenesis through Akt, glucokinase, and SREBP1c. *Cell metabolism* 15, 725-738.

Haj, F.G., Verveer, P.J., Squire, A., Neel, B.G., and Bastiaens, P.I. (2002). Imaging sites of receptor dephosphorylation by PTP1B on the surface of the endoplasmic reticulum. *Science* 295, 1708-1711.

Harvey, C.D., Ehrhardt, A.G., Cellurale, C., Zhong, H., Yasuda, R., Davis, R.J., and Svoboda, K. (2008). A genetically encoded fluorescent sensor of ERK activity. *Proceedings of the National Academy of Sciences of the United States of America* 105, 19264-19269.

Haystead, T.A., Dent, P., Wu, J., Haystead, C.M., and Sturgill, T.W. (1992). Ordered phosphorylation of p42mapk by MAP kinase kinase. *FEBS letters* 306, 17-22.

Heasley, L.E., and Johnson, G.L. (1992). The beta-PDGF receptor induces neuronal differentiation of PC12 cells. *Molecular biology of the cell* 3, 545-553.

Heldin, C.H., Lu, B., Evans, R., and Gutkind, J.S. (2016). *Signals and Receptors*. Cold Spring Harbor perspectives in biology 8.

Hill, S.M., Nesser, N.K., Johnson-Camacho, K., Jeffress, M., Johnson, A., Boniface, C., Spencer, S.E., Lu, Y., Heiser, L.M., Lawrence, Y., *et al.* (2016). Context Specificity in Causal Signaling Networks Revealed by Phosphoprotein Profiling. *Cell Syst*.

- Hiratsuka, T., Fujita, Y., Naoki, H., Aoki, K., Kamioka, Y., and Matsuda, M. (2015). Intercellular propagation of extracellular signal-regulated kinase activation revealed by in vivo imaging of mouse skin. *eLife* 4, e05178.
- Honegger, A.M., Kris, R.M., Ullrich, A., and Schlessinger, J. (1989). Evidence that autophosphorylation of solubilized receptors for epidermal growth factor is mediated by intermolecular cross-phosphorylation. *Proceedings of the National Academy of Sciences of the United States of America* 86, 925-929.
- Housden, B.E., and Perrimon, N. (2014). Spatial and temporal organization of signaling pathways. *Trends in biochemical sciences* 39, 457-464.
- Hsueh, R.C., Natarajan, M., Fraser, I., Pond, B., Liu, J., Mumby, S., Han, H., Jiang, L.I., Simon, M.I., Taussig, R., *et al.* (2009). Deciphering signaling outcomes from a system of complex networks. *Science signaling* 2, ra22.
- Hubbard, S.R. (2004). Juxtamembrane autoinhibition in receptor tyrosine kinases. *Nature reviews Molecular cell biology* 5, 464-471.
- Hubbard, S.R., and Till, J.H. (2000). Protein tyrosine kinase structure and function. *Annu Rev Biochem* 69, 373-398.
- Hughes, A.J., Spelke, D.P., Xu, Z., Kang, C.C., Schaffer, D.V., and Herr, A.E. (2014). Single-cell western blotting. *Nat Methods* 11, 749-755.
- Hung, Y.P., Albeck, J.G., Tantama, M., and Yellen, G. (2011). Imaging cytosolic NADH-NAD(+) redox state with a genetically encoded fluorescent biosensor. *Cell metabolism* 14, 545-554.
- Illmer, T., Schaich, M., Platzbecker, U., Freiberg-Richter, J., Oelschlagel, U., von Bonin, M., Pursche, S., Bergemann, T., Ehninger, G., and Schleyer, E. (2004). P-glycoprotein-mediated drug efflux is a resistance mechanism of chronic myelogenous leukemia cells to treatment with imatinib mesylate. *Leukemia* 18, 401-408.
- Inoki, K., Li, Y., Zhu, T., Wu, J., and Guan, K.L. (2002). TSC2 is phosphorylated and inhibited by Akt and suppresses mTOR signalling. *Nature cell biology* 4, 648-657.
- Inoue, M., Takeuchi, A., Horigane, S., Ohkura, M., Gengyo-Ando, K., Fujii, H., Kamijo, S., Takemoto-Kimura, S., Kano, M., Nakai, J., *et al.* (2015). Rational design of a high-affinity, fast, red calcium indicator R-CaMP2. *Nat Methods* 12, 64-70.
- Itoh, R.E., Kurokawa, K., Ohba, Y., Yoshizaki, H., Mochizuki, N., and Matsuda, M. (2002). Activation of rac and cdc42 video imaged by fluorescent resonance energy transfer-based single-molecule probes in the membrane of living cells. *Molecular and cellular biology* 22, 6582-6591.
- Janes, K.A., Albeck, J.G., Gaudet, S., Sorger, P.K., Lauffenburger, D.A., and Yaffe, M.B. (2005). A systems model of signaling identifies a molecular basis set for cytokine-induced apoptosis. *Science* 310, 1646-1653.

Bibliography

Junttila, M.R., and de Sauvage, F.J. (2013). Influence of tumour micro-environment heterogeneity on therapeutic response. *Nature* *501*, 346-354.

Kaimachnikov, N.P., and Kholodenko, B.N. (2009). Toggle switches, pulses and oscillations are intrinsic properties of the Src activation/deactivation cycle. *The FEBS journal* *276*, 4102-4118.

Karunakaran, D., Tzahar, E., Beerli, R.R., Chen, X., Graus-Porta, D., Ratzkin, B.J., Seger, R., Hynes, N.E., and Yarden, Y. (1996). ErbB-2 is a common auxiliary subunit of NDF and EGF receptors: implications for breast cancer. *The EMBO journal* *15*, 254-264.

Katayama, H., Yamamoto, A., Mizushima, N., Yoshimori, T., and Miyawaki, A. (2008). GFP-like proteins stably accumulate in lysosomes. *Cell Struct Funct* *33*, 1-12.

Kermorgant, S., and Parker, P.J. (2008). Receptor trafficking controls weak signal delivery: a strategy used by c-Met for STAT3 nuclear accumulation. *The Journal of cell biology* *182*, 855-863.

Kholodenko, B.N., Hancock, J.F., and Kolch, W. (2010). Signalling ballet in space and time. *Nature reviews Molecular cell biology* *11*, 414-426.

Kim, S.M., Kim, H., Yun, M.R., Kang, H.N., Pyo, K.H., Park, H.J., Lee, J.M., Choi, H.M., Ellinghaus, P., Ocker, M., *et al.* (2016). Activation of the Met kinase confers acquired drug resistance in FGFR-targeted lung cancer therapy. *Oncogenesis* *5*, e241.

Kleiman, L.B., Maiwald, T., Conzelmann, H., Lauffenburger, D.A., and Sorger, P.K. (2011). Rapid phospho-turnover by receptor tyrosine kinases impacts downstream signaling and drug binding. *Molecular cell* *43*, 723-737.

Klinghoffer, R.A., Hamilton, T.G., Hoch, R., and Soriano, P. (2002). An allelic series at the PDGF α R locus indicates unequal contributions of distinct signaling pathways during development. *Developmental cell* *2*, 103-113.

Knowlden, J.M., Hutcheson, I.R., Barrow, D., Gee, J.M., and Nicholson, R.I. (2005). Insulin-like growth factor-I receptor signaling in tamoxifen-resistant breast cancer: a supporting role to the epidermal growth factor receptor. *Endocrinology* *146*, 4609-4618.

Kodama, Y., and Hu, C.D. (2012). Bimolecular fluorescence complementation (BiFC): a 5-year update and future perspectives. *Biotechniques* *53*, 285-298.

Kolch, W., Halasz, M., Granovskaya, M., and Kholodenko, B.N. (2015). The dynamic control of signal transduction networks in cancer cells. *Nature reviews Cancer* *15*, 515-527.

Kolch, W., and Pitt, A. (2010). Functional proteomics to dissect tyrosine kinase signalling pathways in cancer. *Nature reviews Cancer* *10*, 618-629.

Komatsu, N., Aoki, K., Yamada, M., Yukinaga, H., Fujita, Y., Kamioka, Y., and Matsuda, M. (2011). Development of an optimized backbone of FRET biosensors for kinases and GTPases. *Molecular biology of the cell* *22*, 4647-4656.

Koushik, S.V., Chen, H., Thaler, C., Puhl, H.L., 3rd, and Vogel, S.S. (2006). Cerulean, Venus, and VenusY67C FRET reference standards. *Biophysical journal* *91*, L99-L101.

Ku, H.H. (1966). Notes on the use of propagation of error formulas. *Journal of Research of the National Bureau of Standards (National Bureau of Standards)* *70C (4)*: 262. .

Kubota, H., Noguchi, R., Toyoshima, Y., Ozaki, Y., Uda, S., Watanabe, K., Ogawa, W., and Kuroda, S. (2012). Temporal coding of insulin action through multiplexing of the AKT pathway. *Molecular cell* *46*, 820-832.

Kuchenov, D., Laketa, V., Stein, F., Salopiata, F., Klingmuller, U., and Schultz, C. (2016). High-Content Imaging Platform for Profiling Intracellular Signaling Network Activity in Living Cells. *Cell Chem Biol* *23*, 1550-1559.

Kumagai, Y., Naoki, H., Nakasyo, E., Kamioka, Y., Kiyokawa, E., and Matsuda, M. (2015). Heterogeneity in ERK activity as visualized by in vivo FRET imaging of mammary tumor cells developed in MMTV-Neu mice. *Oncogene* *34*, 1051-1057.

Lai, A.Z., Cory, S., Zhao, H., Gigoux, M., Monast, A., Guiot, M.C., Huang, S., Tofigh, A., Thompson, C., Naujokas, M., *et al.* (2014). Dynamic reprogramming of signaling upon met inhibition reveals a mechanism of drug resistance in gastric cancer. *Science signaling* *7*, ra38.

Laketa, V., Zarbakhsh, S., Traynor-Kaplan, A., Macnamara, A., Subramanian, D., Putyrski, M., Mueller, R., Nadler, A., Mentel, M., Saez-Rodriguez, J., *et al.* (2014). PIP(3) induces the recycling of receptor tyrosine kinases. *Science signaling* *7*, ra5.

Landry, B.D., Clarke, D.C., and Lee, M.J. (2015). Studying Cellular Signal Transduction with OMIC Technologies. *J Mol Biol* *427*, 3416-3440.

Langeberg, L.K., and Scott, J.D. (2015). Signalling scaffolds and local organization of cellular behaviour. *Nature reviews Molecular cell biology* *16*, 232-244.

Lee, M.J., and Yaffe, M.B. (2016). Protein Regulation in Signal Transduction. *Cold Spring Harbor perspectives in biology* *8*.

Lehr, S., Kotzka, J., Avci, H., Sickmann, A., Meyer, H.E., Herkner, A., and Muller-Wieland, D. (2004). Identification of major ERK-related phosphorylation sites in Gab1. *Biochemistry* *43*, 12133-12140.

Lemmon, M.A., Freed, D.M., Schlessinger, J., and Kiyatkin, A. (2016). The Dark Side of Cell Signaling: Positive Roles for Negative Regulators. *Cell* *164*, 1172-1184.

Lemmon, M.A., and Schlessinger, J. (2010). Cell signaling by receptor tyrosine kinases. *Cell* *141*, 1117-1134.

Li, J., Zhao, W., Akbani, R., Liu, W., Ju, Z., Ling, S., Vellano, C.P., Roebuck, P., Yu, Q., Eterovic, A.K., *et al.* (2017). Characterization of Human Cancer Cell Lines by Reverse-phase Protein Arrays. *Cancer cell* *31*, 225-239.

Bibliography

- Lin, C.W., Jao, C.Y., and Ting, A.Y. (2004). Genetically encoded fluorescent reporters of histone methylation in living cells. *Journal of the American Chemical Society* *126*, 5982-5983.
- Lin, C.W., and Ting, A.Y. (2004). A genetically encoded fluorescent reporter of histone phosphorylation in living cells. *Angewandte Chemie* *43*, 2940-2943.
- Liu, B.A., Jablonowski, K., Raina, M., Arce, M., Pawson, T., and Nash, P.D. (2006). The human and mouse complement of SH2 domain proteins-establishing the boundaries of phosphotyrosine signaling. *Molecular cell* *22*, 851-868.
- Liu, L., Greger, J., Shi, H., Liu, Y., Greshock, J., Annan, R., Halsey, W., Sathe, G.M., Martin, A.M., and Gilmer, T.M. (2009). Novel mechanism of lapatinib resistance in HER2-positive breast tumor cells: activation of AXL. *Cancer research* *69*, 6871-6878.
- Liu, P., Begley, M., Michowski, W., Inuzuka, H., Ginzberg, M., Gao, D., Tsou, P., Gan, W., Papa, A., Kim, B.M., *et al.* (2014). Cell-cycle-regulated activation of Akt kinase by phosphorylation at its carboxyl terminus. *Nature* *508*, 541-545.
- Long, X., Lin, Y., Ortiz-Vega, S., Yonezawa, K., and Avruch, J. (2005). Rheb binds and regulates the mTOR kinase. *Current biology : CB* *15*, 702-713.
- Love, M.I., Huber, W., and Anders, S. (2014). Moderated estimation of fold change and dispersion for RNA-seq data with DESeq2. *Genome Biol* *15*, 550.
- Lun, X.K., Zanutelli, V.R., Wade, J.D., Schapiro, D., Tognetti, M., Dobberstein, N., and Bodenmiller, B. (2017). Influence of node abundance on signaling network state and dynamics analyzed by mass cytometry. *Nature biotechnology*.
- Luo, W., Friedman, M.S., Shedden, K., Hankenson, K.D., and Woolf, P.J. (2009). GAGE: generally applicable gene set enrichment for pathway analysis. *BMC Bioinformatics* *10*, 161.
- Ma, L., Chen, Z., Erdjument-Bromage, H., Tempst, P., and Pandolfi, P.P. (2005). Phosphorylation and functional inactivation of TSC2 by Erk implications for tuberous sclerosis and cancer pathogenesis. *Cell* *121*, 179-193.
- Mank, M., Reiff, D.F., Heim, N., Friedrich, M.W., Borst, A., and Griesbeck, O. (2006). A FRET-based calcium biosensor with fast signal kinetics and high fluorescence change. *Biophysical journal* *90*, 1790-1796.
- Margolis, B., Rhee, S.G., Felder, S., Mervic, M., Lyall, R., Levitzki, A., Ullrich, A., Zilberstein, A., and Schlessinger, J. (1989). EGF induces tyrosine phosphorylation of phospholipase C-II: a potential mechanism for EGF receptor signaling. *Cell* *57*, 1101-1107.
- Martin, B., Brenneman, R., Golden, E., Walent, T., Becker, K.G., Prabhu, V.V., Wood, W., 3rd, Ladenheim, B., Cadet, J.L., and Maudsley, S. (2009). Growth factor signals in neural cells: coherent patterns of interaction control multiple levels of molecular and phenotypic responses. *The Journal of biological chemistry* *284*, 2493-2511.

- McCawley, L.J., Li, S., Wattenberg, E.V., and Hudson, L.G. (1999). Sustained activation of the mitogen-activated protein kinase pathway. A mechanism underlying receptor tyrosine kinase specificity for matrix metalloproteinase-9 induction and cell migration. *The Journal of biological chemistry* 274, 4347-4353.
- McKeithan, T.W. (1995). Kinetic proofreading in T-cell receptor signal transduction. *Proceedings of the National Academy of Sciences of the United States of America* 92, 5042-5046.
- Mendoza, M.C., Er, E.E., and Blenis, J. (2011). The Ras-ERK and PI3K-mTOR pathways: cross-talk and compensation. *Trends in biochemical sciences* 36, 320-328.
- Miller-Jensen, K., Janes, K.A., Brugge, J.S., and Lauffenburger, D.A. (2007). Common effector processing mediates cell-specific responses to stimuli. *Nature* 448, 604-608.
- Miura, H., Matsuda, M., and Aoki, K. (2014). Development of a FRET biosensor with high specificity for Akt. *Cell Struct Funct* 39, 9-20.
- Miyake, M., Yoshikawa, T., Fujita, S., and Miyake, J. (2009). Transfection microarray and the applications. *Molecular bioSystems* 5, 444-449.
- Miyamoto, T., Rho, E., Sample, V., Akano, H., Magari, M., Ueno, T., Gorshkov, K., Chen, M., Tokumitsu, H., Zhang, J., *et al.* (2015). Compartmentalized AMPK signaling illuminated by genetically encoded molecular sensors and actuators. *Cell reports* 11, 657-670.
- Miyawaki, A. (2003). Visualization of the spatial and temporal dynamics of intracellular signaling. *Developmental cell* 4, 295-305.
- Miyawaki, A. (2011). Development of probes for cellular functions using fluorescent proteins and fluorescence resonance energy transfer. *Annu Rev Biochem* 80, 357-373.
- Miyawaki, A., and Niino, Y. (2015). Molecular spies for bioimaging--fluorescent protein-based probes. *Molecular cell* 58, 632-643.
- Mizutani, T., Kondo, T., Darmanin, S., Tsuda, M., Tanaka, S., Tobiume, M., Asaka, M., and Ohba, Y. (2010). A novel FRET-based biosensor for the measurement of BCR-ABL activity and its response to drugs in living cells. *Clinical cancer research : an official journal of the American Association for Cancer Research* 16, 3964-3975.
- Mochizuki, N., Yamashita, S., Kurokawa, K., Ohba, Y., Nagai, T., Miyawaki, A., and Matsuda, M. (2001). Spatio-temporal images of growth-factor-induced activation of Ras and Rap1. *Nature* 411, 1065-1068.
- Monick, M.M., Powers, L.S., Gross, T.J., Flaherty, D.M., Barrett, C.W., and Hunninghake, G.W. (2006). Active ERK contributes to protein translation by preventing JNK-dependent inhibition of protein phosphatase 1. *J Immunol* 177, 1636-1645.

Murphy, J.E., Padilla, B.E., Hasdemir, B., Cottrell, G.S., and Bunnett, N.W. (2009). Endosomes: a legitimate platform for the signaling train. *Proceedings of the National Academy of Sciences of the United States of America* *106*, 17615-17622.

Nadler, A., Reither, G., Feng, S., Stein, F., Reither, S., Muller, R., and Schultz, C. (2013). The fatty acid composition of diacylglycerols determines local signaling patterns. *Angewandte Chemie* *52*, 6330-6334.

Nagashima, T., Shimodaira, H., Ide, K., Nakakuki, T., Tani, Y., Takahashi, K., Yumoto, N., and Hatakeyama, M. (2007). Quantitative transcriptional control of ErbB receptor signaling undergoes graded to biphasic response for cell differentiation. *The Journal of biological chemistry* *282*, 4045-4056.

Nagy, P., Claus, J., Jovin, T.M., and Arndt-Jovin, D.J. (2010). Distribution of resting and ligand-bound ErbB1 and ErbB2 receptor tyrosine kinases in living cells using number and brightness analysis. *Proceedings of the National Academy of Sciences of the United States of America* *107*, 16524-16529.

Nagy, P., Friedlander, E., Tanner, M., Kapanen, A.I., Carraway, K.L., Isola, J., and Jovin, T.M. (2005). Decreased accessibility and lack of activation of ErbB2 in JIMT-1, a herceptin-resistant, MUC4-expressing breast cancer cell line. *Cancer research* *65*, 473-482.

Nakakuki, T., Birtwistle, M.R., Saeki, Y., Yumoto, N., Ide, K., Nagashima, T., Brusch, L., Ogunnaik, B.A., Okada-Hatakeyama, M., and Kholodenko, B.N. (2010). Ligand-specific c-Fos expression emerges from the spatiotemporal control of ErbB network dynamics. *Cell* *141*, 884-896.

Nakaoka, S., Sasaki, K., Ito, A., Nakao, Y., and Yoshida, M. (2016). A Genetically Encoded FRET Probe to Detect Intranucleosomal Histone H3K9 or H3K14 Acetylation Using BRD4, a BET Family Member. *ACS chemical biology* *11*, 729-733.

Natarajan, M., Lin, K.M., Hsueh, R.C., Sternweis, P.C., and Ranganathan, R. (2006). A global analysis of cross-talk in a mammalian cellular signalling network. *Nature cell biology* *8*, 571-580.

Neumann, B., Held, M., Liebel, U., Erfle, H., Rogers, P., Pepperkok, R., and Ellenberg, J. (2006). High-throughput RNAi screening by time-lapse imaging of live human cells. *Nat Methods* *3*, 385-390.

Newman, R.H., Fosbrink, M.D., and Zhang, J. (2011). Genetically encodable fluorescent biosensors for tracking signaling dynamics in living cells. *Chemical reviews* *111*, 3614-3666.

Newman, R.H., and Zhang, J. (2008). Visualization of phosphatase activity in living cells with a FRET-based calcineurin activity sensor. *Molecular bioSystems* *4*, 496-501.

Nguyen, T.T., Scimeca, J.C., Filloux, C., Peraldi, P., Carpentier, J.L., and Van Obberghen, E. (1993). Co-regulation of the mitogen-activated protein kinase, extracellular signal-regulated kinase 1, and the 90-kDa ribosomal S6 kinase in PC12 cells. Distinct effects of the neurotrophic

factor, nerve growth factor, and the mitogenic factor, epidermal growth factor. *The Journal of biological chemistry* 268, 9803-9810.

Ni, Q., Ganesan, A., Aye-Han, N.N., Gao, X., Allen, M.D., Levchenko, A., and Zhang, J. (2011). Signaling diversity of PKA achieved via a Ca²⁺-cAMP-PKA oscillatory circuit. *Nature chemical biology* 7, 34-40.

Niu, X.L., Peters, K.G., and Kontos, C.D. (2002). Deletion of the carboxyl terminus of Tie2 enhances kinase activity, signaling, and function. Evidence for an autoinhibitory mechanism. *The Journal of biological chemistry* 277, 31768-31773.

Odaka, H., Arai, S., Inoue, T., and Kitaguchi, T. (2014). Genetically-encoded yellow fluorescent cAMP indicator with an expanded dynamic range for dual-color imaging. *PloS one* 9, e100252.

Oh, D., Ogiue-Ikeda, M., Jadwin, J.A., Machida, K., Mayer, B.J., and Yu, J. (2012). Fast rebinding increases dwell time of Src homology 2 (SH2)-containing proteins near the plasma membrane. *Proceedings of the National Academy of Sciences of the United States of America* 109, 14024-14029.

Ohnishi, Y., Huber, W., Tsumura, A., Kang, M., Xenopoulos, P., Kurimoto, K., Oles, A.K., Arauzo-Bravo, M.J., Saitou, M., Hadjantonakis, A.K., *et al.* (2014). Cell-to-cell expression variability followed by signal reinforcement progressively segregates early mouse lineages. *Nature cell biology* 16, 27-37.

Olayioye, M.A., Neve, R.M., Lane, H.A., and Hynes, N.E. (2000). The ErbB signaling network: receptor heterodimerization in development and cancer. *The EMBO journal* 19, 3159-3167.

Oldach, L., and Zhang, J. (2014). Genetically encoded fluorescent biosensors for live-cell visualization of protein phosphorylation. *Chemistry & biology* 21, 186-197.

Ouyang, M., Sun, J., Chien, S., and Wang, Y. (2008). Determination of hierarchical relationship of Src and Rac at subcellular locations with FRET biosensors. *Proceedings of the National Academy of Sciences of the United States of America* 105, 14353-14358.

Parrini, M.C., Camonis, J., Matsuda, M., and de Gunzburg, J. (2009). Dissecting activation of the PAK1 kinase at protrusions in living cells. *The Journal of biological chemistry* 284, 24133-24143.

Patterson, J.C., Klimenko, E.S., and Thorner, J. (2010). Single-cell analysis reveals that insulation maintains signaling specificity between two yeast MAPK pathways with common components. *Science signaling* 3, ra75.

Pawson, T. (2004). Specificity in signal transduction: from phosphotyrosine-SH2 domain interactions to complex cellular systems. *Cell* 116, 191-203.

Pazarentzos, E., and Bivona, T.G. (2015). Adaptive stress signaling in targeted cancer therapy resistance. *Oncogene* 34, 5599-5606.

Bibliography

Piljic, A., de Diego, I., Wilmanns, M., and Schultz, C. (2011). Rapid development of genetically encoded FRET reporters. *ACS chemical biology* 6, 685-691.

Purvis, J.E., and Lahav, G. (2013). Encoding and decoding cellular information through signaling dynamics. *Cell* 152, 945-956.

Regot, S., Hughey, J.J., Bajar, B.T., Carrasco, S., and Covert, M.W. (2014). High-sensitivity measurements of multiple kinase activities in live single cells. *Cell* 157, 1724-1734.

Rodriguez-Viciano, P., Warne, P.H., Dhand, R., Vanhaesebroeck, B., Gout, I., Fry, M.J., Waterfield, M.D., and Downward, J. (1994). Phosphatidylinositol-3-OH kinase as a direct target of Ras. *Nature* 370, 527-532.

Ronan, T., Macdonald-Obermann, J.L., Huelsmann, L., Bessman, N.J., Naegle, K.M., and Pike, L.J. (2016). Different Epidermal Growth Factor Receptor (EGFR) Agonists Produce Unique Signatures for the Recruitment of Downstream Signaling Proteins. *The Journal of biological chemistry* 291, 5528-5540.

Salcini, A.E., McGlade, J., Pelicci, G., Nicoletti, I., Pawson, T., and Pelicci, P.G. (1994). Formation of Shc-Grb2 complexes is necessary to induce neoplastic transformation by overexpression of Shc proteins. *Oncogene* 9, 2827-2836.

San Martin, A., Ceballo, S., Baeza-Lehnert, F., Lerchundi, R., Valdebenito, R., Contreras-Baeza, Y., Alegria, K., and Barros, L.F. (2014). Imaging mitochondrial flux in single cells with a FRET sensor for pyruvate. *PloS one* 9, e85780.

San Martin, A., Ceballo, S., Ruminot, I., Lerchundi, R., Frommer, W.B., and Barros, L.F. (2013). A genetically encoded FRET lactate sensor and its use to detect the Warburg effect in single cancer cells. *PloS one* 8, e57712.

Santos, S.D., Verveer, P.J., and Bastiaens, P.I. (2007). Growth factor-induced MAPK network topology shapes Erk response determining PC-12 cell fate. *Nature cell biology* 9, 324-330.

Sasaki, K., Ito, T., Nishino, N., Khochbin, S., and Yoshida, M. (2009). Real-time imaging of histone H4 hyperacetylation in living cells. *Proceedings of the National Academy of Sciences of the United States of America* 106, 16257-16262.

Sauro, H.M., and Kholodenko, B.N. (2004). Quantitative analysis of signaling networks. *Prog Biophys Mol Biol* 86, 5-43.

Schindelin, J., Arganda-Carreras, I., Frise, E., Kaynig, V., Longair, M., Pietzsch, T., Preibisch, S., Rueden, C., Saalfeld, S., Schmid, B., *et al.* (2012). Fiji: an open-source platform for biological-image analysis. *Nat Methods* 9, 676-682.

Schleifenbaum, A., Stier, G., Gasch, A., Sattler, M., and Schultz, C. (2004). Genetically encoded FRET probe for PKC activity based on pleckstrin. *Journal of the American Chemical Society* 126, 11786-11787.

- Scholler, P., Moreno-Delgado, D., Lecat-Guillet, N., Doumazane, E., Monnier, C., Charrier-Savournin, F., Fabre, L., Chouvet, C., Soldevila, S., Lamarque, L., *et al.* (2017). HTS-compatible FRET-based conformational sensors clarify membrane receptor activation. *Nature chemical biology*.
- Sears, R., Nuckolls, F., Haura, E., Taya, Y., Tamai, K., and Nevins, J.R. (2000). Multiple Ras-dependent phosphorylation pathways regulate Myc protein stability. *Genes Dev* *14*, 2501-2514.
- Selimkhanov, J., Taylor, B., Yao, J., Pilko, A., Albeck, J., Hoffmann, A., Tsimring, L., and Wollman, R. (2014). Systems biology. Accurate information transmission through dynamic biochemical signaling networks. *Science* *346*, 1370-1373.
- Seong, J., Ouyang, M., Kim, T., Sun, J., Wen, P.C., Lu, S., Zhuo, Y., Llewellyn, N.M., Schlaepfer, D.D., Guan, J.L., *et al.* (2011). Detection of focal adhesion kinase activation at membrane microdomains by fluorescence resonance energy transfer. *Nature communications* *2*, 406.
- Shaner, N.C., Lambert, G.G., Chamma, A., Ni, Y., Cranfill, P.J., Baird, M.A., Sell, B.R., Allen, J.R., Day, R.N., Israelsson, M., *et al.* (2013). A bright monomeric green fluorescent protein derived from *Branchiostoma lanceolatum*. *Nat Methods* *10*, 407-409.
- Shcherbakova, D.M., Hink, M.A., Joosen, L., Gadella, T.W., and Verkhusha, V.V. (2012). An orange fluorescent protein with a large Stokes shift for single-excitation multicolor FCCS and FRET imaging. *Journal of the American Chemical Society* *134*, 7913-7923.
- Shcherbakova, D.M., and Verkhusha, V.V. (2013). Near-infrared fluorescent proteins for multicolor in vivo imaging. *Nat Methods* *10*, 751-754.
- Shimobayashi, M., and Hall, M.N. (2014). Making new contacts: the mTOR network in metabolism and signalling crosstalk. *Nature reviews Molecular cell biology* *15*, 155-162.
- Sieg, D.J., Hauck, C.R., Ilic, D., Klingbeil, C.K., Schaefer, E., Damsky, C.H., and Schlaepfer, D.D. (2000). FAK integrates growth-factor and integrin signals to promote cell migration. *Nature cell biology* *2*, 249-256.
- Sigismund, S., Woelk, T., Puri, C., Maspero, E., Tacchetti, C., Transidico, P., Di Fiore, P.P., and Polo, S. (2005). Clathrin-independent endocytosis of ubiquitinated cargos. *Proceedings of the National Academy of Sciences of the United States of America* *102*, 2760-2765.
- Sneppen, K., Krishna, S., and Semsey, S. (2010). Simplified models of biological networks. *Annu Rev Biophys* *39*, 43-59.
- Stauber, D.J., DiGabriele, A.D., and Hendrickson, W.A. (2000). Structural interactions of fibroblast growth factor receptor with its ligands. *Proceedings of the National Academy of Sciences of the United States of America* *97*, 49-54.
- Stein, F. (2014). Lipid and image analysis tools for studying lipid-protein binding dynamics in living cells. PhD diss *University of Heidelberg*.

Stein, F., Kress, M., Reither, S., Piljic, A., and Schultz, C. (2013). FluoQ: a tool for rapid analysis of multiparameter fluorescence imaging data applied to oscillatory events. *ACS chemical biology* 8, 1862-1868.

Stokoe, D., Macdonald, S.G., Cadwallader, K., Symons, M., and Hancock, J.F. (1994). Activation of Raf as a result of recruitment to the plasma membrane. *Science* 264, 1463-1467.

Straussman, R., Morikawa, T., Shee, K., Barzily-Rokni, M., Qian, Z.R., Du, J., Davis, A., Mongare, M.M., Gould, J., Frederick, D.T., *et al.* (2012). Tumour micro-environment elicits innate resistance to RAF inhibitors through HGF secretion. *Nature* 487, 500-504.

Takanaga, H., Chaudhuri, B., and Frommer, W.B. (2008). GLUT1 and GLUT9 as major contributors to glucose influx in HepG2 cells identified by a high sensitivity intramolecular FRET glucose sensor. *Biochimica et biophysica acta* 1778, 1091-1099.

Takaya, A., Ohba, Y., Kurokawa, K., and Matsuda, M. (2004). RalA activation at nascent lamellipodia of epidermal growth factor-stimulated Cos7 cells and migrating Madin-Darby canine kidney cells. *Molecular biology of the cell* 15, 2549-2557.

Tallquist, M.D., French, W.J., and Soriano, P. (2003). Additive effects of PDGF receptor beta signaling pathways in vascular smooth muscle cell development. *PLoS biology* 1, E52.

Tantama, M., Martinez-Francois, J.R., Mongeon, R., and Yellen, G. (2013). Imaging energy status in live cells with a fluorescent biosensor of the intracellular ATP-to-ADP ratio. *Nature communications* 4, 2550.

Tay, S., Hughey, J.J., Lee, T.K., Lipniacki, T., Quake, S.R., and Covert, M.W. (2010). Single-cell NF-kappaB dynamics reveal digital activation and analogue information processing. *Nature* 466, 267-271.

Team, R.C. (2012). R: A Language and Environment for Statistical Computing, R Foundation for Statistical Computing.

Terai, K., and Matsuda, M. (2005). Ras binding opens c-Raf to expose the docking site for mitogen-activated protein kinase kinase. *EMBO reports* 6, 251-255.

Terai, K., and Matsuda, M. (2006). The amino-terminal B-Raf-specific region mediates calcium-dependent homo- and hetero-dimerization of Raf. *The EMBO journal* 25, 3556-3564.

Tewson, P., Westenberg, M., Zhao, Y., Campbell, R.E., Quinn, A.M., and Hughes, T.E. (2012). Simultaneous detection of Ca²⁺ and diacylglycerol signaling in living cells. *PloS one* 7, e42791.

Therrien, M., Michaud, N.R., Rubin, G.M., and Morrison, D.K. (1996). KSR modulates signal propagation within the MAPK cascade. *Genes Dev* 10, 2684-2695.

Thestrup, T., Litzlbauer, J., Bartholomaeus, I., Mues, M., Russo, L., Dana, H., Kovalchuk, Y., Liang, Y., Kalamakis, G., Laukat, Y., *et al.* (2014). Optimized ratiometric calcium sensors for functional in vivo imaging of neurons and T lymphocytes. *Nat Methods* 11, 175-182.

- Tischer, C., and Bastiaens, P.I. (2003). Lateral phosphorylation propagation: an aspect of feedback signalling? *Nature reviews Molecular cell biology* 4, 971-974.
- Toettcher, J.E., Weiner, O.D., and Lim, W.A. (2013). Using optogenetics to interrogate the dynamic control of signal transmission by the Ras/Erk module. *Cell* 155, 1422-1434.
- Tornillo, G., Bisaro, B., Camacho-Leal Mdel, P., Galie, M., Provero, P., Di Stefano, P., Turco, E., Defilippi, P., and Cabodi, S. (2011). p130Cas promotes invasiveness of three-dimensional ErbB2-transformed mammary acinar structures by enhanced activation of mTOR/p70S6K and Rac1. *Eur J Cell Biol* 90, 237-248.
- van der Geer, P., Hunter, T., and Lindberg, R.A. (1994). Receptor protein-tyrosine kinases and their signal transduction pathways. *Annu Rev Cell Biol* 10, 251-337.
- Vasudevan, H.N., Mazot, P., He, F., and Soriano, P. (2015). Receptor tyrosine kinases modulate distinct transcriptional programs by differential usage of intracellular pathways. *eLife* 4.
- Verstraete, K., and Savvides, S.N. (2012). Extracellular assembly and activation principles of oncogenic class III receptor tyrosine kinases. *Nature reviews Cancer* 12, 753-766.
- Violin, J.D., Zhang, J., Tsien, R.Y., and Newton, A.C. (2003). A genetically encoded fluorescent reporter reveals oscillatory phosphorylation by protein kinase C. *The Journal of cell biology* 161, 899-909.
- Volinsky, N., and Kholodenko, B.N. (2013). Complexity of receptor tyrosine kinase signal processing. *Cold Spring Harbor perspectives in biology* 5, a009043.
- Wagner, J.P., Wolf-Yadlin, A., Sevecka, M., Grenier, J.K., Root, D.E., Lauffenburger, D.A., and MacBeath, G. (2013). Receptor tyrosine kinases fall into distinct classes based on their inferred signaling networks. *Science signaling* 6, ra58.
- Wang, H., Yang, C., Leskow, F.C., Sun, J., Canagarajah, B., Hurley, J.H., and Kazanietz, M.G. (2006). Phospholipase Cgamma/diacylglycerol-dependent activation of beta2-chimaerin restricts EGF-induced Rac signaling. *The EMBO journal* 25, 2062-2074.
- Wang, Y., Botvinick, E.L., Zhao, Y., Berns, M.W., Usami, S., Tsien, R.Y., and Chien, S. (2005). Visualizing the mechanical activation of Src. *Nature* 434, 1040-1045.
- Ward, C.W., Lawrence, M.C., Streltsov, V.A., Adams, T.E., and McKern, N.M. (2007). The insulin and EGF receptor structures: new insights into ligand-induced receptor activation. *Trends in biochemical sciences* 32, 129-137.
- Warnes, G., Bolker, B., Bonebakker, L., Gentleman, R., and Huber, W. (2012). Package 'gplots'. <http://cran.r-project.org>.
- Wehrman, T., He, X., Raab, B., Dukipatti, A., Blau, H., and Garcia, K.C. (2007). Structural and mechanistic insights into nerve growth factor interactions with the TrkA and p75 receptors. *Neuron* 53, 25-38.

Bibliography

Welch, C.M., Elliott, H., Danuser, G., and Hahn, K.M. (2011). Imaging the coordination of multiple signalling activities in living cells. *Nature reviews Molecular cell biology* 12, 749-756.

Wickham, H. (2009). *ggplot2: Elegant Graphics for Data Analysis*. Springer: New York.

Wilke, B.U., Lindner, M., Greifenberg, L., Albus, A., Kronimus, Y., Bunemann, M., Leitner, M.G., and Oliver, D. (2014). Diacylglycerol mediates regulation of TASK potassium channels by Gq-coupled receptors. *Nature communications* 5, 5540.

Wilson, T.R., Fridlyand, J., Yan, Y., Penuel, E., Burton, L., Chan, E., Peng, J., Lin, E., Wang, Y., Sosman, J., *et al.* (2012). Widespread potential for growth-factor-driven resistance to anticancer kinase inhibitors. *Nature* 487, 505-509.

Yonesaka, K., Zejnullahu, K., Okamoto, I., Satoh, T., Cappuzzo, F., Souglakos, J., Ercan, D., Rogers, A., Roncalli, M., Takeda, M., *et al.* (2011). Activation of ERBB2 signaling causes resistance to the EGFR-directed therapeutic antibody cetuximab. *Sci Transl Med* 3, 99ra86.

Yoshizaki, H., Ohba, Y., Kurokawa, K., Itoh, R.E., Nakamura, T., Mochizuki, N., Nagashima, K., and Matsuda, M. (2003). Activity of Rho-family GTPases during cell division as visualized with FRET-based probes. *The Journal of cell biology* 162, 223-232.

Yu, C.F., Liu, Z.X., and Cantley, L.G. (2002). ERK negatively regulates the epidermal growth factor-mediated interaction of Gab1 and the phosphatidylinositol 3-kinase. *The Journal of biological chemistry* 277, 19382-19388.

Yu, Y., Yoon, S.O., Poulogiannis, G., Yang, Q., Ma, X.M., Villen, J., Kubica, N., Hoffman, G.R., Cantley, L.C., Gygi, S.P., *et al.* (2011). Phosphoproteomic analysis identifies Grb10 as an mTORC1 substrate that negatively regulates insulin signaling. *Science* 332, 1322-1326.

Yuan, T.L., and Cantley, L.C. (2008). PI3K pathway alterations in cancer: variations on a theme. *Oncogene* 27, 5497-5510.

Yuan, T.L., Wulf, G., Burga, L., and Cantley, L.C. (2011). Cell-to-cell variability in PI3K protein level regulates PI3K-AKT pathway activity in cell populations. *Current biology : CB* 21, 173-183.

Yun, C.H., Mengwasser, K.E., Toms, A.V., Woo, M.S., Greulich, H., Wong, K.K., Meyerson, M., and Eck, M.J. (2008). The T790M mutation in EGFR kinase causes drug resistance by increasing the affinity for ATP. *Proceedings of the National Academy of Sciences of the United States of America* 105, 2070-2075.

Yuzawa, S., Opatowsky, Y., Zhang, Z., Mandiyan, V., Lax, I., and Schlessinger, J. (2007). Structural basis for activation of the receptor tyrosine kinase KIT by stem cell factor. *Cell* 130, 323-334.

Zanella, F., Rosado, A., Garcia, B., Carnero, A., and Link, W. (2008). Chemical genetic analysis of FOXO nuclear-cytoplasmic shuttling by using image-based cell screening. *Chembiochem* 9, 2229-2237.

Zhang, X., Gureasko, J., Shen, K., Cole, P.A., and Kuriyan, J. (2006). An allosteric mechanism for activation of the kinase domain of epidermal growth factor receptor. *Cell* 125, 1137-1149.

Zheng, Y., Zhang, C., Croucher, D.R., Soliman, M.A., St-Denis, N., Pasculescu, A., Taylor, L., Tate, S.A., Hardy, W.R., Colwill, K., *et al.* (2013). Temporal regulation of EGF signalling networks by the scaffold protein Shc1. *Nature* 499, 166-171.

Zhu, J., Blenis, J., and Yuan, J. (2008). Activation of PI3K/Akt and MAPK pathways regulates Myc-mediated transcription by phosphorylating and promoting the degradation of Mad1. *Proceedings of the National Academy of Sciences of the United States of America* 105, 6584-6589.

Ziauddin, J., and Sabatini, D.M. (2001). Microarrays of cells expressing defined cDNAs. *Nature* 411, 107-110.

Zimmermann, S., and Moelling, K. (1999). Phosphorylation and regulation of Raf by Akt (protein kinase B). *Science* 286, 1741-1744.

Acknowledgements

First and foremost I would like to express my thanks to Carsten Schultz for giving me the opportunity to pursue my PhD in his laboratory. His consistent support kept me in a good intelligent and emotional shape to develop my own ideas throughout the doctoral work. He has pushed me to think broader and encouraged me to pursue ideas that expanded the limits of what I thought possible for me to do.

I sincerely thank the members of my thesis advisory committee: Rainer Pepperkok, Ursula Klingmüller and Wolfgang Huber for reviewing my work and advising me with their valuable comments and suggestions over the years.

Many thanks also to Rainer Pepperkok, Ursula Klingmüller, Martin Jechlinger and Walter Nickel for being a member in my thesis defense committee.

This study would not be possible without excellent work of the EMBL Core facilities and their excellent technical support during my time at EMBL. A special thank goes to Beate Neumann who helped me with a microarray spotting. I will never forget her ability to dedicate her own time to assisting me.

I would like to thank everybody from the Schultz laboratory who created stimulating, exciting and collaborative environment. I would like especially thank Vibor Laketa for all his support within and outside the field of cellular signaling. Through his inspiring actions Vibor taught me not only how to be a great scientist, but also how to be a great mentor. I am truly grateful to

Frank Stein who helped me to move my first steps in the R programming and Madeleine Schultz for reading and improving this manuscript. Another big thank you goes to Jan-Erik Hoffman for a urgent translation of the thesis abstract to German.

Most importantly, I would like to thank my family, especially my wife, Katya, for her love, patience, great care and unwavering support throughout my studies as well as long discussions about my project. Without all of you, everything would not be possible.